

DEGRADATION OF MICROPLASTIC FIBERS  
IN LAUNDRY WASTEWATER VIA  
IMMOBILIZED SILVER-TITANIUM DIOXIDE  
BASED PHOTOCATALYTIC MEMBRANE  
REACTOR

**BIAO WANG**

FACULTY OF ENGINEERING  
UNIVERSITI MALAYA  
KUALA LUMPUR

2025

**DEGRADATION OF MICROPLASTIC FIBERS IN  
LAUNDRY WASTEWATER VIA IMMOBILIZED  
SILVER-TITANIUM DIOXIDE BASED  
PHOTOCATALYTIC MEMBRANE REACTOR**

**BIAO WANG**

**DISSERTATION SUBMITTED IN FULFILMENT OF  
THE REQUIREMENTS FOR THE DEGREE OF MASTER  
OF ENGINEERING SCIENCE**

**FACULTY OF ENGINEERING  
UNIVERSITI MALAYA  
KUALA LUMPUR**

**2025**

**UNIVERSITI MALAYA**  
**ORIGINAL LITERARY WORK DECLARATION**

Name of Candidate: **BIAO WANG**

Matric No: **S2124866**

Name of Degree: **MASTER OF ENGINEERING SCIENCE**

Title of Project Paper/Research Report/Dissertation/Thesis (“this Work”):

**Degradation of microplastic fibers in laundry wastewater via TiO<sub>2</sub> photocatalytic membrane reactor**

Field of Study: **Separation Processes (NEC 524: Chemical and Process)**

I do solemnly and sincerely declare that:

- (1) I am the sole author/writer of this Work;
- (2) This Work is original;
- (3) Any use of any work in which copyright exists was done by way of fair dealing and for permitted purposes and any excerpt or extract from, or reference to or reproduction of any copyright work has been disclosed expressly and sufficiently and the title of the Work and its authorship have been acknowledged in this Work;
- (4) I do not have any actual knowledge nor do I ought reasonably to know that the making of this work constitutes an infringement of any copyright work;
- (5) I hereby assign all and every rights in the copyright to this Work to the Universiti Malaya (“UM”), who henceforth shall be owner of the copyright in this Work and that any reproduction or use in any form or by any means whatsoever is prohibited without the written consent of UM having been first had and obtained;
- (6) I am fully aware that if in the course of making this Work I have infringed any copyright whether intentionally or otherwise, I may be subject to legal action or any other action as may be determined by UM.

Candidate’s Signature

Date: 15/08/2024

Subscribed and solemnly declared before,

Witness’s Signature

Date: 15/08/2024

Name:

Designation:

## ABSTRAK

Pencemaran mikroplastik (MP), terutamanya daripada gentian mikroplastik poliester (PMPF) yang dikeluarkan semasa proses dobi, telah menjadi isu alam sekitar yang ketara. Kajian ini meneroka penyelesaian yang berkesan untuk menolak dan merendahkan kedua-dua simulasi dan PMPF sebenar dalam air sisa dobi menggunakan reaktor membran fotomangkin (PMR) berasaskan  $\text{TiO}_2$ . PMR tidak bergerak menyepadukan mangkin  $\text{TiO}_2$  (Ag- $\text{TiO}_2$ ) yang dihias Ag pada membran seramik  $\text{Al}_2\text{O}_3$ , menggabungkan keupayaan fotokatalitik  $\text{TiO}_2$  dengan kecekapan dipertingkat yang disediakan oleh kesan plasmonik nanopartikel perak. Peralatan ini bertujuan untuk mengoptimumkan degradasi PMPF di bawah penyinaran cahaya ultraviolet-C (UVC). Prestasi PMR tidak bergerak telah dinilai dengan simulasi dan air sisa dobi sebenar yang mengandungi PMPF. Keputusan menunjukkan bahawa membran pemangkin Ag- $\text{TiO}_2$  mencapai penolakan sehingga 99.9% bagi kedua-dua simulasi dan PMPF sebenar, dan kadar degradasi 23.2% bagi PMPF simulasi selepas 48 jam penyinaran UVC. Analisis morfologi terperinci melalui FESEM dan pencirian kimia melalui FTIR dan GC/MS mengesahkan degradasi gentian poliester yang ketara. Kajian ini menunjukkan potensi PMR tak bergerak berasaskan  $\text{TiO}_2$  sebagai penyelesaian berskala dan cekap untuk mengurangkan pencemaran MP berserabut dalam air sisa. Pendekatan ini menggabungkan degradasi fotokatalitik dengan penapisan membran, menolak dan merendahkan ahli parlimen berserabut dengan berkesan, dengan itu mengurangkan kesan alam sekitar mereka.

Kata kunci: Mikroplastik; Poliester;  $\text{TiO}_2$ ; reaktor membran fotokatalitik; Pemisahan dan degradasi

## ACKNOWLEDGEMENTS

As I near the end of my graduate studies, I would like to express my heartfelt gratitude to those who have supported and helped me throughout this journey.

First and foremost, I want to thank my family. Your unwavering support and encouragement have been my driving force. To my parents in particular, your selfless dedication and endless support have given me the strength to persevere through challenges. I know that I could not have reached this point without you.

Secondly, I want to thank my friends; Ong Lide, Zhang Zhiqian, Aubaid Ullah, Muhammed Sahal Siddique, Mustapha Mohammed Grema. Your encouragement and comfort during times of confusion and fatigue have been invaluable. Your companionship has filled my research life with laughter and warmth. Especially during stressful moments, your understanding and support have allowed me to keep moving forward.

A special thanks to my supervisor; Associate Professor Ir. Dr. Nur Awanis Binti Hashim, Dr. Mohamad Fairus Bin Rabuni. Throughout the research process, you have provided me with patient guidance and invaluable advice. Your academic expertise and rigorous attitude have had a profound impact on me. Thank you for your encouragement and assistance when I faced difficulties. Your support has enabled me to overcome many challenges and continually improve my research skills.

Lastly, I want to thank all my partners in the department of Chemical Engineering. Thank you for your help and cooperation in the experiments, and for the inspiration and support during academic discussions. Your wisdom and efforts have made my research journey less lonely, and we have shared many unforgettable moments together.

I sincerely thank each and every one of you. It is your support and help that have made me who I am today.

## TABLE OF CONTENTS

Abstract .....	iii
Abstrak .....	iv
Acknowledgements .....	v
Table of Contents .....	vi
List of Figures .....	ix
List of Tables.....	xi
List of Symbols and Abbreviations.....	xii
<b>CHAPTER 1: INTRODUCTION .....</b>	<b>1</b>
1.1 Background.....	1
1.2 Problem statement .....	6
1.3 Objectives .....	8
1.4 Scope of the study.....	9
1.5 Significance of the study .....	11
1.6 Outline of the thesis .....	12s
<b>CHAPTER 2: LITERATURE REVIEW.....</b>	<b>13</b>
2.1 MPs fiber released in laundry wastewater.....	13
2.2 Analytical techniques for MPs detection in wastewater.....	14
2.2.1 MPs identification .....	14
2.2.2 MPs quantification.....	16
2.3 Existing and potential removal methods of MPs in wastewater treatment plants .	17
2.3.1 Primary treatment .....	18
2.3.2 Secondary treatment .....	25
2.3.3 Advanced treatment.....	26

2.4	Existing and potential removal methods of MPs in drinking water treatment plants.....	28
2.5	Existing and potential removal technologies for MPs in other water treatment processes.....	32
2.6	Photocatalytic for water treatment.....	32
2.7	PMR for MPs degradation.....	34
2.8	Summary of literature review.....	40
<b>CHAPTER 3: MATERIALS AND METHODS.....</b>		<b>43</b>
3.1	Materials.....	43
3.2	Photocatalytic reactors.....	44
3.3	Preparation of photocatalytic membrane.....	44
3.4	Preparation of PMPF.....	46
3.5	Photocatalytic experiments.....	47
3.5.1	PMR optimization via MG degradation.....	47
3.5.2	Simulated-PMPF elimination experiments.....	48
3.6	Characterization of membranes and microplastics.....	49
<b>CHAPTER 4: RESULTS AND DISCUSSION.....</b>		<b>53</b>
4.1	Characterization, photocatalytic performance, and optimization for Al <sub>2</sub> O <sub>3</sub> ceramic membrane with TiO <sub>2</sub> (CMT) membranes in immobilized-PMR.....	53
4.1.1	Characterization of CMT membranes.....	53
4.1.2	Photocatalytic performance in three photocatalytic experiments via MG degradation.....	58
4.2	Impact of process parameters on TIM-PMR performance.....	65
4.3	Stability of the TIM-PMR.....	69
4.4	Characterization of Al <sub>2</sub> O <sub>3</sub> , TiO <sub>2</sub> and Ag-TiO <sub>2</sub> membranes.....	70

4.4.1	Morphological property of membranes .....	70
4.4.2	Crystal property of Ag-TiO <sub>2</sub> membranes .....	73
4.4.3	Optical property of catalytic membranes .....	74
4.4.4	Porosity and pore size of membranes .....	77
4.4.5	Contact angle of membranes .....	79
4.5	Characterization, elimination, degradation mechanism of PMPF .....	79
4.5.1	Characterization of PMPF .....	79
4.5.1.1	Morphology analysis of simulated-PMPF .....	79
4.5.1.2	FTIR-ATR spectroscopy for simulated-PMPF .....	82
4.5.1.3	Photodegradation by-products of simulated-PMPF via GC/MS .....	84
4.5.2	Membranes performance for PMPF rejection and degradation .....	87
4.5.2.1	Simulated-PMPF rejection via membranes .....	87
4.5.2.2	Simulated-PMPF degradation via membranes .....	90
4.5.2.3	Performance comparison of immobilized-PMR and other studies .....	91
4.5.2.4	Pure water flux and anti-fouling performance .....	95
4.5.2.5	Effect of concentration for simulated-PMPF removal .....	98
4.5.2.6	Removal of real-PMPF in actual laundry wastewater .....	100
4.5.3	Possible degradation mechanism of simulated-PMPF .....	103
<b>CHAPTER 5: CONCLUSION .....</b>		<b>105</b>
References .....		106
List of Publications and Papers Presented .....		128
Appendix .....		129



## LIST OF FIGURES

Figure 1.1:	Global fiber production in 2022.	2
Figure 2.1:	Photocatalytic degradation mechanism.	33
Figure 2.2:	Configurations of PMR. (a) Slurry reactor followed by a membrane filtration unit; (b) submerged membrane in a slurry reactor; (c) submerged membrane in TiO <sub>2</sub> coated reactor; and (d) photocatalytic membrane.	37
Figure 3.1:	Flow chart of the study	43
Figure 3.2:	Laboratory-scale (a) sludge photocatalytic reactor (SPR) and (b) PMR system.	44
Figure 3.3:	The preparation procedure of (a) real-PMPF and (b) simulated-PMPF.	46
Figure 4.1:	FESEM surface images of (a) CMT <sub>0</sub> , (b) CMT <sub>5</sub> , (c) CMT <sub>50</sub> , and (d) CMT <sub>100</sub> .	54
Figure 4.2:	Cross-sectional views of (a) CMT <sub>5</sub> , (b) CMT <sub>50</sub> , and (c) CMT <sub>100</sub> , along with EDS (d) mapping and (e) weight ratio results of CMT <sub>50</sub> surface.	56
Figure 4.3:	AFM 3D images of (a) CMT <sub>0</sub> and (b) CMT <sub>50</sub> ; (c) XRD pattern of TiO <sub>2</sub> powder, Al <sub>2</sub> O <sub>3</sub> , and CMT <sub>50</sub> .	58
Figure 4.4:	(a) hydraulic permeability of the CMT <sub>0</sub> and CMT <sub>50</sub> ; (b) MG removal rate in three systems; (c) photodegradation model of the three systems by using first-order kinetics plots; (d) comparison of anti-fouling properties. (TiO <sub>2</sub> = 50 mg, CFV = 100 cm <sup>3</sup> /min, TMP = 0.2 bar)	63
Figure 4.5:	Effect of (a) TiO <sub>2</sub> concentration; (b) TMP and (c) CFV on MG degradation; (d) cycles of MG removal.	67
Figure 4.6:	(a) original Al <sub>2</sub> O <sub>3</sub> ceramic membrane; (b) TiO <sub>2</sub> catalytic membrane; (c) Ag-TiO <sub>2</sub> catalytic membrane; (d) diameter of Ag-TiO <sub>2</sub> particles; (e) and (f) EDS element mapping images of Ag, Ti, Al, Ti and O on Ag-TiO <sub>2</sub> membrane; (g) weight ratio results of Ag-TiO <sub>2</sub> membrane.	72
Figure 4.7:	XRD pattern of Al <sub>2</sub> O <sub>3</sub> and Ag-TiO <sub>2</sub> membrane.	74

Figure 4.8:	(a) UV-Vis DRS spectra and (b) Tauc plots for the optical band gap of TiO <sub>2</sub> and Ag-TiO <sub>2</sub> membrane.	76
Figure 4.9:	(a) Porosity and (b) contact angle value of Al <sub>2</sub> O <sub>3</sub> , TiO <sub>2</sub> and Ag-TiO <sub>2</sub> membrane.	78
Figure 4.10:	FESEM images of degraded simulated-PMPF by TiO <sub>2</sub> membranes in (a) 0, (b) 24 and (c) 48 h, and by Ag-TiO <sub>2</sub> membranes in (d) 0, (e) 24 and (f) 48 h.	81
Figure 4.11:	(a) FTIR-ATR spectra of degraded simulated-PMPF by Ag-TiO <sub>2</sub> membranes in 0, 24 and 48 h with enlarged region between (b) 1800-600 cm <sup>-1</sup> .	84
Figure 4.12:	Major possible intermediate products by GC/MS.	87
Figure 4.13:	Rejection of simulated-PMPF.	89
Figure 4.14:	Degradation of simulated-PMPF.	91
Figure 4.15:	(a) Pure water flux under different TMP; (b) normalized permeate flux of all membranes.	97
Figure 4.16:	The (a) rejection and (b) degradation of Ag-TiO <sub>2</sub> membrane for simulated-PMPF with different concentrations.	99
Figure 4.15:	(a) Normalized permeate flux; (b) rejection of real-PMPF.	102
Figure 4.16:	Diagram of possible mechanism of simulated-PMPF degradation.	104

## LIST OF TABLES

Table 2.1	MPs removal efficiency in WWTPs.	21
Table 2.2	Photocatalytic performance comparison	39
Table 4.1:	MG degradation rate and permeate flux deterioration after 4 h reaction.	62
Table 4.2:	The information of the possible intermediate products.	86
Table 4.3:	Comparison of the polyester microplastic degradation in this study and other research.	93

Universiti Malaya

## LIST OF SYMBOLS AND ABBREVIATIONS

MPs	:	microplastics
Ag	:	silver
PMR	:	photocatalytic membrane reactors
PMPF	:	polyester microplastic fibers
WWTP	:	wastewater treatment plant
TiO <sub>2</sub>	:	titanium dioxide
CFV	:	crossflow velocity
TMP	:	transmembrane pressure
MG	:	malachite green
PET	:	polyethylene terephthalate
PAN	:	polyacrylonitrile
PP	:	polypropylene
PU	:	polyurethane
AMX	:	amoxicillin
Al <sub>2</sub> O <sub>3</sub>	:	alumina
DMSO	:	dimethyl sulfoxide
H <sub>2</sub> SO <sub>4</sub>	:	sulfuric acid
SPR	:	sludge photocatalytic reactor
CMT	:	ceramic membrane with TiO <sub>2</sub>
Ag-TiO <sub>2</sub>	:	Ag-decorated TiO <sub>2</sub>
TIS-PMR	:	TiO <sub>2</sub> in suspension
TIM-PMR	:	TiO <sub>2</sub> immobilized on the membrane
FESEM	:	field emission scanning electron microscopy
EDS	:	energy dispersive X-ray spectrometer

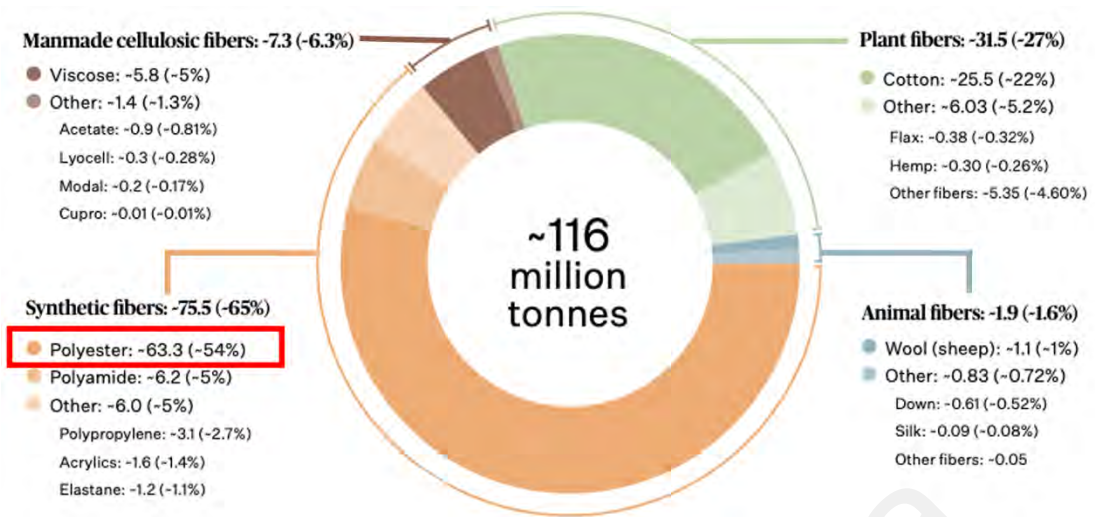
XRD	:	X-ray diffraction
UV-DRS	:	UV-visible diffuse reflectance spectroscopy
FTIR	:	fourier transform infrared
FTIR-ATR	:	FTIR-attenuated total reflectance
GC/MS	:	gas chromatography-mass spectrometry
Al	:	aluminium
O	:	oxygen
Ti	:	titanium
PDF	:	Powder Diffraction File
LSPR	:	localized surface plasmon resonance
He	:	helium
EI	:	electron ionization
ROS	:	reactive oxygen species
$\cdot\text{OH}$	:	hydroxyl radical
$\cdot\text{O}_2^-$	:	superoxide anion
$^1\text{O}_2$	:	singlet oxygen

## CHAPTER 1: INTRODUCTION

### 1.1 Background

Microplastics (MPs), particles size  $\leq 5$  mm, have garnered widespread attention due to their toxicity to organisms and broader environmental impact (Yuan et al., 2022). Recent studies and media coverage have underscored the pollution caused by washing synthetic textiles, which releases these fibrous MPs into the environment (Liu et al., 2021; Wang et al., 2024). During laundry processes, mechanical forces continuously release synthetic fibers, particularly shorter ones (de Oliveira et al., 2023; Y.-Q. Zhang et al., 2021). It is estimated that over 840 million washing machines globally contribute to approximately 500,000 tons of fibrous MPs entering the oceans annually (Cesa et al., 2020; S. Mishra et al., 2021).

The increase in the production of low-cost synthetic clothing over the past two decades is expected to further amplify the release of fiber MPs in the future (Ütebay et al., 2020). As shown in Fig. 1, data from 2022 reveal that synthetic fibers constituted 65% of global fiber production, totaling 116 million tonnes, with polyester comprising 54% of this total (Exchange, 2023). However, other significant fiber sources also contribute to the textile market, including natural fibers (cotton, wool, and silk), cellulosic fibers (viscose, lyocell, and modal), and bio-based synthetic fibers. Projections suggest that by 2030, synthetic fibers will make up 73% of all textile fibers, with polyester representing 85% of this category (Foundation, 2021; Suaria et al., 2020). This trend emphasizes the growing role of polyester fibers released during laundry in contributing to MP pollution.



**Fig. 1.1. Global fiber production in 2022.**

In addition, MPs pose risks to both human health and aquatic ecosystems. There is an increasing volume of research investigating the impact of MPs on human health and ecosystems (Al Mamun et al., 2023; Blackburn & Green, 2022). Studies indicate that MPs can enter the human body through ingestion and skin contact (Prata et al., 2020; Vethaak & Legler, 2021). When ingested, MPs are not fully excreted through feces. For instance, Leslie et al. found that the average concentration of plastic particles detected in human blood was 1.6  $\mu\text{g}/\text{ml}$  (Leslie et al., 2022; J. Zhang et al., 2021). Within the digestive system, MPs may trigger inflammatory responses, disrupt gut microbiota, and increase intestinal permeability (H. Chen et al., 2022; Ji et al., 2023). Medical literature also suggests that skin contact with plastics can lead to low-grade inflammation and foreign body reactions (Salthouse & Matlaga, 1975). Additionally, MPs pose various potential risks to organisms, depending on exposure levels and sensitivity (Anbumani & Kakkar, 2018; Kim et al., 2023). For instance, the high surface area and persistent nature of microplastics may lead to oxidative stress, cytotoxicity, and translocation to other tissues, potentially causing chronic inflammation and an increased cancer risk (Deng et al., 2018; Furukuma & Fujii, 2016). MPs have also been linked to a higher incidence of immune and neurodegenerative diseases (D  tr  e & Gallardo-Esc  rate, 2018). Furthermore, MPs

can release chemicals from their structure, absorb environmental contaminants, or act as vectors for harmful microorganisms (Crawford & Quinn, 2017; Kirstein et al., 2016).

Despite the high removal efficiency of MPs in wastewater treatment plant (WWTP), significant quantities still enter aquatic environments due to the large volumes of sewage processed daily (Alvim et al., 2020; Gao et al., 2022; N. Tang et al., 2020). Fibrous MPs, in particular, are prevalent in WWTP effluents and pose serious ecological risks because of their widespread distribution (Cheng et al., 2021; Lee et al., 2020; Singh et al., 2020). Furthermore, humans are estimated to ingest between 0.1 and 5 grams of MPs weekly, with traces found in lung tissue, the placenta, and blood, highlighting the urgent need for effective removal strategies (Sajid et al., 2022; Sangkham et al., 2022).

Photocatalytic degradation has emerged as a promising method for breaking down various organic pollutants, noted for its feasibility, cost-effectiveness, and energy efficiency (Paiman et al., 2023; Saifuddin et al., 2022). Titanium dioxide ( $\text{TiO}_2$ ) is a commonly used photocatalyst in wastewater treatment due to its non-toxicity, high electron mobility, and strong redox potential (Heris et al., 2023; Kanakaraju & Chandrasekaran, 2023; Madkhali et al., 2023). Studies have demonstrated the effectiveness of  $\text{TiO}_2$ -based systems in degrading plastics, with the degradation rate of polyester MPs ranging from 6.23% to 28.96 % (Blanco-Gutiérrez et al., 2022; Ge et al., 2022; Peng et al., 2023; Zhou, Luo, et al., 2022). Enhancing photocatalytic activity by coupling  $\text{TiO}_2$  with silver (Ag) has proven effective, as Ag improves efficiency through the plasmonic effect and by acting as an electron acceptor for  $\text{TiO}_2$  (Khan & Shah, 2023; Kumar et al., 2022; Li et al., 2024; Tseng & Chen, 2019; Wodka et al., 2010).

Despite their potential,  $\text{TiO}_2$ -based catalysts face challenges such as recovery, reuse, and maintaining stability in suspension (Ahmad et al., 2024; Chen et al., 2015; Singh et al., 2013; G. Zhang et al., 2023). Membrane separation, another key wastewater treatment



technology, is also used for eliminating MPs (Zhao et al., 2024). Techniques combining coagulation with ultrafiltration have shown rejection rates up to 85% for polyethylene, while membrane bioreactors have achieved a 99.9% rejection rate for MPs (Ma et al., 2019; Talvitie, Mikola, Koistinen, et al., 2017). Nonetheless, membrane separation is prone to fouling and often requires chemical pre-treatments to mitigate this issue, presenting operational challenges (Y. Zhang et al., 2021).

To address these limitations, a novel integrated approach known as the "photocatalytic membrane reactor (PMR)" has been developed (Binazadeh et al., 2023). PMR can be categorized as suspended or immobilized, depending on whether the catalyst is suspended in the solution or immobilized onto the membrane (Mozia, 2010). While suspended-PMR offer high photocatalytic degradation rate through full contact between the catalyst and pollutants, they can cause significant membrane fouling (Rani et al., 2021; Zhang et al., 2016). In contrast, immobilized-PMR, though slightly less efficient, offer enhanced stability, high-quality permeate, and potential antifouling properties (Kusworo et al., 2022; Mozia, 2010).

Ceramic membranes were chosen as substrates for the photocatalytic membranes due to their durability and chemical stability, offering advantages over polymer membranes (Bet-Moushoul et al., 2016; Danfá et al., 2021). Photocatalytic reactions often require UVC irradiation, which can degrade polymer films, making ceramic membranes more suitable (Horovitz et al., 2020). Moreover, ceramic membranes demonstrate better antifouling performance and are easier to backwash and restore flux after fouling occurs. For instance, Kim et al. reported that zirconia-titania (Z-T) ceramic membranes, compared to polyether sulfone (PES) polymer membranes with similar pore sizes, exhibit superior anti-pollution capabilities, achieving a 99.96% rejection rate of MPs (Kim et al., 2024). Also, Poerio et al. found that in a suspended-PMR system achieving nearly 100 %

rejection rate and 13.52% degradation rate of MPs, while the flux of polymer membranes in PMR with pore sizes of 0.1  $\mu\text{m}$ , 0.03  $\mu\text{m}$ , and 2 kDa decreased by more than 90% after 5-h filtration, with flux recovery proving difficult even after applying a cleaning solution (Poerio et al., 2024).

Investigating the removal and degradation of MPs presents significant challenges because, to date, there is no standardized method for detecting micron-sized MPs in wastewater. Variations in detection methods and operating procedures complicate the comparison of results across different studies (Gong & Xie, 2020). Consequently, selecting appropriate detection methods is crucial for accurate quantification. Common techniques for detecting MPs in water include turbidity measurements, ultraviolet-visible (UV-vis) spectroscopy, and Fourier Transform Infrared Spectroscopy (FTIR) (Bayarkhuu & Byun, 2022; Biao et al., 2024; Corami et al., 2020; Fan et al., 2022). To assess the degradation rate of simulated polyester microplastic fibers (PMPF), changes in concentration were monitored using UV-vis spectroscopy, which boasts an accuracy rate exceeding 95% (Fan et al., 2022). The evaluation of membrane's rejection rate for both real and simulated-PMPF can be done by measuring the concentration of MPs before and after filtration. Given that immobilized-PMR combines the benefits of membrane separation and catalytic properties, both degradation and rejection rates are crucial for determining the overall efficiency of the process.

Additionally, research on preparing micron-sized fibrous MPs in wastewater is limited, posing challenges for lab-scale studies and practical applications (Cole, 2016; Lee et al., 2020; Zhou, Wang, et al., 2022). Manually screening real-PMPF with consistent size and properties from actual laundry wastewater is also difficult. Therefore, this study prepared real-PMPF for practical applications and simulated-PMPF with similar characteristics for evaluating rejection and degradation rates and exploring degradation mechanisms.

In this study, we employed a photoreduction method to prepare an Ag-TiO<sub>2</sub> catalyst, which was then applied to a flat-sheet ceramic membrane via crossflow filtration. To our knowledge, this represents the first use of an immobilized-PMR to remove PMPF from simulated and real laundry wastewater. The research aimed to reduce the release of PMPF at its source and minimize its entry into wastewater treatment facilities. Additionally, the study explored the degradation mechanisms of polyester to provide deeper insights into the photocatalytic degradation process. Furthermore, the research assessed the rejection rate of real-PMPF and examined the anti-fouling performance of the photocatalytic membranes, focusing on the practical application of the immobilized-PMR.

## **1.2 Problem statement**

The use of plastics is rapidly growing due to their advantages, such as being lightweight, having good chemical stability, and being cost-effective. Global plastic production is projected to reach 33 billion tons by 2050 (Gu et al., 2020; Kutralam-Muniasamy et al., 2020). This surge in plastic usage has also resulted in a significant increase in plastic waste (Alabi et al., 2019). Over time, these waste plastics can gradually break down into smaller fragments, which are categorized by size as macro-plastics (> 2 cm), meso-plastics (5 mm to 2 cm), micro-plastics (< 5 mm), and nano-plastics (< 1 μm) (Blettler et al., 2017; Taylor et al., 2016). In addition to secondary MPs formed from the breakdown of larger plastic particles, MPs also include primary plastics manufactured for specific uses (Li, 2018). It is estimated that approximately 1.5 million tons of MPs are released into aquatic environments annually due to years of poor management and improper disposal of plastic materials (Kumar et al., 2023; Pico et al., 2019). MPs are increasingly found in aquatic ecosystems, including beaches, surface water, the water column, and subtidal sediments, with their prevalence on the rise (Coyle et al., 2020; Leslie et al., 2017; Li et al., 2023; Thompson et al., 2004). The world will face significant

challenges as plastic disposal rates exceed environmental limits (Kurniawan et al., 2023; Persson et al., 2022).

With the exponential rise in synthetic textile production and the corresponding surge in microplastic pollution, there is a pressing need for effective mitigation strategies. Existing measures are insufficient, as they do not fully tackle the dual challenges of minimizing fiber shedding during textile use and improving the capture and removal of microplastics in wastewater treatment processes. Consequently, innovative solutions are necessary to mitigate the environmental and health risks posed by microplastics, especially those derived from synthetic textiles.

Investigating the removal and degradation of MPs presents significant challenges because, to date, there is no standardized method for detecting micron-sized MPs in wastewater. Variations in detection methods and operating procedures complicate the comparison of results across different studies (Gong & Xie, 2020). Consequently, selecting appropriate detection methods is crucial for accurate quantification. Common techniques for detecting MPs in water include turbidity measurements, ultraviolet-visible (UV-vis) spectroscopy, and Fourier Transform Infrared Spectroscopy (FTIR) (Bayarkhuu & Byun, 2022; Biao et al., 2024; Corami et al., 2020; Fan et al., 2022). To assess the degradation rate of simulated polyester microplastic fibers (PMPF), changes in concentration were monitored using UV-vis spectroscopy, which boasts an accuracy rate exceeding 95% (Fan et al., 2022). The evaluation of membrane's rejection rate for both real and simulated-PMPF can be done by measuring the concentration of MPs before and after filtration. Given that immobilized-PMR combines the benefits of membrane separation and catalytic properties, both degradation and rejection rates are crucial for determining the overall efficiency of the process.

Additionally, research on preparing micron-sized fibrous MPs in wastewater is limited, posing challenges for lab-scale studies and practical applications (Cole, 2016; Lee et al., 2020; Zhou, Wang, et al., 2022). Manually screening real-PMPF with consistent size and properties from actual laundry wastewater is also difficult. Therefore, this study prepared real-PMPF for practical applications and simulated-PMPF with similar characteristics for evaluating rejection and degradation rates and exploring degradation mechanisms.

To mitigate the environmental and health risks posed by microplastics, this study employs a PMR designed for the degradation of polyester microplastic fibers (PMPF) from laundry wastewater. The TiO<sub>2</sub>-based immobilized-PMR system integrates membrane filtration with photocatalysis, ensuring both the physical rejection and chemical degradation of microplastics. The study explores Ag-TiO<sub>2</sub> as an enhanced photocatalyst, leveraging silver's plasmonic effect to improve light absorption and electron transfer, thereby increasing degradation efficiency. Additionally, operational optimizations such as crossflow velocity (CFV) and transmembrane pressure (TMP) are evaluated to maximize microplastic removal efficiency while minimizing membrane fouling.

### **1.3 Objectives**

The aim of the research is to develop a photocatalytic membrane reactor to degrade polyester microplastic fiber (PMPF) from laundry wastewater. Provide guidance on PMPF degradation mechanism to reduce MPs pollution. The present study has the following objectives:

- i. To design a photocatalytic reactor and optimize the catalyst loading on the membrane for PMPF elimination.
- ii. To assess the effect of reactor operating on MG dye degradation in different CFV and TMP.

- iii. To evaluate the effect of membrane performance using both simulated and real PMPF.

#### **1.4 Scope of the study**

This study focuses on the development and evaluation of a TiO<sub>2</sub>-based PMR system specifically designed for treating laundry wastewater contaminated with PMPF. The research encompasses the preparation and detailed characterization of the photocatalytic membrane, optimization of reactor operating conditions, and performance evaluation using both model pollutants and real wastewater samples. The study is limited to utilizing TiO<sub>2</sub> as the photocatalyst and targeting polyester fibers as the primary pollutant of interest.

The scope includes:

The flat-sheet alumina (Al<sub>2</sub>O<sub>3</sub>) ceramic membrane with a pore size of 0.1 μm and thickness of 6 mm was used as the substrate. The photocatalyst consisted of TiO<sub>2</sub> (99.5% purity) and Ag-TiO<sub>2</sub> (1 wt.% Ag), with catalyst loadings of 5, 20, 50, and 100 mg. The photocatalytic membrane was prepared through ball milling, sonication, crossflow filtration, drying at 50°C, and calcination at 400°C for 4 hours to ensure uniform catalyst immobilization.

For microplastic fiber degradation studies, simulated-PMPF was prepared by shredding 100% polyester fabric into fibers (<5 mm), treating them in DMSO at 90°C for 15 minutes, washing with ethanol, and filtering to obtain fibers <1000 μm. In contrast, real-PMPF was collected from actual laundry wastewater using a washing machine with a 15-minute cycle, 24 L of water, and 10 mL of detergent. Wastewater samples were taken from the wash, rinse, and spin cycles, combined, and filtered before testing.

Various characterization techniques were employed to analyze both the membranes and microplastic fibers. FESEM (AURIGA, ZEISS) with EDS mapping was used to

examine surface morphology and elemental composition. XRD (Rigaku SmartLab) identified the crystalline phases of TiO<sub>2</sub> and Ag-TiO<sub>2</sub> coatings. UV-Vis DRS (Perkin Elmer Lambda 750) measured optical properties, while FTIR-ATR (Perkin Elmer, USA) tracked chemical transformations in degraded polyester fibers. Additionally, GC-MS (Shimadzu, GCMS-QP 2010 Plus) was used to identify degradation by-products, confirming the breakdown of microplastics into smaller molecules.

To optimize the photocatalytic membrane reactor (PMR), key operating parameters were studied, including crossflow velocity (CFV), transmembrane pressure (TMP), and catalyst concentration. The CFV values tested were 10, 50, and 100 cm<sup>3</sup>/min, while TMP varied between 0.2, 0.5, 0.8, and 1.0 bar. Catalyst concentration was adjusted at 5, 20, 50, and 100 mg TiO<sub>2</sub>, with an additional 1 wt.% Ag in Ag-TiO<sub>2</sub> membranes. These conditions were optimized to balance photocatalytic efficiency, membrane permeability, and fouling resistance.

For degradation studies, malachite green (MG, 5 mg/L) was selected as a model organic pollutant to evaluate photocatalytic performance, as its degradation kinetics provide insights into the system's efficiency. Additionally, both simulated-PMPF and real-PMPF were tested to assess microplastic rejection and degradation efficiency under optimized PMR conditions. This comprehensive study provides a foundation for developing an efficient and scalable solution to mitigate microplastic pollution from laundry wastewater.

By focusing on these specific aspects, this study aims to contribute insights into the development of effective PMR technologies for mitigating microplastic pollution originating from synthetic textile laundering processes.

## 1.5 Significance of the study

The successful implementation of this research holds significant implications for addressing the pervasive issue of microplastic pollution in wastewater generated from synthetic textile laundering processes. By focusing on the development and application of a TiO<sub>2</sub>-based PMR system, this study aims to offer a sustainable and effective solution for mitigating microplastic contamination.

1. Environmental protection: The findings from this study could lead to a practical method for removing PMPF from wastewater, thereby preventing their entry into natural ecosystems such as rivers, lakes, and oceans. This contributes directly to safeguarding aquatic habitats and biodiversity.

2. Public health impact: Minimizing fibrous MPs contamination in wastewater can potentially reduce human exposure to harmful chemicals associated with MPs, addressing concerns about their impact on public health.

3. Technological advancement: By advancing TiO<sub>2</sub>-based photocatalytic membrane technology, this research paves the way for enhanced water treatment processes. These advancements could benefit various industrial and municipal applications beyond textile wastewater treatment.

4. Sustainability: Implementing effective microplastic removal techniques aligns with global sustainability goals, promoting responsible consumption and production practices within the textile industry.

5. Policy and regulation: Insights gained from this study may inform future policy decisions aimed at regulating MPs discharge from textile manufacturing and laundering operations, contributing to broader environmental stewardship efforts.



Overall, the outcomes of this research have the potential to catalyze positive changes in environmental management strategies, emphasizing the importance of addressing microplastic pollution at its source and promoting sustainable practices across industries.

## **1.6 Outline of the thesis**

This thesis is structured into five chapters. Chapter 1 provides an introduction to the research background, problem statement, objectives, scope, and significance. Chapter 2 reviews the relevant literature on MPs release and MPs degradation. Chapter 3 details the methodologies and materials used in the study. Chapter 4 presents and discusses the results obtained from the experiments. Finally, Chapter 5 concludes the study and suggests future research directions.

Universiti Malaysia

## CHAPTER 2: LITERATURE REVIEW

### 2.1 MPs fiber released in laundry wastewater

The apparel industry uses around 69.7 million tons of fibers annually, with synthetic fibers accounting for nearly 60 % of this type of fiber (De Falco, Cocca, et al., 2019). Household laundry wastewater releases large quantities of plastic microfibers into the environment from the shedding of various textiles. Synthetic fibers released during the washing process mainly include polyethylene terephthalate (PET), nylon, polyacrylonitrile (PAN), polypropylene (PP), and polyurethane (PU) (De Falco, Di Pace, et al., 2019). These MPs fibers represent most types of MPs in the environment. Research shows that the pollution due to synthetic fibers in clothing in Asia is higher than the global average, with laundry washing in India and Southeast Asia accounting for 15.9% of global microplastics to the environment (Boucher & Friot, 2017). Each garment is estimated to release more than 1,900 microfibers to the WWTP during a single wash cycle. A study on MPs releases from washing machines in Kuala Lumpur showed that fragments and fibers were detected in laundry wastewater, with an average content of 0.068 g/m<sup>3</sup> and an average length of 2258.59 μm (Praveena et al., 2021). More than 50% of laundry machine-washed clothing is made of nylon and polyester, and FTIR analysis indicates the presence of polyester, nylon, and acrylic in these laundry samples. Carmichael reported that polyester is the most dominant man-made plastic fiber, followed by nylon (Carmichael, 2015). Although the discharge of MPs is a multifactorial result, there is no doubt that household laundry wastewater is one of the important sources of MPs in WWTP.

Due to the sharp increase in demand for synthetic fabrics over the past decade, it is projected to grow at an annual rate of over 7% in the next ten years (Exchange, 2019). Asia is expected to see a faster compound annual growth rate because of significant economic development in the region. Currently, synthetic fabrics make up 63% of the

global fabric market, with the majority being polyester. Polyester is widely used across various applications due to its mechanical strength, aesthetic appeal, lightness, and low cost. Global fiber production has reached 113 tons, with polyester (the primary component of polyester) accounting for over half of all synthetic fibers (Pepper & Truscott, 2021).

## **2.2 Analytical techniques for MPs detection in wastewater**

Identifying and profiling MPs in aquatic environments is crucial for devising effective removal strategies. Common morphologies of MPs in water encompass fragments, microbeads, and fibers. The prevalent types of MPs in wastewater include PA, PET, PE, PS, and PP, constituting 11-20.5%, 14.3-41.79%, 11.6-15.52%, 3.35-9.8%, and 8.9-11% respectively (Cristaldi et al., 2020; Jiang et al., 2020; Xu et al., 2019). However, as MPs migrate from their sources to water systems, they undergo aging, deformation, and wear, complicating their classification (He et al., 2023; Raju et al., 2023). Additionally, subjective human errors can emerge during MPs quantitative detection and identification. To surmount these obstacles, researchers have turned to advanced characterization techniques.

### **2.2.1 MPs identification**

Scanning Electron Microscopy (SEM) provides insights into the size and morphology of MPs. It distinguishes morphological alterations occurring during MPs degradation, such as the emergence of cracks and cavities (Kamalian et al., 2020; Y.-T. Zhang et al., 2022). SEM remains instrumental in grasping the physical attributes of MPs, steering the evolution of efficient removal methods.

Dynamic Light Scattering (DLS) analyses a wide spectrum of liquid samples to determine MPs size distribution and concentration (Batool & Valiyaveetil, 2021; Caputo et al., 2021). While optimally used for spherical particles, it can detect various particle

shapes in rotational motion (Arenas-Guerrero et al., 2018). Nonetheless, its capacity to differentiate MPs from other light-scattering particles is limited, which can mask the presence of minuscule particles (Carr & Wright, 2008).

Fourier Transform Infrared Spectroscopy (FTIR), a non-invasive technique, can identify MP particles using micro-FTIR (Schymanski et al., 2021). However, micro-FTIR struggles with particles smaller than 10  $\mu\text{m}$ , especially if they are irregular or opaque, due to diffraction limits (Cabernard et al., 2018; Renner et al., 2017).

Raman Spectroscopy (RS), known for its high spatial resolution and minimal sensitivity to water, can be coupled with microscopy for swift and automated data acquisition. Micro-Raman spectroscopy addresses some of FTIR constraints with its spectral resolution nearing 1  $\mu\text{m}$  (Käppler et al., 2016). Nevertheless, the interpretation of Raman spectra mandates caution as they can be influenced by biological and other chemical entities (Imhof et al., 2016; J. Li et al., 2018).

More advanced techniques like Surface-Enhanced Raman Spectroscopy (SERS) and Raman tweezers have further improved MPs identification (Pérez-Jiménez et al., 2020; Saletnik et al., 2021) (Gillibert et al., 2019). SERS intensifies the Raman signal by leveraging corrugated metal nanoparticles, enhancing detection sensitivity (Lv et al., 2020). Raman tweezers merge RS with optical tweezers, granting the capability to seize and manipulate MPs using light forces (Gillibert et al., 2019). These innovations extend spectroscopic capabilities, enlarging the detectable MPs spectrum and enabling their differentiation in complex environments.

When comparing sample spectra from RS with MPs reference spectra, a spectral similarity threshold of 70% has been set for reliable MPs identification (Fraser et al., 2020). This precise benchmark minimizes the risks of misinterpretation, providing

researchers with confidence in their conclusions. Consequently, these innovative spectroscopic techniques are driving MPs research forward, shedding light on their prevalence and characteristics in water systems.

Specifically, FTIR and Raman Spectroscopy can confirm the polymer composition, while SEM imaging provides morphological insights. This will help distinguish between polyester, nylon, and other synthetic fibers commonly found in laundry wastewater.

### **2.2.2 MPs quantification**

To precisely measure the presence of MPs in aquatic environments, a variety of quantification techniques are in play, each presenting its advantages and shortcomings. Counting methods, utilizing microscopic techniques and hemacytometers, offer a direct observation of MPs. After collecting the plastic particles via filtration, they are subjected to a washing, rinsing, and drying process, after which they are inspected under a stereo microscope (Hanvey et al., 2017; Song et al., 2015). Hemacytometers, which feature uniformly sized rectangular chambers, serve to enumerate the cumulative count of MPs (Prata et al., 2021). The weighing method necessitates the drying and subsequent weighing of MPs gathered through filtration, offering a quantitative understanding of the MPs mass (Zhou et al., 2021).

Absorbance methods by using ultraviolet-visible (UV-Vis) spectroscopy, the peak absorbance of MPs solution is determined. To measure the concentration of MPs, the observed absorbance is compared with a calibration curve derived using standard MPs solutions (Yang et al., 2022). Nonetheless, this technique might not be appropriate for MPs of lower density, as their buoyancy could cause them to float, thereby affecting the results.

Turbidity methods establish a standard curve for MPs concentration by measuring the turbidity of solutions with known MPs concentrations. The fluctuations in turbidity over time mirror the changes in the concentration of MPs (Rajala et al., 2020). Turbidimeters, tools that measure the cloudiness of a fluid, showcase heightened sensitivity in detecting MPs when compared with absorbance techniques (Skaf et al., 2020).

Each quantitative method has its own merits and drawbacks. The choice of method depends on specific research needs and the characteristics of the MPs being analyzed. A point of caution for researchers: expressing MPs concentrations in grams per liter (g/L) may make the values appear small, potentially understating the serious nature of MPs pollution to the general public. On the other hand, representing in terms of particles per liter (particles/L) can lead to pronounced counting errors given the diminutive size of MPs (Priya et al., 2023). Overall, it is important to carefully consider the most suitable methods for quantifying MPs to determine their level of presence in the water bodies.

### **2.3 Existing and potential removal methods of MPs in wastewater treatment plants**

Wastewater treatment plants (WWTPs), with their conventionally employed processes, mainly aim to remove pollutants such as solids and organic matter from wastewater using physical, chemical, and biological treatments (Mujeriego & Asano, 1999; Sun et al., 2019). However, the emerging concern of MPs demands a closer examination of the suitability of these treatments to remove MPs as literature indicates that the conventional WWTPs are not designed to perform such a task. The processes in WWTPs are described in order of increasing levels of treatment, commonly used terms are primary, secondary, and advanced treatment (Krishnan et al., 2023; Sonune & Ghate, 2004). To date, a few European countries are trying to develop a fourth treatment to improve the effluent quality further (Kosek et al., 2020). Although the intent of these processes is not primarily to

remove MPs, observational data suggests a considerable reduction in the amount of MPs post each stage, with removal efficiencies spanning a broad range from as low as 10.2% to as high as 100% (Bayo et al., 2020; Cheng et al., 2021; Conley et al., 2019; Z. Xu et al., 2021).

The wide range in reported removal rates of MPs in various WWTPs is attributed to differences in treatment methods and the diverse characteristics of MPs, including their concentration, shape, and size, which vary across regions (Long et al., 2019; Yang et al., 2021). Notably, WWTP's primary and secondary treatments play a substantial role in promoting MPs removal. Advanced treatment processes, such as membrane separation technology, can further enhance MPs removal, effectively preventing MPs from entering natural water bodies (Yang et al., 2023). Despite this promising outcome, some advanced treatments might offer marginal benefits or even exacerbate the issue through MPs fragmentation (Talvitie, Mikola, Setälä, et al., 2017; Ziajahromi et al., 2017). Therefore, a thorough understanding of each treatment stage's mechanisms and their collective impact on MPs is necessary. This would pave the way for designing tailored treatment combinations, maximizing the removal of MPs from wastewater.

### **2.3.1 Primary treatment**

The primary treatment facilities in WWTPs, act as the initial barrier against pollutants, typically consisting of grids/screens, grit chambers, primary sedimentation/clarification tanks, and, in some cases, flotation tanks (Ou & Zeng, 2018; Wu et al., 2021). Table 2.1 presents the MPs removal rate in those primary treatment facilities like grids, grit chambers, primary sedimentation tanks, and air flotation tanks exhibit MPs removal efficiencies ranging from 2.7% to 70.5%, 57.0%, 19.1% to 99.0%, and 95.0%, respectively. The removal efficiency of coarse grid treatment in Jiang et al. varies significantly, showing values of 2.7% and 70.5%. This discrepancy arises due to

differences in grid spacing, flow conditions, and MP size distribution. Coarse grids with larger spacing are primarily designed to capture macroscopic debris, resulting in lower MP removal (2.7%), while finer grids with smaller spacing retain more microplastics, achieving higher efficiency (70.5%).

Grids and screens, as the first line to prevent solid pollutants in wastewater, are effective in removing larger solids like cloth, paper, and plastic, and they also capture a fraction of smaller MPs that might adhere to the larger solids (Hamidian et al., 2021; Tchobanoglous et al., 1991). To enhance MPs removal, researchers have incorporated fine/ultra-fine grids or small filters downstream of coarse grids. However, issues such as filter clogging and challenges related to backwashing have been encountered in these setups (Ali et al., 2019; Arslan et al., 2023; Bao et al., 2022).

Grit chambers play a crucial role in removing heavier particles from wastewater, preventing operational issues in treatment systems. These chambers help settle coarse materials like sand and gravel before the water moves further in the process. Various studies have highlighted the efficiency of different types of grit chambers in removing unwanted particles from wastewater. For example, study by Liu (Liu et al., 2019) showed that both grid-based and aerated grit chambers (AGC) effectively retain debris and suspended particles larger than 6 mm. AGC, in particular, improve sedimentation by altering flow dynamics with aeration. This process enhances wastewater treatment efficiency by reducing clogging, equipment wear, and maintenance costs.

Primary sedimentation/clarification tanks work on the principle of density separation. Heavier MPs, such as polybutylene terephthalate (PBT), PE, and polyvinyl chloride (PVC), tend to settle at the bottom due to gravity, making sedimentation tanks highly effective in their removal (Kernchen et al., 2022). Remarkably, in many WWTPs, over 90% of such MPs are eliminated through this method. However, some MPs with densities



exceeding 1 g/cm<sup>3</sup>, like PET and PA fibers, might persist in the effluent after primary sedimentation (Bayo et al., 2020; Murphy et al., 2016).

In contrast to sedimentation, air flotation is particularly efficient in removing low to medium density MPs or those with a higher specific surface area (Hou et al., 2021) (Kökkılıç et al., 2022). Dissolved air flotation (DAF) technology is an excellent example of this treatment category (Monira et al., 2023) (Reddy & Nair, 2022; Talvitie, Mikola, Koistinen, et al., 2017). Notably, combining sedimentation and flotation techniques offers a promising method to address both high and low-density MPs simultaneously (Z. Xu et al., 2021).

Universiti Malaysia

**Table 2.1. MPs removal efficiency in WWTPs.**

<b>Country/ region</b>	<b>Treatment levels</b>	<b>Unit operations</b>	<b>Removal efficiency (%)</b>	<b>Ref.</b>
China	Primary	Coarse grid	2.7	(Jiang et al., 2022)
	treatment	Coarse grid	70.5	
Finland	Primary	Coarse grid	55.7	(Salmi et al., 2021)
	treatment			
Turkey	Primary	Coarse and fine grids	41.3	(Üstün et al., 2022)
	treatment			
China	Primary treatment	Grit chamber	57.0	(Dong et al., 2022)
US	Primary treatment	Grids and grit chamber	35.1	(Michielssen et al., 2016)
Korea	Primary treatment	Fine grid and vortex- type grit chamber	25.8	(B. Zhang et al., 2023a)
		Fine grid and aerated grit chamber	56.8	
		Ultra-fine grill and aerated grit chamber	60.3	
Spain	Primary treatment	Primary sedimentation tank	19.1	(Bayo et al., 2020)
	Primary treatment	Primary sedimentation tank	91.7	

**Table 2.1 continued.**

Finland	Primary treatment	Primary sedimentation tank	99	(Lares et al., 2018)
Finland	Secondary treatment	Dissolved air flotation	95	(Talvitie, Mikola, Koistinen, et al., 2017)
Finland	Secondary treatment	Conventional activated sludge process (CASP)	66.7	(Lares et al., 2018)
		MBR	99.4	
Scotland	Secondary treatment	CASP	92.6	(Murphy et al., 2016)
China	Secondary treatment	Cyclic activated sludge system (CASS)	10.39-28.83	(Luo et al., 2023)
Vietnam	Secondary treatment	Sequencing batch reactor (SBR)	25.3	(Van Do et al., 2022)
Korea	Secondary treatment	SBR	85-92	(Lee & Kim, 2018)
China	Secondary treatment	anaerobic/aerobic (A/O)	16.9	(Jiang et al., 2020)
China	Secondary treatment	anaerobic/anoxic/aerobic (A/A/O)	15	(Lv et al., 2019)
Spain	Secondary treatment	A/A/O	93.7	(Edo et al., 2020)

**Table 2.1 continued.**

China	Secondary treatment	A/A/O	37.3	(B. Zhang et al., 2023a)
		SBR	47.5	
		CASS	13.8	
China	Secondary treatment	A/A/O + Constructed wetlands	100	(Wei et al., 2020)
China	Secondary treatment	Oxidation ditch (OD)	72.1	(Yang et al., 2021)
China	Secondary treatment	OD	16.5	(Lv et al., 2019)
Finland	Secondary treatment	MBR	99.9	(Talvitie, Mikola, Koistinen, et al., 2017)
Swedish	Secondary treatment	MBR	100	(Baresel et al., 2019)
* India	Advanced treatment	Micro-filtration (MF)	99.3	(Yaranal et al., 2021)
* Australia	Advanced treatment	MF	91	(Pramanik et al., 2021)
	Advanced treatment	Ultra-filtration (UF)	96	
Australia	Advanced treatment	Reverse osmosis (RO)	90	(Ziajahromi et al., 2017)

**Table 2.1 continued.**

---

Finland	Advanced treatment	MBR	98.3	(Lares et al., 2018)
China	Advanced treatment	Dynamic membrane (DM)	99.5	(L. Li et al., 2018)
* China	Advanced treatment	Adsorption	66.63	(F. Yuan et al., 2020)
* Finland	Advanced treatment	Adsorption	100	(Siipola et al., 2020)
* UK	Advanced treatment	Photocatalysis	97	(Lee et al., 2020)
* Sweden	Advanced treatment	Photocatalysis	65	(Uheida et al., 2021)
* China	Advanced treatment	Photocatalysis	10.23	(Zhou, Wang, et al., 2022)

---

### 2.3.2 Secondary treatment

The secondary treatment in WWTP relies on biological degradation, biological flocculation, precipitation, as well as chemical reactions between microorganisms and pollutants to remove contaminants from water (W. Tang et al., 2020). As presented in Table 1, the removal efficiencies of MPs in the secondary treatment ranged from 10.39 % to 100%. Compared to primary sedimentation, secondary sedimentation removed an average of 71.3% of fibers (Hidayaturrehman & Lee, 2019; Ruan et al., 2019).

The most widely used biological methods to date are activated sludge and biofilm methods (Falås et al., 2013). Activated sludge can adsorb pollutants, while microorganisms on activated sludge can degrade micropollutants, facilitating MPs removal (R. Chen et al., 2022; B. Zhang et al., 2023b). In addition to the conventional activated sludge process (CASP), there are many variants of the activated sludge process such as sequencing batch reactor (SBR), anaerobic/aerobic (A/O), and anaerobic/anoxic/aerobic (A/A/O), etc (Zhang et al., 2017). Among these methods, CASP, SBR, A/A/O, and membrane bioreactors (MBR) can effectively remove more than 90% of MPs, with efficiency ranging from 66.7% to 92.6%, 25.3% to 92%, and 15% to 93.7%, respectively. However, some methods, such as the A/O process, exhibit significantly lower performance, removing only around 16.9% of MPs from sewage (Jiang et al., 2020). On the other hand, Wei et al. found that combining the A/A/O process with constructed wetlands could achieve up to 100% removal efficiency (Wei et al., 2020).

The biofilm method, involving continuous flow of sewage through solid fillers, forms a sludge-like biofilm and has shown removal efficiencies of 50%-80% using bioreactors like bio-trickling filters, rotating bio-contractors, and bio-fluidized beds (Ali et al., 2021; Wang et al., 2019; Zhang, 2020). Both activated sludge and biofilm methods are based

on microbial degradation and aggregation technologies to treat pollutants and MPs (J. Yuan et al., 2020).

However, MPs could negatively impact the efficiency of activated sludge and biofilm methods (Tao et al., 2023; J. Xu et al., 2021). Oxygen in wastewater interacts with MPs active sites, generating reactive oxygen species and causing sludge particle degradation (Guan et al., 2020; Mu & Chen, 2011). Research indicates that high concentrations of specific MPs like PET-MPs reduce the production of extracellular polymeric substances (EPS) within sludge, impacting crucial acidogens and methanogens to affect the efficiency of sewage treatment (Zhang et al., 2020). Additionally, certain MP types, such as polyethersulfone resin (PES)-MPs and PA-MPs, inhibit nitrification and denitrification reactions, reducing wastewater treatment efficiency and increasing excess sludge production (Li et al., 2020; Zhao et al., 2020). Notably, 93% of the MPs removed by sewage treatment plants become entrained in sludge (Gies et al., 2018). Therefore, the integration of microbial methods into existing WWTP systems for MPs removal should not undermine the plant's primary wastewater treatment function. Besides, further research is necessary for effective sludge treatment to prevent MPs in dried sludge from re-entering the environment.

### **2.3.3 Advanced treatment**

Advanced (or tertiary) treatment in WWTPs aims for an advanced level of water purification, achieving higher quality effluent than the preceding secondary treatments (Sonune & Ghate, 2004). The main focus of tertiary treatments is on refining and polishing the effluent, making it suitable for specific uses like industrial water supply or safe in sensitive ecosystems. This advanced level of treatment has displayed the potential to reduce MPs concentration significantly. Studies have indicated that after tertiary treatment, the concentration of MPs in wastewater is reduced, ranging from 10.23 % to

100 % of the influent concentration on average. However, post-treatment effluents still commonly retain small-sized MPs, especially those measuring less than 190  $\mu\text{m}$  (Blair et al., 2019; Iyare et al., 2020; Patil et al., 2023; Z. Xu et al., 2021).

Various technologies, such as membrane filtration, MBR, advanced oxidation, dissolved air flotation, and activated carbon adsorption, are employed within tertiary treatments (Cheng et al., 2021). Such technologies, particularly MBRs, have demonstrated near-complete MPs removal, thus producing effluent with negligible MPs content (Lv et al., 2019; Talvitie, Mikola, Koistinen, et al., 2017). However, membrane clogging remains a primary concern, necessitating frequent backwashing, which, in turn, may release MPs back into the environment. Other filtration methods, including rapid sand and disc filters, face similar challenges of clogging and the associated need for periodic backwashing (Hidayaturrehman & Lee, 2019; Talvitie, Mikola, Koistinen, et al., 2017).

While tertiary treatment methods have shown promise, they do not consistently guarantee better MPs removal across different WWTPs. Mason et al. highlighted this inconsistency after investigating 17 distinct WWTPs in the United States (Mason et al., 2016). The study found no discernible correlation between tertiary treatment stages and MPs removal efficiency (Ziajahromi et al., 2017). For instance, advanced membrane technologies like reverse osmosis (RO), which theoretically boasts the smallest pore size, showed an underwhelming removal rate of just 2.8% (Cheng et al., 2021). Moreover, some bioactive filters were not only ineffective but counterproductive, with a reported negative removal rate of 72.7% (Talvitie, Mikola, Setälä, et al., 2017).

Such disparities in the reported efficiencies of tertiary treatments across different setups emphasize the need for further in-depth research. There is a particular emphasis on the removal of small molecule MPs, such as microbeads and fibers. Recognizing the



limitations of conventional tertiary treatments, some European nations like Sweden and Germany have pioneered the adoption of an additional fourth level of treatment. This step primarily revolves around the use of activated carbon filters and a synergistic blend of advanced oxidation technologies with granular activated carbon (GAC) to amplify MPs removal (Kosek et al., 2020). Future research efforts should focus on improving MPs removal, particularly for smaller MPs, to ensure the effectiveness of tertiary treatments in preventing MPs from entering natural water bodies.

#### **2.4 Existing and potential removal methods of MPs in drinking water treatment plants**

Drinking water treatment plants (DWTPs) are important in ensuring the supply of clean and safe water fit for human consumption. Conventional DWTPs methods focus on removing various pollutants, including suspended particles, heavy metals, and harmful microorganisms, from raw water sources (Shen et al., 2020). These plants employ a multifaceted approach, utilizing processes such as coagulation and flocculation, sedimentation, filtration, and clarification to achieve this goal (Sarkar et al., 2021).

Removing MPs in DWTPs is challenging due to their similar physical properties to other solids in water (Pivokonsky et al., 2018). This similarity makes it difficult to isolate and target MPs for their effective removal. Although the abundance of MPs can decrease after DWTP treatment, there is currently no specialized technology designed for the direct removal of MPs from drinking water. Additionally, there are no established legislative limits for MPs in drinking water (Novotna et al., 2019). Given the vital role of DWTPs in preventing the transfer of MPs from their sources to our taps, there is an urgent need to thoroughly explore both existing solutions and potential innovations aimed at removing MPs within these facilities.

The coagulation stage, a fundamental component of the drinking DWTPs process, utilizes the collective capabilities of coagulation, sedimentation, and filtration to efficiently eliminate impurities from raw water. At the core of this phase lies the mechanism through which MPs aggregate and precipitate, a transformation facilitated by the presence of coagulants and flocculants. Exploring both established and emerging technological tools, several options show significant potential in enhancing MPs removal during the coagulation process.

Coagulation-flocculation-sedimentation (CFS) is a widely used technique in DWTP and WWTP to remove suspended materials. This process involves the addition of coagulants that destabilize fine particles, allowing flocculants to aggregate them into larger, more easily removable clusters. Through this mechanism, CFS effectively aids in the elimination of small pollutants, colloidal substances, and dissolved MPs from water. However, the efficiency of this method can vary significantly due to several influencing factors, including the type and dosage of coagulants used, pH levels, and the specific morphology of the MPs present. Optimizing these parameters is crucial to ensuring consistent and effective removal of contaminants in water treatment processes.

Electrocoagulation (EC) is an advanced water treatment technique that leverages electrolysis to introduce coagulant agents into wastewater. By applying an electrical current through metal electrodes, metallic ions are released into the water, which act as coagulating agents that facilitate the aggregation and settling of MPs. This method is particularly effective in MP removal, as the metallic ions enhance the destabilization and binding of these particles. Additionally, EC offers several advantages over conventional coagulation methods, including a reduction in chemical usage and the potential to simultaneously remove multiple pollutants. Due to its efficiency and environmental

benefits, EC is considered a valuable complementary approach to traditional CFS processes in water treatment facilities.

Magnetization technology presents an innovative approach to MPs removal by introducing magnetic particles into the water, which subsequently bind with MPs to form magnetized conglomerates. Once these magnetized clusters are formed, a magnetic field can be applied to quickly and efficiently extract them from the water, streamlining the purification process. This technique is particularly advantageous due to its rapid action, high specificity, and ability to function effectively even in environments with high MPs concentrations. Furthermore, the use of magnetic separation reduces the reliance on chemical additives, making it a more environmentally friendly solution. As research advances, magnetization technology continues to show great promise in improving MPs removal in both drinking water and wastewater treatment applications.

Micro-machines, inspired by advancements in nanotechnology, are microscopic entities engineered to navigate through water sources to target and capture MPs. These tiny devices are designed to either bind with or trap MPs, allowing for their efficient transportation to designated extraction points within the treatment system. Their small size and high maneuverability make them particularly well-suited for operation in complex water matrices where traditional filtration methods may be less effective. Additionally, their specificity in targeting MPs enhances removal efficiency while minimizing unintended interactions with other waterborne substances. The integration of micro-machines into water treatment technologies represents a significant step forward in the ongoing quest for highly efficient and targeted MPs removal strategies.

Incorporating these advanced technologies into the coagulation stage of water treatment requires careful planning and optimization to ensure seamless integration and maximum efficiency. Each method presents unique advantages and operational

considerations that must be tailored to the specific characteristics of the water being treated. By strategically combining these approaches, water treatment facilities can enhance MPs removal while improving overall water quality. The continuous evolution of these technologies underscores the importance of innovation in addressing the challenges posed by microplastic contamination in drinking water sources. As research progresses, further advancements in these fields will likely lead to even more effective and sustainable solutions for water purification.

Rapid sand filtration (RSF), a pivotal process within DWTP, relies on natural substrates: quartz sand and anthracite (Pivokonsky et al., 2018). Current analyses highlight MPs removal efficiencies in DWTP via RSF as oscillating between 18.9% and 50.9% (Gao et al., 2022; Z. Wang et al., 2020). Noteworthy is the complete absence of small MPs (<10  $\mu\text{m}$ ) in treated effluents (Gao et al., 2022; Z. Wang et al., 2020). Specifically, removal efficacies observed for fibrous, spherical, and fragmented MPs have been demonstrated at 30.9%-49.3%, 23.5%-50.9%, and 18.9%-27.5%, respectively (Estahbanati et al., 2023). To date, RSF has been used in WWTP as a tertiary treatment to purge suspended particulates and a spectrum of aquatic biota (Reddy & Nair, 2022; Z. Xu et al., 2021). Within the WWTP settings, RSF shows a superior MPs removal prowess, achieving removal efficiency nearing 97%, plausibly attributed to the hydrophilic affinities between MPs and the sand matrix (Talvitie, Mikola, Koistinen, et al., 2017). Therefore, differences in MPs removal between DWTPs and WWTPs necessitate further research to elucidate influencing factors.

Nevertheless, to ensure long-term and stable performance, issues related to microbial colonization must be tackled. Persistent microbial colonization of filtration mediums, even in the face of rigorous cleaning protocols, can result in MPs-rich aggregate formation (Gülay et al., 2016). Such agglomerates pose a significant risk of RSF

obstruction, thereby affecting its MPs removal consistency. Although MPs adsorption to silica particles presents a pathway, the efficacy is inherently capped by the finite adsorptive capacity of these substrates (Z. Xu et al., 2021).

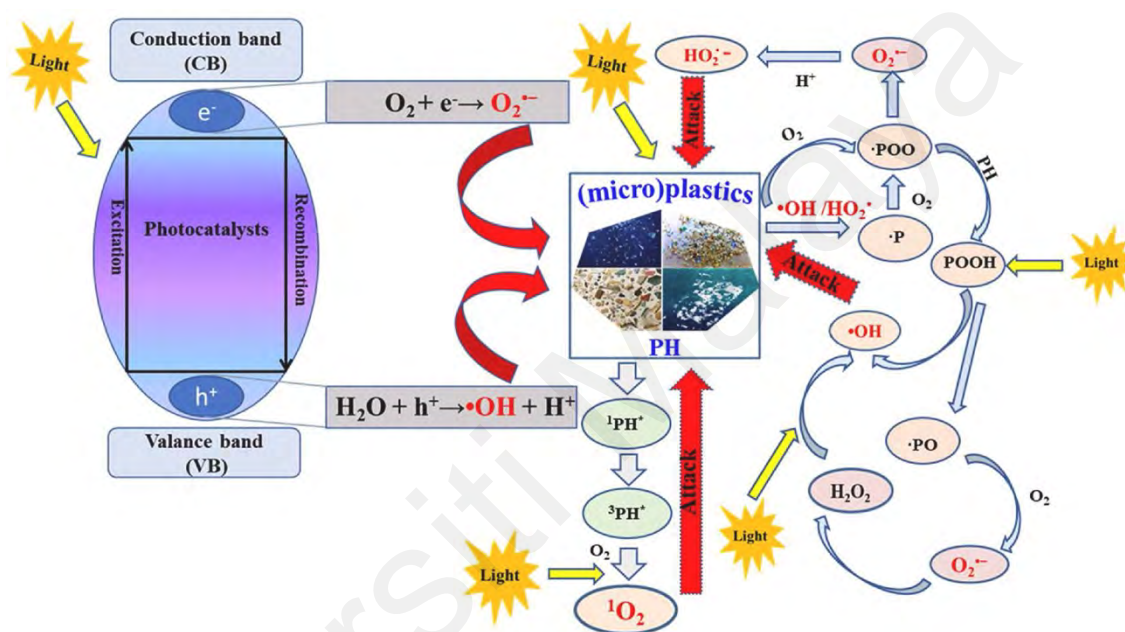
## **2.5 Existing and potential removal technologies for MPs in other water treatment processes**

While there are a range of technologies that exist to remove MPs in WWTP and DWTP as discussed above, alternative strategies such as constructed wetlands (CWs) and oil film separation present additional technologies for MPs removal. CWs, in particular, showcase impressive filtration capabilities. However, their effectiveness could be limited in areas with significant sewage inflows, and their widespread implementation might strain natural wetland ecosystems. Conversely, oil film separation stands out for its effectiveness, though its seamless integration into pre-existing water treatment frameworks poses its own set of challenges. As navigate the complexities of MPs contamination, the integration of CWs and oil film separation into comprehensive water treatment paradigms necessitates a nuanced understanding of regional contexts, the intrinsic properties of MPs, and potential unforeseen challenges.

## **2.6 Photocatalytic for water treatment**

To address the MPs pollution issue, photocatalytic oxidation appears to be one of the possible solutions. This process, which is efficient, long-lasting, and cost-effective, utilizes photooxidation to degrade MPs. Under light exposure, MPs undergo processes such as chain crosslinking, chain scission, and mineralization, ultimately transforming from large molecular polymers into smaller molecules like water and carbon dioxide. The introduction of a photocatalyst can accelerate this typically slow chemical reaction. As illustrated in Fig. 2.1, when a semiconductor material, capable of acting as a photocatalyst, is stimulated by light with energy equal to or greater than its bandgap, charge separation

occurs. Electrons ( $e^-$ ) from the valence band are elevated to the conduction band (Kusworo et al., 2022). This shift creates a band of positively charged holes ( $h^+$ ) in the valence band. These electrons and holes then react with water molecules, hydroxyl groups, and oxygen, generating hydroxyl radicals and superoxide reactive species that attack the polymer chains of MPs, leading to their rapid degradation into smaller molecular entities (Rodriguez-Narvaez et al., 2021).



**Fig. 2.1. Photocatalytic degradation mechanism (Ge et al., 2022).**

Li et al. synthesized a  $MoS_2/Cd_xZn_{1-x}S$  catalyst by combining  $CxZ_{1-x}S$  with  $MoS_2$ , aiming to leverage the synergistic benefits of enhanced charge separation efficiency, improved light absorption, and appropriate oxidation potential. This catalyst was used to generate hydrogen and degrade PET into small molecular organic compounds (Li et al., 2021). In another study, Uheida et al. employed zinc oxide nanorods as catalysts, achieving a reduction of more than 65% in the volume of PP microplastics after 456 hours of visible light exposure (Uheida et al., 2021). Additionally, Saifuddin et al. developed  $TiO_2@NC$  for the degradation of polypropylene (PP) globules, with results indicating that 1 mg of this catalyst could degrade 0.843 mg of PP within 400 hours (Saifuddin et al.,

2022). Lee et al. reported that PA66 microfibers exhibited a mass loss of 97% in 100 mg/L TiO<sub>2</sub> solution after 48 hours of irradiation with UCV (Lee et al., 2020). Zhou et al. synthesized Bi<sub>2</sub>O<sub>3</sub>@N-TiO<sub>2</sub> to degrade about 10.23 ± 1.91 wt % of polyethylene terephthalate at pH = 9 (Zhou, Wang, et al., 2022).

Several factors influence the efficiency of photocatalytic degradation, including catalyst porosity and surface area, as well as the crystallite structure and the presence of additives (Liu et al., 2022). Photocatalytic degradation of microplastics (MPs) primarily takes place on the surface of the catalyst; therefore, a greater contact area between the MPs and the catalyst generally results in higher degradation efficiency. The crystalline structure of the catalyst plays a significant role in determining the bandgap of the semiconductor, as quantum confinement and variations in carrier density can influence this property. Higher crystallinity tends to lower the bandgap, reducing the energy required for the excitation process (Domínguez-Jaimes et al., 2021). It is important to note that the performance of a single catalyst is often limited; however, the introduction of additives can enhance photocatalytic efficiency (Kamalian et al., 2020). Consequently, developing a cost-effective catalyst or composite catalyst is crucial for improving the photocatalytic degradation of MPs

## **2.7 PMR for MPs degradation**

Photocatalytic membrane reactors are currently categorized into four distinct configurations (Fig. 2.2): (a) a slurry photocatalytic reactor with an individual membrane unit, (b) a membrane submerged in a slurry photocatalytic reactor, (c) a submerged membrane in a TiO<sub>2</sub>-coated reactor, and (d) a photocatalytic membrane, such as a pure TiO<sub>2</sub> porous membrane or a TiO<sub>2</sub> composite membrane. Each configuration has unique advantages and limitations that influence its applicability in water treatment.

In the slurry photocatalytic reactor with an individual membrane unit (Fig. 2.2 (a)), the photocatalytic reaction occurs in a separate reactor before the treated water is passed through a membrane for filtration. This design allows efficient pollutant degradation but requires an additional separation step to recover suspended photocatalysts, which can complicate the operation. Similarly, in the submerged membrane configuration within a slurry photocatalytic reactor (Fig. 2.2 (b)), the membrane is directly immersed in the slurry, enabling simultaneous filtration and photocatalysis. However, the presence of suspended  $\text{TiO}_2$  particles can lead to membrane fouling and higher operational costs due to the need for catalyst recovery.

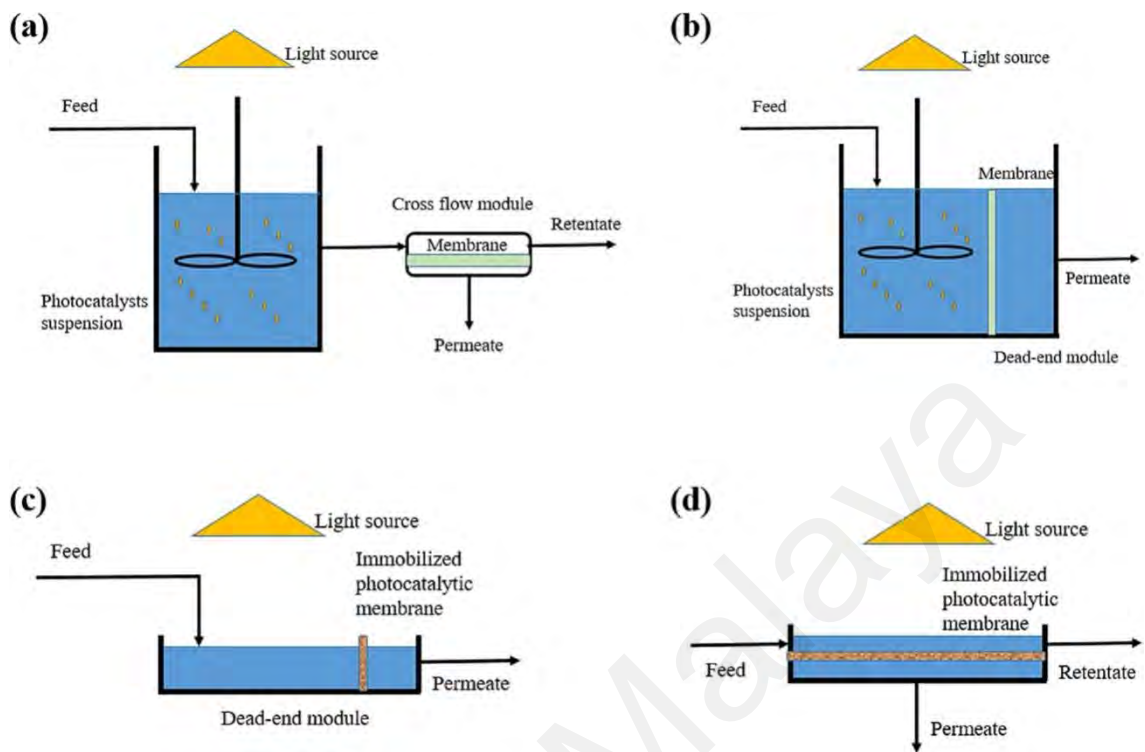
The third configuration, a submerged membrane in a  $\text{TiO}_2$ -coated reactor (Fig. 2.2 (c)), employs a membrane placed inside a reactor with immobilized  $\text{TiO}_2$ . This setup minimizes catalyst loss and simplifies operation, but the fixed photocatalyst layer may limit photocatalytic efficiency due to reduced surface area and light penetration. Finally, the photocatalytic membrane configuration (Fig. 2.2 (d)) integrates photocatalysis directly into the membrane structure using a  $\text{TiO}_2$ -coated or  $\text{TiO}_2$ -composite membrane. This approach offers several advantages, including simultaneous filtration and organic degradation, reduced membrane fouling, and enhanced antibacterial properties. It also eliminates the need for catalyst recovery and minimizes retentate pollution.

Moreover, photocatalytic membranes generally outperform conventional membranes by mitigating fouling and improving permeate quality. Membrane processes have gained prominence as effective water treatment technologies due to their compact design, high separation efficiency, and ease of maintenance. However, traditional membranes often suffer from fouling, where the accumulation of contaminants forms a cake layer, leading to pore blockage, reduced water flux, and increased operational costs. Additionally, conventional filtration mainly concentrates pollutants in the retentate, requiring further



treatment before disposal. In contrast, photocatalytic membrane processes actively degrade pollutants in the feed solution by generating reactive oxygen species under UV light exposure. This degradation reduces cake layer formation, minimizes pore blockage, lowers retentate pollutant concentration, and significantly improves permeate quality.

The efficacy of PMR systems is significantly influenced by parameters including pH, temperature, TiO<sub>2</sub> concentration, TMP, CFV, and hydraulic retention time (HRT). Previous research has indicated that the impact of pH on PMR performance is closely associated with the specific pollutants being treated (L. Chen et al., 2022; J. Zhang et al., 2023). Temperature influences PMR effectiveness by affecting the adsorption-desorption equilibrium between the catalytic membrane and the pollutants (Zheng et al., 2017). In addition, optimal photomineralization temperatures for PMRs are reported to be between 20 and 80 °C (Malato et al., 2009; Molinari et al., 2023). Consequently, this study did not further investigate the effects of pH and temperature on PMR performance.



**Fig. 2.2. Configurations of PMR. (a) slurry photocatalytic reactor with individual membrane unit, (b) membrane submerged in slurry photocatalytic reactor; (c) submerged membrane in  $\text{TiO}_2$  coated reactor; and (d) photocatalytic membrane.**

Zhang et al. investigated the rejection of Direct Black 168 using a  $\text{TiO}_2/\text{Al}_2\text{O}_3$  membrane under UV light at varying pH levels of wastewater. Their results showed that 82% of Direct Black 168 was removed after 300 minutes of UV irradiation with the  $\text{TiO}_2/\text{Al}_2\text{O}_3$  composite membrane (Zhang et al., 2006). Li et al. developed a submerged ceramic membrane photocatalytic reactor (SCMPR) specifically for photocatalytic degradation, which demonstrated high removal efficiency and stability for amoxicillin (AMX) degradation across a broad pH range, from 6.5 to 9.0 (Li et al., 2019). Vatanpour et al. reported the use of visible light in a submerged photocatalytic membrane reactor (PMR) equipped with flat-sheet PVDF MF membranes operating with an N- $\text{TiO}_2$  photocatalyst, achieving a decolorization efficiency of 84.2% during the decomposition

of Reactive Orange 29 (RO29) after 240 minutes (Vatanpour et al., 2019). Therefore, photocatalytic membrane reactors show great promise for practical applications in wastewater treatment, particularly for wastewater containing micropollutants such as microplastics, microplastic fibers, and even nanoplastics.

Photocatalytic degradation is an advanced oxidation process that efficiently degrades MPs into smaller molecules through photocatalytic reactions. When a semiconductor photocatalyst, such as  $\text{TiO}_2$  or zinc oxide ( $\text{ZnO}$ ), absorbs light energy equal to or greater than its bandgap, it generates electron-hole pairs. These reactive species interact with oxygen and water to produce hydroxyl radicals and superoxide anions, which break down polymer chains via chain scission, crosslinking, and mineralization into  $\text{CO}_2$  and  $\text{H}_2\text{O}$ .

Photocatalytic membranes integrate membrane filtration with photocatalytic oxidation, enhancing pollutant removal efficiency while minimizing membrane fouling. These membranes typically incorporate photocatalysts like  $\text{TiO}_2$ ,  $\text{ZnO}$ , or  $\text{BiVO}_4$  into polymeric or ceramic supports. Upon light activation, reactive oxygen species (ROS) generated on the membrane surface degrade organic pollutants, including MPs, while simultaneously filtering suspended particles. However, challenges such as catalyst leaching, membrane fouling, and limited visible-light absorption necessitate further research to enhance the durability and efficiency of photocatalytic membranes.

The efficiency of photocatalytic reactors is influenced by several operational parameters. Light intensity and wavelength directly affect catalyst activation, with UV and visible-light-responsive photocatalysts demonstrating varying degradation efficiencies. The catalyst dosage plays a critical role, as excessive loading can lead to agglomeration, reducing the active surface area and photon penetration. Reaction temperature and pH also impact photocatalytic activity, influencing charge carrier dynamics and radical formation. Additionally, the presence of competing contaminants,

such as natural organic matter and heavy metals, can interfere with MPs degradation by scavenging reactive species. Optimizing these factors is crucial for achieving high degradation rates in large-scale water treatment applications.

Table 2.2 presents a comparative analysis of various photocatalytic methods used for degrading polyester-based MPs. It categorizes degradation based on polymer shape (fragments, fibers, or powder) and the photocatalysts used. The degradation rates vary significantly, with catalysts like Pt@N-TiO<sub>2</sub>-1.5% powder achieving the highest degradation rate (28.96%). The combination of photocatalysis with membrane separation also enhances degradation efficiency. Overall, the table highlights the impact of different catalysts and methods on MPs degradation, showcasing the potential of advanced oxidation processes for wastewater treatment.

**Table. 2. 2. Photocatalytic performance comparison**

<b>Polyester shape</b>	<b>Degradation method</b>	<b>Catalyst</b>	<b>Degradation rate (%)</b>	<b>Ref</b>
fragment	Photocatalysis	TiO <sub>2</sub> /MIL-100 (Fe) in fine mesh	-	(Rojas-Guerrero et al., 2023)
fiber	Photocatalysis	Ni <sub>5</sub> P <sub>4</sub> /TiO <sub>2</sub> /C nanofilm	6.23	(Peng et al., 2023)
fiber	Photocatalysis	Bi <sub>2</sub> O <sub>3</sub> @N-TiO <sub>2</sub> powder	10.23	(Zhou, Wang, et al., 2022)
fiber	Photocatalysis + membrane separation	TiO <sub>2</sub> + MF/UF membrane	13.52	(Poerio et al., 2024)
-	Photocatalysis	Fe <sub>3</sub> O <sub>4</sub> @SiO <sub>2</sub> powder	13.65	(Blanco-Gutiérrez et al., 2022)
powder	Photocatalysis	C,N-TiO <sub>2</sub> /SiO <sub>2</sub> powder	16.22	(Ariza-Tarazona et al., 2023)
fiber	Photocatalysis	Pt@N-TiO <sub>2</sub> -1.5% powder	28.96	(Zhou, Luo, et al., 2022)

## 2.8 Summary of literature review

The literature review highlights the significant environmental threat posed by MPs fiber, particularly those released through household laundry wastewater. With synthetic fibers like polyester, nylon, and polyacrylonitrile constituting a major portion of global fiber production, the problem of MPs pollution is extensive and pervasive. The review demonstrates that Asia, with its rapidly expanding demand for synthetic fabrics, is a notable contributor to this issue, particularly through laundry processes. Research consistently shows that these fibers are a dominant form of MPs in the environment, and their release during washing poses a severe challenge to WWTP.

Analytical techniques for detecting and characterizing MPs in wastewater have evolved, addressing the complexities introduced by the aging and deformation of MPs during their migration in water systems. Techniques like SEM, DLS, FTIR, and RS have been instrumental in advancing our understanding of MPs. However, each technique has its limitations, particularly when distinguishing MPs from other particles or when dealing with very small MPs. The use of advanced methods, such as SERS and Raman tweezers, represents significant progress in this field, allowing for more precise identification and quantification of MPs in complex environments.

The review also examines the effectiveness of existing and potential removal methods for MPs in WWTPs. It is clear that while conventional primary, secondary, and tertiary treatments were not designed with MPs in mind, they still contribute to significant reductions in MP concentrations. The effectiveness of these treatments varies widely, influenced by factors such as MP characteristics and regional differences in treatment technologies. Primary treatments, such as grids, grit chambers, and sedimentation tanks, show varying degrees of success, while secondary treatments like activated sludge and biofilm methods offer more consistent results. Advanced treatments, particularly

membrane-based technologies, show promise in further reducing MPs but face challenges such as membrane fouling and inconsistent performance across different WWTPs.

In addition to WWTPs, the review considers the role of DWTPs in managing MPs. While conventional DWTP processes are effective in removing various pollutants, they struggle with MPs due to the physical similarities between MPs and other suspended solids. The potential integration of emerging technologies, such as electrocoagulation, magnetization, and micro-machines, into existing DWTP processes, could enhance MPs removal, but these approaches require further research and development.

Finally, the review explores photocatalytic methods as a promising approach for MP degradation. Photocatalytic oxidation, especially when enhanced by catalysts like  $\text{TiO}_2$ , offers a cost-effective and efficient solution for breaking down MPs into smaller, less harmful molecules. The development of PMR represents a significant advancement, combining physical separation with catalytic degradation in a single unit. These reactors not only improve MPs removal but also address common issues such as membrane fouling, making them a viable option for future wastewater treatment strategies.

In summary, the literature review underscores the complexity and scale of the MPs pollution problem, particularly in the context of laundry wastewater. It also highlights the ongoing advancements in detection, characterization, and removal technologies, while identifying areas where further research is needed. The review also highlights the persistence of MPs in wastewater treatment plants (WWTP) and drinking water treatment plants (DWTP), emphasizing that current treatment methods do not fully remove MPs. This highlights the necessity for advanced treatment technologies like  $\text{TiO}_2$ -based photocatalytic membrane reactor.

Current wastewater treatment methods, such as membrane filtration (MBR, ultrafiltration), coagulation-flocculation, adsorption, and conventional oxidation processes, face limitations like membrane fouling, incomplete removal of small MPs, high operational costs, and potential secondary pollution. While MBRs achieve high removal efficiency (up to 99.9%), they only separate MPs without degrading them. Adsorption is effective but costly, and coagulation requires excessive chemical use. In contrast, a photocatalytic membrane reactor (PMR) with  $\text{TiO}_2$  as a photocatalyst not only removes but fully degrades MPs into  $\text{CO}_2$  and water, eliminating pollution at its source.  $\text{TiO}_2$  was selected due to its strong oxidative power, chemical stability, non-toxicity, low cost, and ability to be activated under UV light, making it ideal for environmental applications. It operates with minimal chemical additives, integrates well with existing treatment systems, and can utilize solar energy, making it an efficient, sustainable, and scalable solution. Unlike filtration, which simply traps MPs, PMR with  $\text{TiO}_2$  ensures complete mineralization, addressing the root cause of microplastic pollution in laundry wastewater.

## CHAPTER 3: MATERIALS AND METHODS

### 3.1 Flowchart of the study

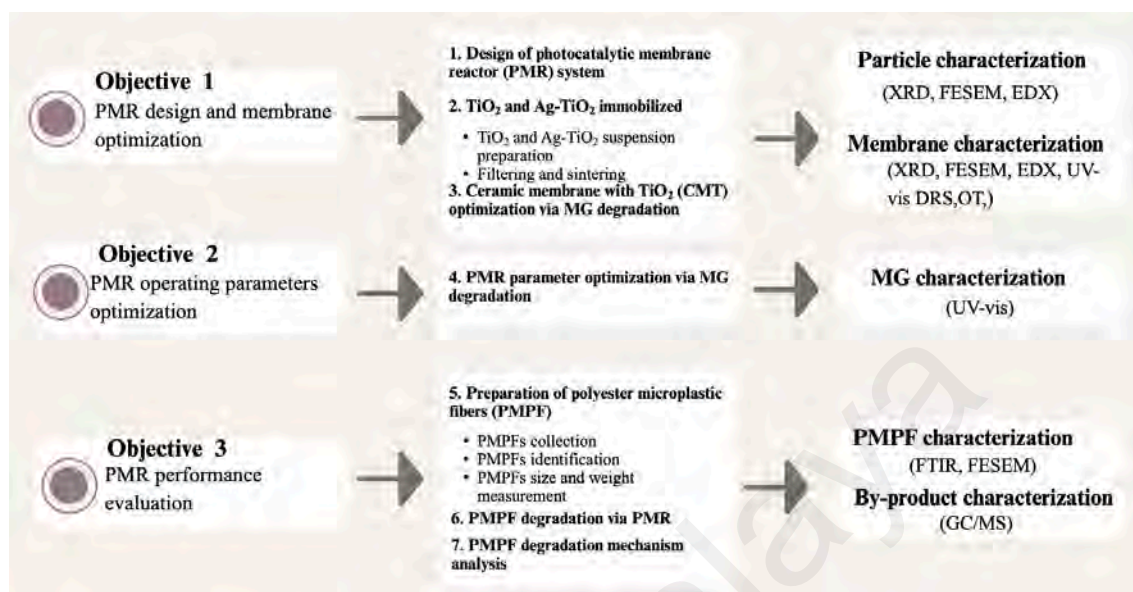


Fig. 3.1. Flow chart of the study

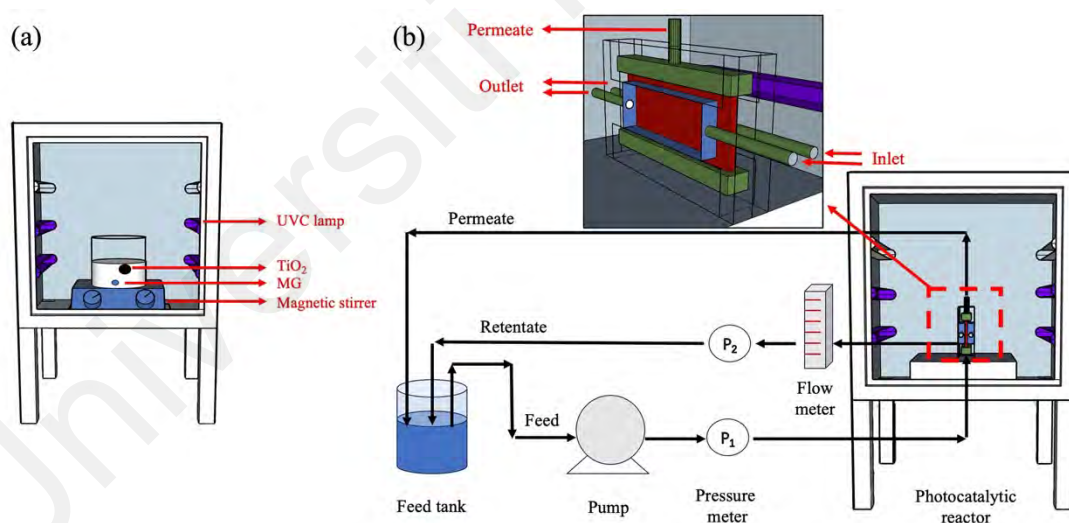
### 3.2 Materials

The flat-sheet alumina (Al<sub>2</sub>O<sub>3</sub>) ceramic membrane (pore size 0.1 μm, thickness 6 mm) was supplied by Shandong Guiyuan New Material Co., Ltd., China. The TiO<sub>2</sub> photocatalyst (purity-99.5%) and silver nitrate (purity-99.5%) were obtained from Sigma-Aldrich. Additionally, dimethyl sulfoxide (DMSO, purity ≥ 99.9%), 95-97% sulfuric acid (H<sub>2</sub>SO<sub>4</sub>), malachite green (MG) and sodium chloride (NaCl, 99.5% purity) were obtained from Merck. Garments composed of 100% polyester were purchased from fashion stores in Malaysia. Distilled water, simulated-PMPF, and real-PMPF were prepared in-laboratory for experimental use. It is worth noting that the polyester garments contained minimal impurities due to their intended use in industrial manufacturing rather than laboratory studies.



### 3.3 Photocatalytic reactors

This study employed two types of photocatalytic reactors: a sludge photocatalytic reactor (SPR) and a scalable PMR. The SPR, detailed in Fig. 3.1 (a), consists of a 2 L beaker as a feed tank, a magnetic stirrer (IKA RCT basic), four UVC lamps (Philips T5 8 W,  $\lambda_{\max} = 254$  nm), and a custom-made stainless-steel box. The immobilized-PMR, designed for practical wastewater treatment application and illustrated in Fig. 3.1 (b), features a crossflow system and includes (i) a glass feed tank, (ii) a peristaltic pump (Watson-Marlow 300 series), (iii) two pressure meters, (iv) a flow meter, (v) a stainless-steel box, (vi) four UVC lamps (similar to the ones used in SPR), (vii) self-made photocatalytic modules (quartz), and (viii) a flat-sheet ceramic photocatalytic membrane (effective area:  $2 \times 24$  cm<sup>2</sup>). The module is centrally positioned within the box, equidistant (15 cm) from the lamps on either side.



**Fig. 3.2. Laboratory-scale (a) sludge photocatalytic reactor (SPR) and (b) PMR system.**

### 3.4 Preparation of photocatalytic membrane

To obtain the homogeneous TiO<sub>2</sub> size (0.1-10  $\mu$ m), the powder is ball-milled at 400 rpm for 30 min. A 10 mg/L TiO<sub>2</sub> suspension is prepared by adding 10 mg of TiO<sub>2</sub> in 1 L

distilled water, followed by sonication at 50 kHz for 30 min to uniformly disperse the catalyst particles. This suspension was applied to the ceramic membrane surface via crossflow filtration at a crossflow flow velocity (CFV) of 50 cm<sup>3</sup>/min, a transmembrane pressure (TMP) of 0.8 bar, and a filtration duration of 10 minutes. The resultant membrane with 5 mg TiO<sub>2</sub>, termed CMT<sub>5</sub>, was dried overnight at 50 °C and then calcined at 400°C for 4 hours (10 °C/min heating rate), followed by natural cooling. Additional membranes with 20, 50, 100 mg TiO<sub>2</sub> were marked as CMT<sub>20</sub>, CMT<sub>50</sub>, and CMT<sub>100</sub>, respectively. The original alumina membrane, i.e. without TiO<sub>2</sub> catalyst, is labeled CMT<sub>0</sub>. The total catalyst mass on each membrane was quantified by measuring the turbidity change in the TiO<sub>2</sub> suspension pre- and post-filtration.

TiO<sub>2</sub> (100 mg) and AgNO<sub>3</sub> (1.57 mg) were then sonicated in 1 L of distilled water (50 kHz, 0.5 h), stirred continuously for 24 h under UVC exposure to fabricate the Ag-decorated TiO<sub>2</sub> (Ag-TiO<sub>2</sub>) suspension. The catalyst immobilization on the membrane surface was achieved through crossflow filtration with specific parameters: CFV at 50 cm<sup>3</sup>/min, TMP at 0.8 bar, and a 10 min filtration time. After overnight drying at 50 °C and calcination at 400 °C for 4 h, the photocatalytic membrane was cooled naturally. The turbidity method was employed to measure the catalyst mass loss in the mixture, indicating the amount of Ag-TiO<sub>2</sub> immobilized on the membrane.

Further MG degradation experiments involved Ag-TiO<sub>2</sub> catalysts prepared by incorporating 0.1, 1, and 10 wt.% Ag onto the TiO<sub>2</sub>. The Ag-TiO<sub>2</sub> membrane with 1 wt.% Ag displayed the most effective degradation, aligning with previous research demonstrating optimal photocatalytic activity at this concentration (Anan et al., 2021; Leong et al., 2014; Ma et al., 2009; J. R. Mishra et al., 2021). Therefore, this study only fabricated the 1 wt.% Ag-TiO<sub>2</sub> membrane to further evaluate the removal and degradation efficiency for PMPF.

### 3.5 Preparation of PMPF

Real-PMPF were collected from actual laundry wastewater using the process outlined in Fig. 3.2 (a). The washing machine was operated on a 15 min cycle with 24 L of water, using 10 ml detergent for a single washing. An empty cycle preceded each wash to minimize interference. Wastewater generated from various stages (i.e. wash, rinse, and spin) of a single cycle was mixed. Contact equipment was rinsed with distilled water, and the rinsing water was added to the laundry wastewater before filtering by 0.1  $\mu\text{m}$  filter paper. This actual laundry wastewater and real-PMPF collection process was repeated three times.

Simulated-PMPF were prepared as shown in Fig. 3.2 (b). Polyester clothing was cut into small fragments ( $< 1\text{ cm}$ ) and then shredded into fibers ( $< 5\text{ mm}$ ) using a blender. These fibers were treated in DMSO at  $90\text{ }^\circ\text{C}$  for 15 minutes to remove dyes, followed by washing with ethanol and air-drying. To further reduce fiber size, 10 g of NaCl was mixed with the colorless fibers and processed in a blender. Finally, the mixture was then transferred to distilled water to dissolve the NaCl, and the resulting fibers were filtered to obtain simulated-PMPF with sizes  $< 1000\text{ }\mu\text{m}$ .

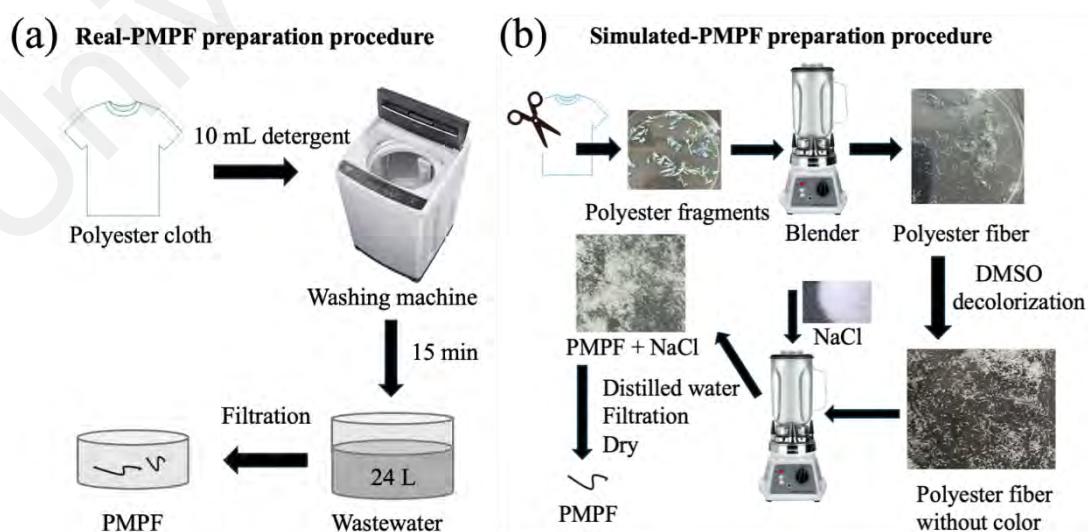


Fig. 3.3. The preparation procedure of (a) real-PMPF and (b) simulated-PMPF.

### 3.6 Photocatalytic experiments

#### 3.6.1 PMR optimization via MG degradation

Malachite green (MG) was chosen as the target pollutant for this study since it is a well-established pollutant for evaluating the catalytic performance of different catalysts (Jose et al., 2023; C. Zhang et al., 2022). In this study, there were two PMR systems investigated and compared: TiO<sub>2</sub> in suspension (TIS-PMR) and TiO<sub>2</sub> immobilized on the membrane (TIM-PMR). Accordingly, three different experiments were conducted using SPR and two types of PMR systems, respectively. Besides, all the experiments were conducted at room temperature (25 ± 2 °C).

Each experiment began with filling the feed tank with 1 L of a 5 mg/L MG solution. In the cases of the SPR and TIS-PMR, TiO<sub>2</sub> suspension was mixed with the MG solution in the feed tank. This mixture was stirred for 30 min in darkness to ensure adsorption/desorption equilibrium before proceeding with the experiment. Similarly, the TIM-PMR system was run in the dark for 30 min to allow the TiO<sub>2</sub> on the photocatalytic membrane and the MG in the solution to reach adsorption/desorption equilibrium. The crossflow parameters for TIS-PMR and TIM-PMR were maintained consistently. In both systems, the MG solution circulated from the feed tank (shielded by tin foil) to the sump on either side of the module, facilitating the photocatalytic reaction. The retentate and permeate were recirculated to the feed tank to maintain a constant solution volume. The reaction duration was 4 h, with hourly sample collection from the feed tank to assess MG degradation performance and membrane fouling in the PMR setups.

The photocatalytic degradation efficiency of MG was calculated by Eq (1):

$$\text{MG Photocatalytic degradation rate} = (C_0 - C_t) / C_0 \times 100\% \quad (1)$$

Where  $C_0$  ( $\text{mg L}^{-1}$ ) is the initial MG concentration and  $C_t$  ( $\text{mg L}^{-1}$ ) is the MG concentration after  $t$  hour irradiation, respectively.

Membrane permeate flux ( $J$ ) was calculated by Eq (2):

$$\text{The membrane permeate flux} = V / (A \times \Delta t) \quad (2)$$

Where  $V$  (L),  $A$  ( $\text{m}^2$ ), and  $\Delta t$  (h) represent the volume of permeate, effective filtration area, and permeation time, respectively.

Furthermore, the stability of MG in darkness was confirmed. The pure MG solution in the feed tank, without  $\text{TiO}_2$ , exhibited less than a 5% change in MG concentration after 4 h under UVC light, indicating the stability of MG under these irradiation conditions.

### 3.6.2 Simulated-PMPF elimination experiments

The effectiveness of simulated-PMPF elimination was evaluated in terms of both degradation and rejection rates as the indicators of simulated-PMPF elimination, leveraging the combined photocatalytic and membrane separation capabilities of the immobilized-PMR. Specifically, simulated-PMPF was suspended in 1 L of distilled water to prepare the feed solution. The crossflow system was set to a CFV of 100 mL/min and a TMP of 0.2 bar and operated for 1 h in the dark to ensure adsorption/desorption equilibrium. Water samples were collected from both the feed and permeate at 12 h intervals over a 48 h UVC photodegradation experiment. Following collection, simulated-PMPF was filtered from the solution, air-dried, and analyzed.

Simulated-PMPF concentrations were measured in the feed tank at 0, 12, 24, 36, and 48 hours of UVC irradiation. UV-vis spectroscopy showed a distinct absorbance signal at 266 nm for simulated-PMPF dissolved in  $\text{H}_2\text{SO}_4$ . To quantify the concentration, absorbances of simulated-PMPF (0, 2, 4, 6, 8, and 10 mg) in 10 mL of 10 M  $\text{H}_2\text{SO}_4$  were

measured to construct a calibration curve. The degradation rate was calculated using the following Equation. (1):

$$\text{PMPF Photocatalytic degradation rate} = (C_0 - C_t)/C_0 \times 100\% \quad (3)$$

where  $C_0$  (mg/L) and  $C_t$  (mg/L) represents the initial concentration of simulated-PMPF and concentration of simulated-PMPF after the photocatalytic degradation in feed.

Since the concentration of simulated-PMPF in the permeate was too low for accurate quantification by UV-vis spectroscopy after the photocatalytic reaction, turbidity measurements were used instead. The turbidity method also provided better accuracy for real-PMPF due to the high level of impurities in laundry wastewater. The rejection rate of membranes was calculated using Equation. (2):

$$\text{Rejection rate} = (1 - C_p/C_f) \times 100\% \quad (4)$$

Where,  $C_p$  and  $C_f$  are the concentrations of simulated- and real- PMPF in the permeated and feed.

### **3.7 Characterization of membranes and microplastics**

The surface morphology of the photocatalytic membranes and PMPF was analyzed using field emission scanning electron microscopy (FESEM, AURIGA, ZEISS, USA) to examine structural characteristics, while energy dispersive X-ray spectroscopy (EDS, GENESIS APEX4, USA) identified the elemental composition. Membrane samples were cut into small sections ( $5 \times 5$  mm), mounted on carbon tape, and sputter-coated with gold or platinum if necessary. Imaging was performed at an accelerating voltage of 2–10 kV in secondary electron mode, while EDS analysis operated at 10–20 kV for elemental mapping.

The chemical composition of the membranes was confirmed through powder X-ray diffraction (XRD, Japan) using a Rigaku SmartLab diffractometer. The optical properties of the photocatalytic membranes were assessed by UV-visible diffuse reflectance spectroscopy (DRS, USA) using a Perkin Elmer Lambda 750 spectrometer. Contact angle of membranes are measured by Contact Angle Measurement (Attension Theta, Sweden).

The crystalline structure of the membranes was confirmed using powder XRD with a Rigaku SmartLab diffractometer. Dried membrane samples were ground into fine powder and placed on a silicon or glass holder. The analysis was conducted using Cu K $\alpha$  radiation over a scanning range of 5°–80° (2 $\theta$ ) with a step size of 0.02° and a scan speed of 1°/min. XRD patterns were compared with standard databases to identify TiO<sub>2</sub> phases.

The optical properties of the photocatalytic membranes were assessed using UV-visible DRS with a Perkin Elmer Lambda 750 spectrometer. Samples were mounted on a BaSO<sub>4</sub>-coated holder, and reflectance was measured over a 200–800 nm wavelength range. The Kubelka-Munk function was applied to estimate bandgap energy and evaluate light absorption efficiency.

Membrane wettability was examined through contact angle measurements using an Attension Theta goniometer. Small membrane pieces (2 × 2 cm) were cleaned and placed on a flat surface before depositing a 2–5  $\mu$ L water droplet. The contact angle was determined using image analysis software, with multiple measurements taken to ensure accuracy. These characterization techniques provided crucial insights into membrane morphology, composition, optical behavior, and surface properties, contributing to performance optimization.

Fourier transform infrared spectroscopy combined with the attenuated total reflectance (FTIR-ATR, FTIR-Spectrum 400, Perkin Elmer, USA) was employed to identify

chemical changes in polyester fibers before and after degradation, providing insights into the degradation process. Additionally, gas chromatography-mass spectrometry (GC/MS, Shimadzu, GCMS-QP 2010 Plus, Japan) was used to demonstrate the effective photocatalytic degradation of simulated-PMPF and to further analyze the by-products after the reaction. Helium (He) was used as the carrier gas at a flow rate of 1.81 mL/min. The GC oven program initiated at 50 °C for 5 min, then increased to 320 °C at a rate of 5 °C/min. The injector temperature was maintained at 320 °C, operating in split mode with a split ratio of 1:60. The pyrolysis products were analyzed using a single quadrupole mass spectrometer with an ion source temperature of 230 °C. Mass data acquisition was performed in electron ionization (EI) positive mode at 70 eV, with a mass-to-charge ratio (m/z) range of 29 - 600 and a scan speed of 1250 u/s.

The reusability of the photocatalytic membranes was assessed by subjecting them to five consecutive cycles of MG degradation experiments. After each cycle, the membranes were carefully washed with deionized water and dried at 60°C before reuse to remove any residual dye or surface contaminants. The photocatalytic performance was evaluated by measuring the degradation efficiency of MG after each cycle using UV-visible spectroscopy. The stability and efficiency retention of the membranes over multiple cycles provided insights into their durability and long-term applicability in wastewater treatment.

Porosity and pore size distribution were analyzed to evaluate membrane filtration properties. The membrane porosity (%) was determined using the gravimetric method, where dry and wet membrane weights were measured before and after soaking in deionized water. The porosity was calculated using the equation:

$$\text{Porosity (\%)} = (W_w - W_d) / \rho_w V \times 100$$



where  $W_w$  and  $W_d$  are the wet and dry membrane weights,  $\rho_w$  is the water density, and  $V$  is the membrane volume.

Pore size distribution was analyzed using FESEM. FESEM images were processed using image analysis software to estimate pore size distribution. These analyses provided critical insights into membrane permeability, filtration efficiency, and potential fouling resistance.

Universiti Malaya

## CHAPTER 4: RESULTS AND DISCUSSION

### 4.1 Characterization, photocatalytic performance, and optimization for Al<sub>2</sub>O<sub>3</sub> ceramic membrane with TiO<sub>2</sub> (CMT) membranes in immobilized-PMR

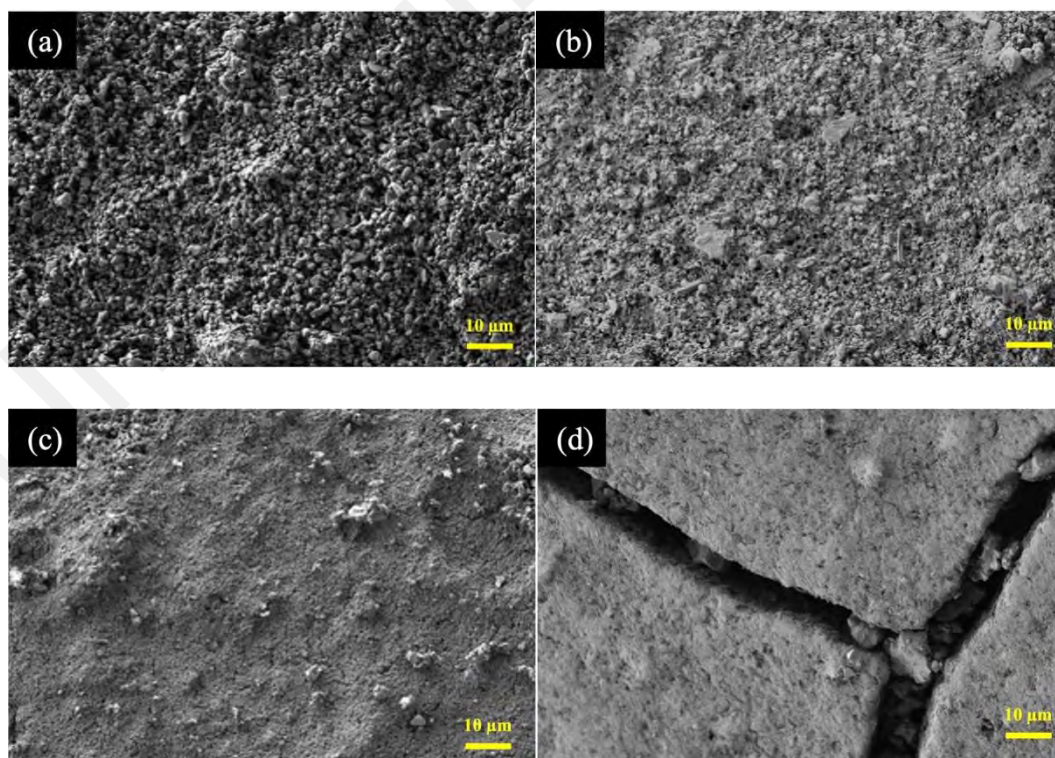
#### 4.1.1 Characterization of CMT membranes

The characterization of photocatalytic membranes is pivotal, particularly because photocatalytic reactions largely occur on the solid surface (Sivaranjani et al., 2022). FESEM was used to examine the morphology of the unmodified ceramic membrane and the TiO<sub>2</sub>-modified photocatalytic membrane. Given that both sides of the membrane showed similar morphologies, this study presents the characteristics of only one side. Fig. 4.1 (a) depicts the surface of the unmodified Al<sub>2</sub>O<sub>3</sub> ceramic membrane, i.e. CMT<sub>0</sub>, characterized by complex-shaped, irregularly distributed pores. This indicates a typical, highly porous, asymmetric structure characteristic of ceramic membranes without noticeable surface defects, suggesting their suitability as high-quality support layers (Yang & Tang, 2018). In addition, Al<sub>2</sub>O<sub>3</sub> is an insulator that can trap photogenerated electrons and prevent their transfer from TiO<sub>2</sub> particles to the interface with the fluid, resulting in a high photocatalytic activity due to a reduced recombination rate of electrons (Deba et al., 2023). These justifications imply that the Al<sub>2</sub>O<sub>3</sub> ceramic membrane used in this study is a potential excellent substrate for photocatalytic membranes.

Fig. 4.1 (b-d) presents the surface morphology of the photocatalytic membranes, namely CMT5, CMT50, and CMT100. TiO<sub>2</sub> amount increases from 5 mg to 50 mg, the catalytic membranes performance gradually improves. However, further increases beyond 50 mg led to a decline in performance. Therefore, CMT50 serves as a critical inflection point, making it a significant focus for further research rather than CMT20.

All catalytic membranes are coated with spherical particle clusters and marginally larger particles, indicating successful TiO<sub>2</sub> deposition. These membranes exhibit a rough

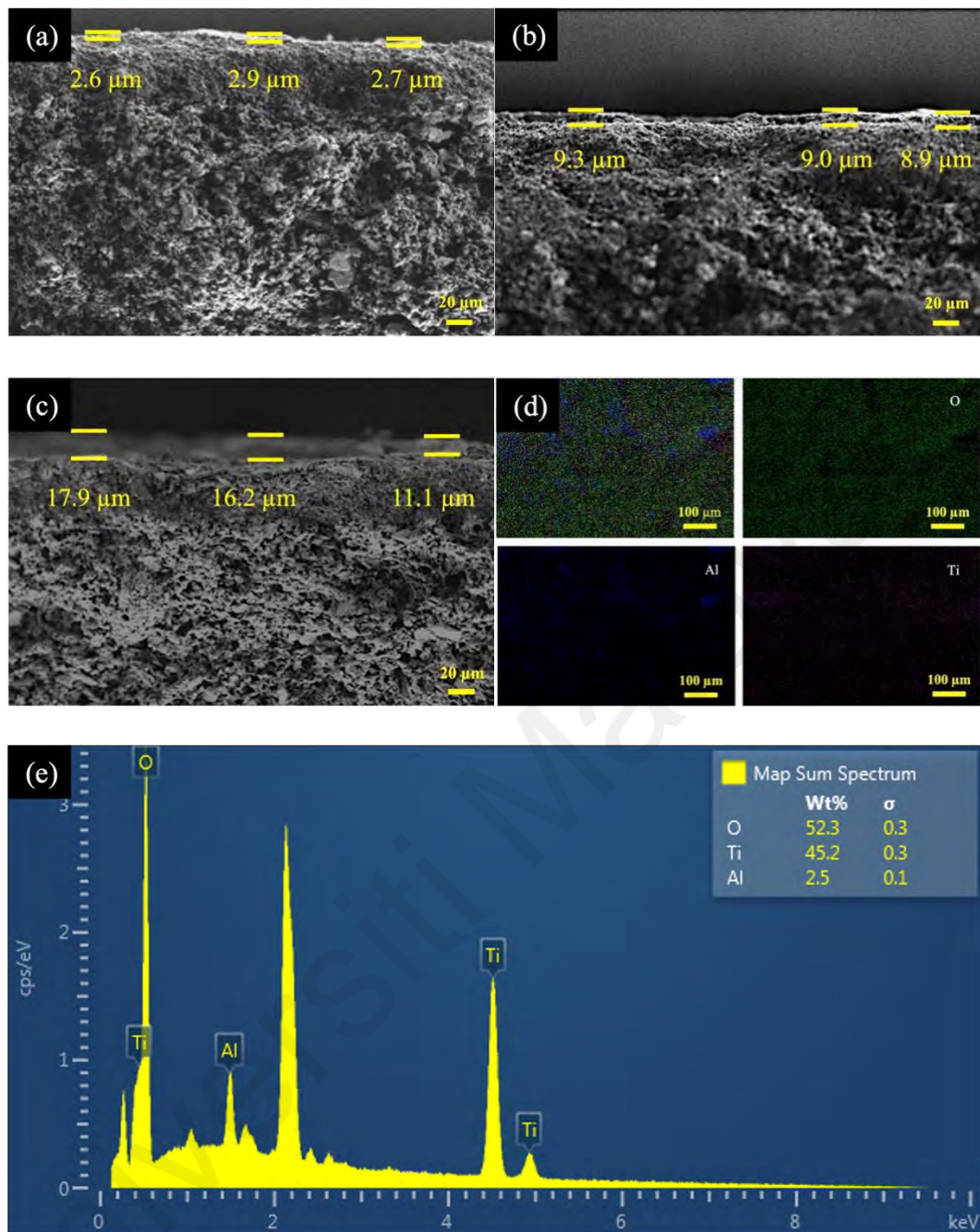
surface texture due to the heterogeneity in size and distribution of particle clusters, implying a great specific surface area favorable for photocatalytic performance. Furthermore, as the  $\text{TiO}_2$  content on top of the membrane increases, these membranes display a denser photocatalytic layer, potentially enhancing their rejection performance at the expense of reduced flux. A critical observation is the identification of a loading threshold, which was around 50 mg, beyond which the  $\text{CMT}_{100}$  membrane shows surface cracking of the catalyst layer upon heat treatment. This phenomenon is attributed to mechanical stresses induced by the thick porous layer during the heating process (Molinari et al., 2021). Consequently, forming a stable photocatalytic layer with over 100 mg of  $\text{TiO}_2$  may prove challenging. While existing studies suggest that lower heating rates during membrane fabrication might mitigate stress caused by differential thermal expansion between the support and  $\text{TiO}_2$  layer (Alem et al., 2009; Fan et al., 2000), this aspect was not investigated in the current study.



**Fig. 4.1. FESEM surface images of (a)  $\text{CMT}_0$ , (b)  $\text{CMT}_5$ , (c)  $\text{CMT}_{50}$ , and (d)  $\text{CMT}_{100}$ .**

The cross-sectional morphology images were instrumental in estimating the thickness of the layers. As illustrated in Fig. 4.2 (a-c), the thickness of the TiO<sub>2</sub> layers increased from 2.6 to 17.9 μm with the increase of TiO<sub>2</sub> loading. These images also substantiated the formation of the TiO<sub>2</sub> skin layer on the photocatalytic membranes. Existing research suggests a minimal correlation between membrane thickness and permeability, indicating that these modifications could potentially enhance retention and shear resistance without adversely impacting the permeate flux (Ahmad et al., 2020).

EDS surface mapping of elements aluminium (Al), oxygen (O), and titanium (Ti) was employed to verify the composition of the layer. Fig. 4.2 (d) displays a homogeneous Ti, O, and Al atoms distribution. From Fig. 4.2 (e), the weight ratio of the elements is shown as 52.3% O, 2.5% Al, and 45.2% Ti. The relatively low percentage of Al can be attributed to minimal exposure of Al, overshadowed by the extensive coverage of TiO<sub>2</sub>. These findings corroborate the successful loading of TiO<sub>2</sub> onto the surface of the alumina membrane, aligning well with observations from FESEM. These findings clearly indicate that the surface coating behaviour of ceramic membranes can be effectively modulated by adjusting the TiO<sub>2</sub> content.

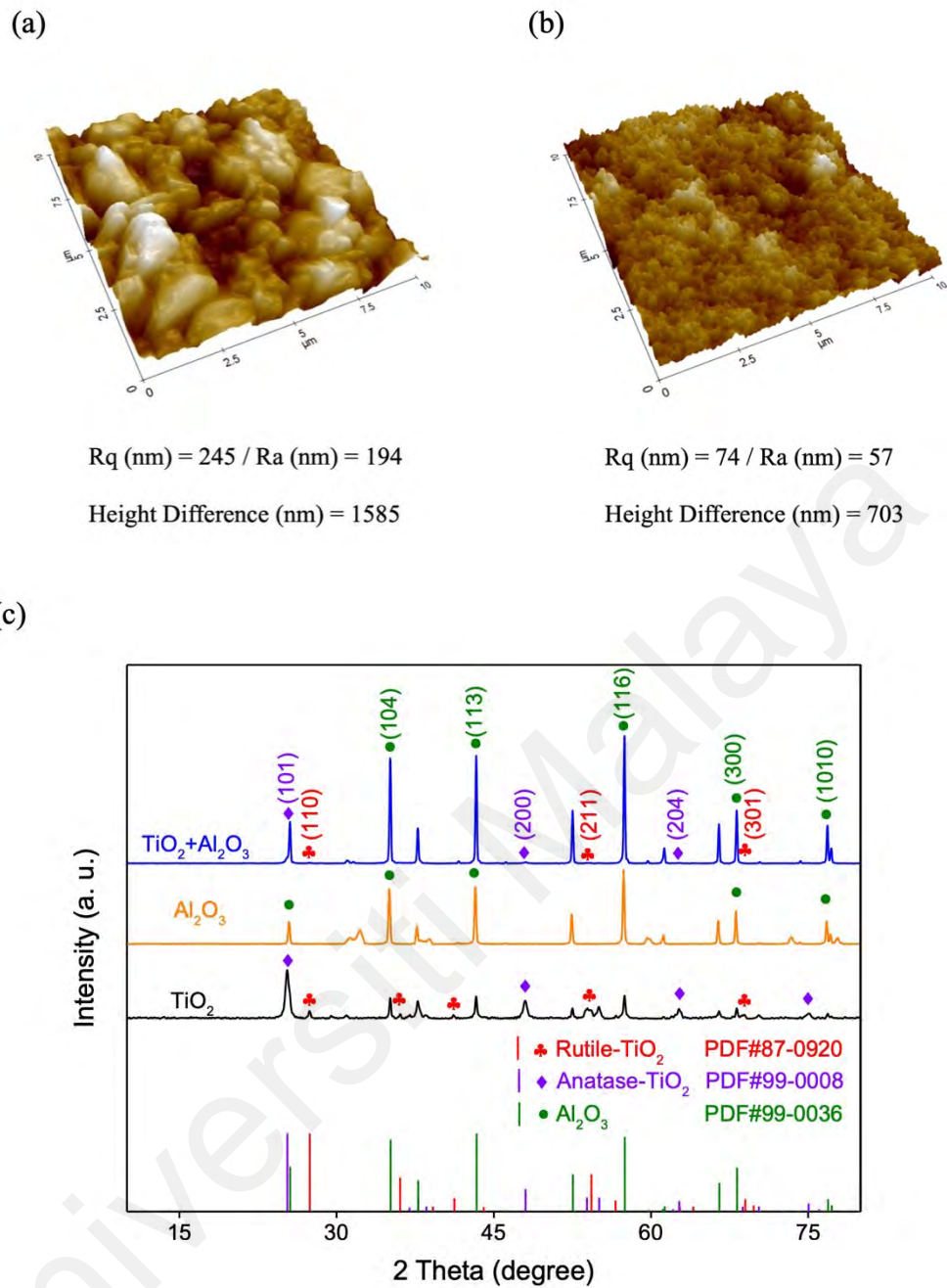


**Fig. 4.2. Cross-sectional views of (a) CMT<sub>5</sub>, (b) CMT<sub>50</sub>, and (c) CMT<sub>100</sub>, along with EDS (d) mapping and (e) weight ratio results of CMT<sub>50</sub> surface.**

AFM 3D imaging was utilized to assess the surface properties of the catalytic film, focusing on their roughness factors. Fig. 4.3 (a) shows that the CMT<sub>0</sub> membrane has a significant height variation of 1585 nm, with the roughness factors  $R_q$  (root mean square roughness) and  $R_a$  (average roughness) measured at 245 and 194 nm, respectively. In contrast, Fig. 4.3 (b) indicates that the CMT<sub>50</sub> membrane has a more uniform surface,

evidenced by a reduced height variation of 703 nm, and significantly lower roughness factors, with  $R_q$  and  $R_a$  measuring 74 and 57 nm, respectively. This increased uniformity is likely attributable to the dense and smooth  $TiO_2$  coating on the membrane top. Such a coating not only enhances the pollution resistance of the photocatalytic film but also potentially improves the stability of catalyst loading, largely due to an increase in shear resistance.

XRD analysis was used to characterize the crystal structure of  $TiO_2$  on the membrane surface. Fig. 4.3 (c) displays the XRD patterns of pure  $TiO_2$ ,  $Al_2O_3$ , and CMT<sub>50</sub> membrane. From Fig. 4.3 (c), both the  $TiO_2$  powder and the photocatalytic membrane exhibit diffraction peaks at  $25.30^\circ$ ,  $48.03^\circ$ , and  $62.68^\circ$ . These peaks correspond to the (101), (200), and (204) crystal planes of the anatase phase of  $TiO_2$ , respectively, as per the Powder Diffraction File (PDF) #99-0008. Additionally, several diffraction peaks at  $2\theta$  values of  $27.43^\circ$ ,  $54.32^\circ$ , and  $68.99^\circ$  correspond to the (110), (211), and (301) crystal planes of the rutile phase of  $TiO_2$  (PDF#87-0920). The XRD pattern indicates that the photocatalytic film maintains its crystal structure without significant phase transformation after calcination at  $400^\circ C$ . Furthermore, the anatase phase constitutes over 90% of the  $TiO_2$  powder and the photocatalytic membrane. Given that anatase is known for its superior photocatalytic activity, these findings suggest that the photocatalytic film examined in this study possesses promising photocatalytic potential. Overall, the XRD results are consistent with observations from FESEM and EDS analyses.



**Fig. 4.3. AFM 3D images of (a) CMT<sub>0</sub> and (b) CMT<sub>50</sub>; (c) XRD pattern of  $TiO_2$  powder,  $Al_2O_3$ , and CMT<sub>50</sub>.**

#### 4.1.2 Photocatalytic performance in three photocatalytic experiments via MG degradation

Table 4.1 demonstrates a significant enhancement in MG degradation across all three systems with the increase in  $TiO_2$  content from 5 to 50 mg. This enhancement is attributed

to the more efficient interaction of UV light with the photocatalyst at the fluid/catalyst interface, increasing photoactive groups capable of degrading pollutants (Ahmed, 2011). Moreover, increasing the catalyst content can increase the adsorption of MG. However, at a concentration of 100 mg/L TiO<sub>2</sub>, while the degradation rates in the SPR and TIS-PMR systems continue to increase, a slight reduction is observed in the TIM-PMR system. This decrease can be ascribed to the complete absorption of light by the thick catalyst layer, which does not change the diffusion length of carriers to the catalyst-liquid interface (Chen et al., 2001; Marinho et al., 2018). Additionally, a smoother surface of the CMT<sub>50</sub> photocatalytic membrane, resultant from higher TiO<sub>2</sub> content, may reduce the effective photocatalytic area, impacting the overall degradation efficiency.

The initial evaluation of hydraulic permeability for selected CMT membranes was conducted using ultrapure water filtration and varying TMP. From Fig. 4.4 (a), the results show a clear linear correlation between pure water flux and TMP for both CMT<sub>0</sub> and CMT<sub>50</sub>, aligning with the principles of Darcy's law. Darcy's Law describes the flow of fluids through porous media, stating that the volume of fluid flowing through a porous material is directly proportional to the hydraulic gradient and the cross-sectional area, and inversely proportional to the fluid viscosity and the length of the flow path. Specifically, Darcy's Law or  $J = V / (A \times t)$ , where J is flux (L/m<sup>2</sup>·h), V is permeate volume (L), A is membrane area (m<sup>2</sup>), and t is time (h). In this study, the TMP and CFV were set as 0 to 1 bar and 100 cm<sup>3</sup>/min. Notably, the membranes exhibited significant permeability values, with CMT<sub>0</sub> and CMT<sub>50</sub> demonstrating rates of 1004 and 762 L/(m<sup>2</sup>·h·bar), respectively, as inferred from the slope in Fig. 4.4 (a). These results effectively demonstrate the high pure water permeability of the ceramic membranes, both before and after catalyst incorporation.



As shown in Fig 4.4 (b), in both PMR systems, the degradation rate of MG exceeds 98%, markedly higher than the 70% achieved in the SPR system. To analyze kinetics, MG degradation experiments were conducted in three systems: SPR, TIS-PMR, and TIM-PMR. A 5 mg/L MG solution was used as the feed, and all experiments were performed at  $25 \pm 2^\circ\text{C}$ . The feed solution was first stirred in the dark for 30 minutes to reach adsorption/desorption equilibrium. The reaction proceeded for 4 hours under UVC irradiation, with hourly sampling to measure MG concentration changes. Fig. 4.4 (c) substantiates that MG degradation in these systems adheres to first-order kinetics, with rate constants for SPR, TIS-PMR, and TIM-PMR at 0.0048, 0.0139, and 0.0184  $\text{min}^{-1}$ , respectively. In addition, studies show that the steepness of these slopes reflects the rapidity of degradation efficiency (Li et al., 2017; G. Zhang et al., 2023). These results highlight the enhanced photocatalytic efficiency of PMR systems over the SPR system.

The TIS-PMR system shows a significant reduction in permeation flux compared to TIM-PMR, particularly at a  $\text{TiO}_2$  concentration of 100 mg, where the flux diminishes to 37% of its original value. This decrease is likely due to the suspended catalyst absorbing the MG solution, leading to the formation of a fouling layer on the membrane surface and the compaction of the filter cake layer over extended filtration periods. The anti-fouling performance of CMT membranes was evaluated using a crossflow filtration system with 100  $\text{cm}^3/\text{min}$  CFV and 0.2 bar TMP. The experiment included 4 hours of UVC irradiation, with flux decline monitored to assess fouling resistance. Interestingly, Fig. 4.4 (d) reveals that both PMR systems exhibit self-cleaning properties, with fluxes recovering to 57% and 98% of their initial values for TIS-PMR and TIM-PMR, respectively, after four hours of reaction. This self-cleaning phenomenon is believed to arise from a synergistic effect of UV photocatalytic activity, hydrophilic conditions, and hydrodynamic shear due to crossflow filtration. Photogenerated electrons react with water molecules to produce hydrophilic hydroxyl radicals, which envelop the  $\text{TiO}_2$  layer's surface and help prevent

attachment of the contaminants to the membrane surface. Hydrodynamic shear also plays a crucial role in minimizing the fouling layer, enhancing the effectiveness of UV irradiation on the photocatalytic membrane surface. Concurrently, the active groups formed by the catalyst under UV irradiation aid in removing pollutants from the membrane.

Notably, the enhancement of the photocatalytic membrane hydrophilicity under UV irradiation is usually verified by measuring the membrane contact angle. However, this study faced experimental limitations in conducting in-situ contact angle measurement during UV exposure. Nevertheless, several studies have validated the phenomenon of light-induced hydrophilicity (Banerjee et al., 2015; Katsumata et al., 2023; Osorio-Vargas et al., 2023).

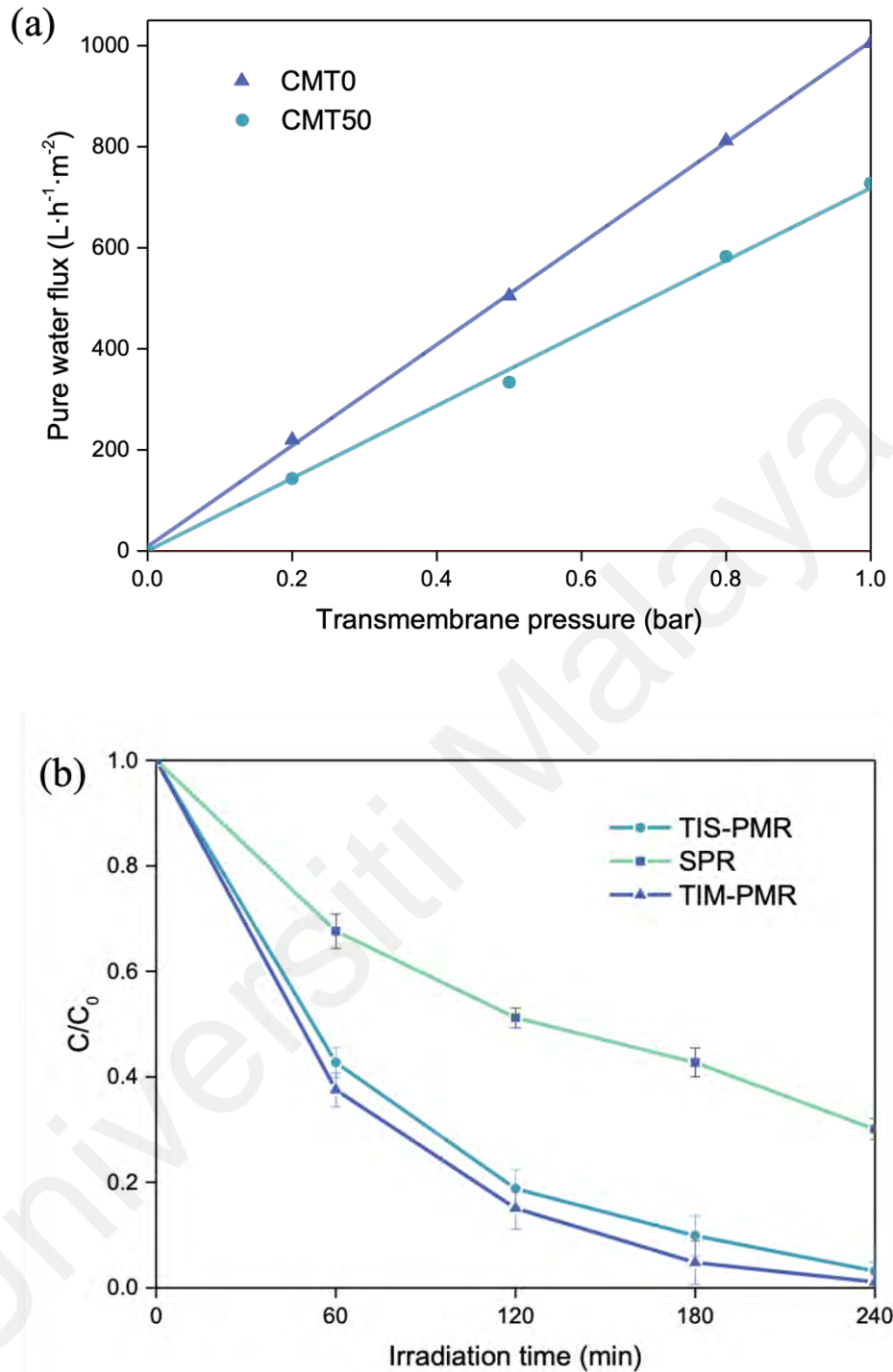
Overall, compared to TIS-PMR, TIM-PMR more effectively combines the advantages of photocatalysis and membrane in the photocatalytic degradation of pollutants. This superior integration indicates that TIM-PMR can more efficiently manage the challenges posed by pollutant degradation, demonstrating a better balance between photocatalytic activity and membrane functionality. In addition, TIM-PMR has more advantages in long-term operation, because the flowing  $\text{TiO}_2$  particles in the TIS-PMR system may cause mechanical damage to the membrane surface.

**Table. 4.1. MG degradation rate and permeate flux deterioration after 4 h reaction.**

Photocatalytic reactor <sup>a</sup>	TiO <sub>2</sub> amount (g)	MG degradation (%)	J/J <sub>0</sub> <sup>b</sup>
SPR	5	44 ± 2	-
	20	58 ± 3	-
	50	70 ± 3	-
	100	77 ± 4	-
TIS-PMR	5	66 ± 3	0.69
	20	82 ± 4	0.65
	50	98 ± 2	0.57
	100	99 ± 1	0.37
TIM-PMR	5	68 ± 3	0.97
	20	86 ± 4	0.98
	50	99 ± 2	0.98
	100	95 ± 3	0.96

<sup>a</sup> TMP and CFV parameters in both PMR systems were set as 0.2 bar and 100 cm<sup>3</sup>/min.

<sup>b</sup> Defined as the ratio between the permeate flux after 4 h of experiment (J) and the initial one (J<sub>0</sub>).



**Fig. 4.4. (a) hydraulic permeability of the CMT<sub>0</sub> and CMT<sub>50</sub>; (b) MG removal rate in three systems; (c) photodegradation model of the three systems by using first-order kinetics plots; (d) comparison of anti-fouling properties. (TiO<sub>2</sub> = 50 mg, CFV = 100 cm<sup>3</sup>/min, TMP = 0.2 bar)**

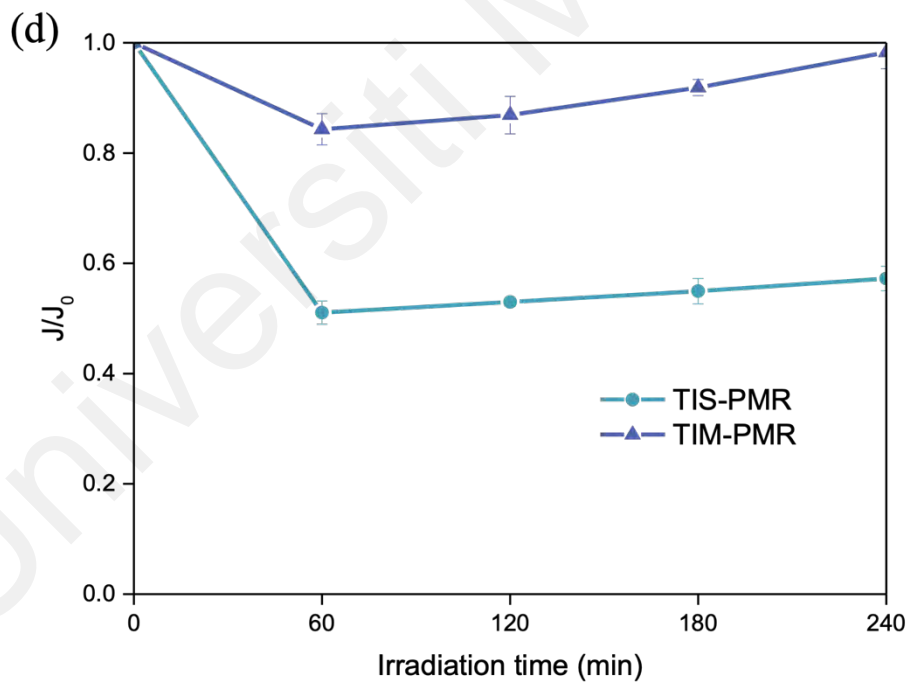
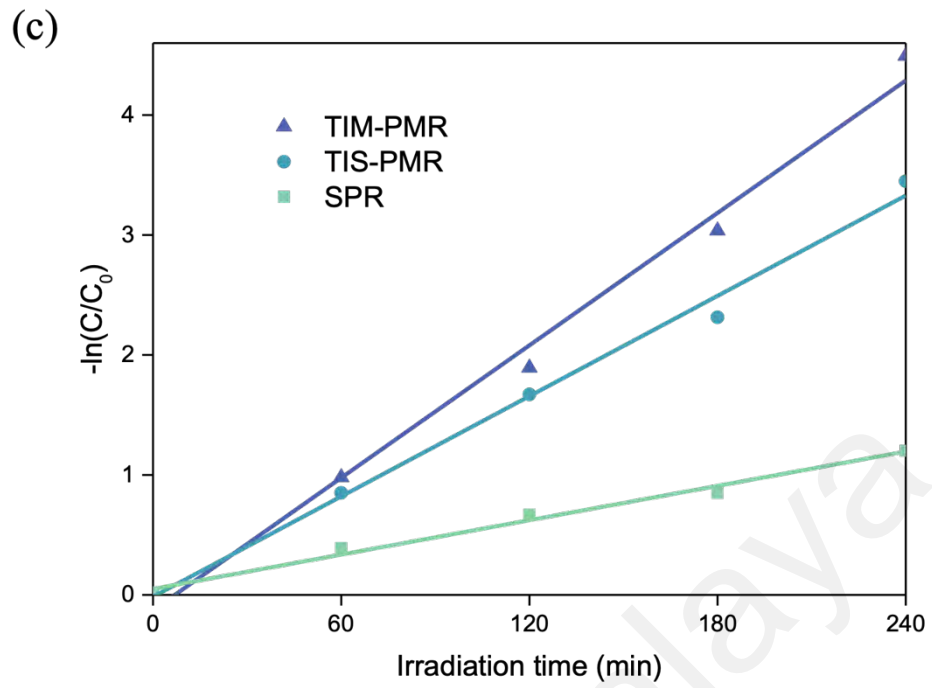


Fig. 4.4, continued.

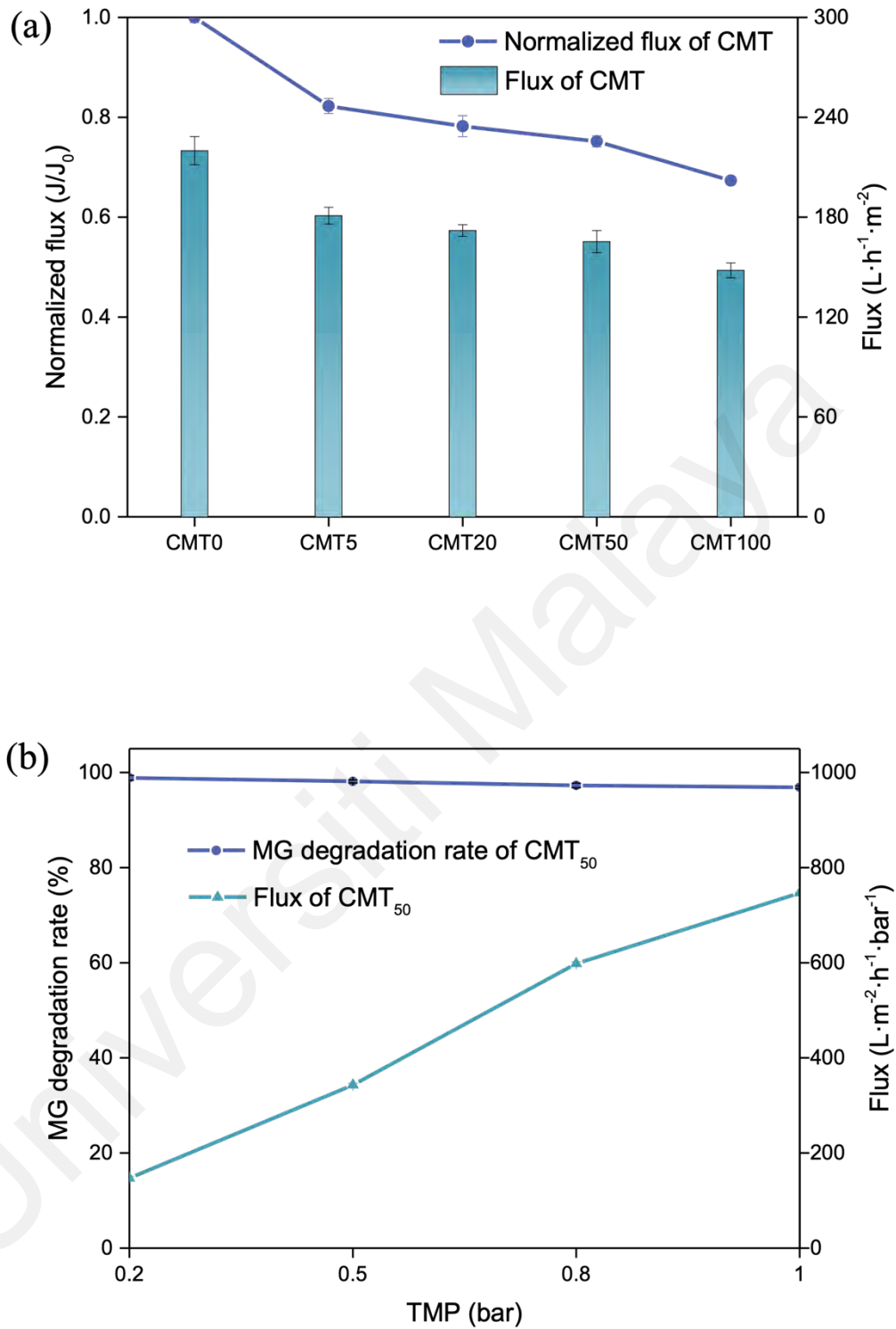
## 4.2 Impact of process parameters on TIM-PMR performance

As discussed in Section 4.1.2, increasing TiO<sub>2</sub> concentration initially significantly enhances MG degradation in the TIM-PMR system, followed by a slight decrease. Fig. 4.5 (a) illustrates a notable reduction in the flux of the photocatalytic film compared to the unmodified membrane (CMT<sub>0</sub>), particularly when the TiO<sub>2</sub> content exceeds 50 mg. Furthermore, research conducted by Ahmad et al. indicates that the permeability of a membrane is more significantly influenced by its porosity and hydrophilicity than by its thickness (Ahmad et al., 2020). Based on this understanding, it can be inferred that the observed reduction in the flux of CMT membranes is likely due to the formation of a denser TiO<sub>2</sub> layer on the surface of the support layer, which results in a decrease in the membrane's porosity. This denser layer of TiO<sub>2</sub>, while beneficial for photocatalytic activity, could impede the flow of water through the membrane, thus reducing its overall permeability.

To explore the impact of different TMPs on the TIM-PMR system, CMT<sub>50</sub> was used with CFV set at 100 cm<sup>3</sup>/min and TMPs at 0.2, 0.5, 0.8, and 1 bar, respectively. As depicted in Fig. 4.5 (b), an increase in TMP corresponded to a linear rise in the permeation flux of the photocatalytic membrane. However, this increase in TMP also led to a slight reduction in the degradation rate of MG. This phenomenon aligns with earlier research findings suggesting that dye decomposition depends on the probability of contact between dye molecules and the active species (Deepracha et al., 2021). FESEM images indicate that the thickness of the CMT<sub>50</sub> is approximately 9 μm. The calculated residence times of MG molecules within this layer under the different TMPs are 0.22, 0.093, 0.053, and 0.043 seconds, respectively. This data implies that the observed decrease in MG degradation rate under higher TMP can be ascribed to the diminished contact time between the MG molecules and the photoactive groups on the membrane. As TMP increases, the faster flow likely reduces the duration for which MG molecules interact

with the catalyst, thereby impacting the efficiency of the photocatalytic degradation process.

Further analysis was conducted on the influence of different CFVs (10, 50, and 100 cm<sup>3</sup>/min) on the TIM-PMR system performance to degrade MG, while maintaining TMP at 0.2 bar. From Fig. 4.5 (c), it is evident that an increase in CFV enhances both the membrane flux and the rate of MG removal. This improvement is due to decreased membrane filtration resistance at higher CFV, resulting in increased permeate flux. Additionally, CFV affects HRT in a fixed PMR reaction module. Adequate HRT allows sufficient time for both pollutant adsorption on the photocatalyst and product desorption from catalyst particles, as well as adequate photooxidation time. In conclusion, the TIM-PMR system shows optimal photocatalytic performance and membrane flux under conditions of low TMP and high CFV.



**Fig. 4.5. Effect of (a) TiO<sub>2</sub> concentration; (b) TMP and (c) CFV on MG degradation; (d) cycles of MG removal.**



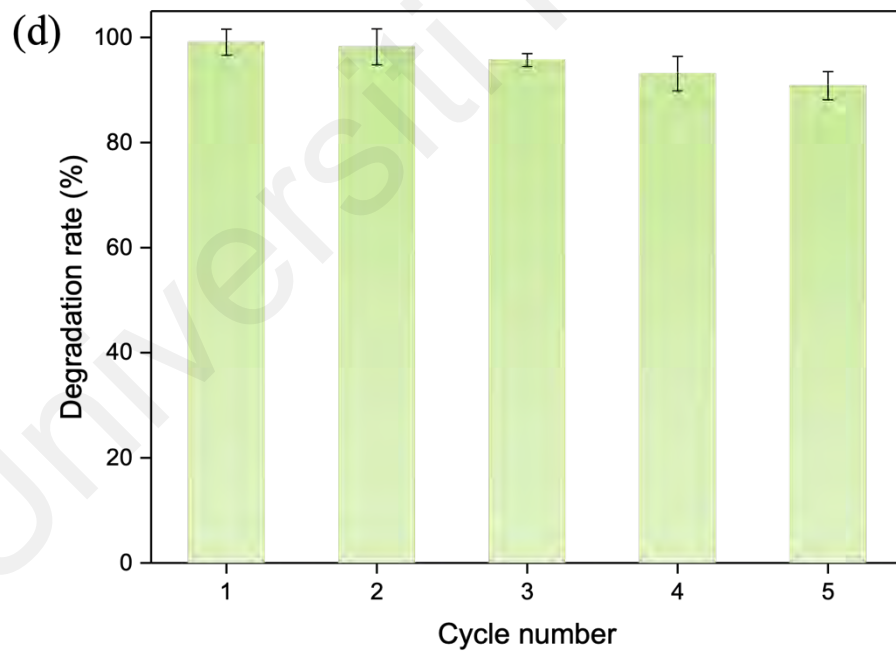
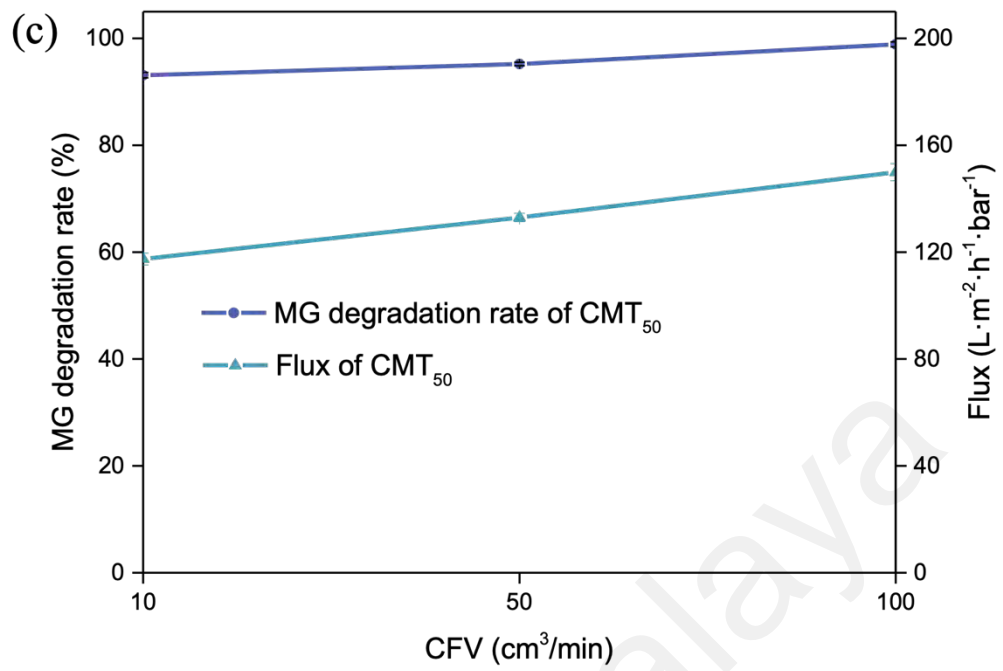


Fig. 4.5, continued.

### 4.3 Stability of the TIM-PMR

The long-term stability of the photocatalytic membrane plays a crucial factor in the industrial application of TIM-PMR. Among all modified membranes, the CMT<sub>50</sub> membrane, selected for its outstanding photocatalytic activity in MG degradation and its efficacy in mitigating membrane fouling, was used to assess membrane reusability by subjecting it to five cycles of MG degradation experiments. Prior to each cycle, the membrane was cleaned using distilled water in a crossflow filtration system for 60 minutes. Simultaneously, four UVC lamps were activated to illuminate the membrane, aiding in removing residual MG from both the filtration system and the membrane surface/interior. From Fig. 4.5 (d), after five cycles, the removal rate of MG remained high at 90.8%. This demonstrates that the TiO<sub>2</sub>-immobilized-membrane, fabricated through crossflow filtration and calcination even without any cross-linking agents or binders, maintains stable MG degradation reusability.

Additionally, these results provide grounds to speculate that the membrane possesses long-term operational stability, further affirming its excellent self-cleaning properties as well. This finding underscores the benefits of the novel photocatalytic membrane system, particularly its ability to restore performance through simple, non-destructive, and eco-friendly ultraviolet irradiation cleaning. This approach contrasts with conventional membrane separation technologies that often require more complex physical and chemical cleaning methods for sustained operation. Therefore, the photocatalytic membrane performance in this context not only highlights its potential for practical application but also emphasizes its advantage in terms of ease for maintenance and environmental sustainability.

## 4.4 Characterization of Al<sub>2</sub>O<sub>3</sub>, TiO<sub>2</sub> and Ag-TiO<sub>2</sub> membranes

### 4.4.1 Morphological property of membranes

The morphology and porosity of the pristine Al<sub>2</sub>O<sub>3</sub> ceramic membrane and the catalytic membranes were examined using FESEM. As shown in 4.6 (a), the Al<sub>2</sub>O<sub>3</sub> ceramic membrane displayed irregular-shaped particles and a highly porous, defect-free surface. This finding indicated the suitability of the Al<sub>2</sub>O<sub>3</sub> ceramic membrane as a high-quality support for photocatalytic applications.

Fig. 4.6 (b) illustrates that the TiO<sub>2</sub> catalytic membrane is covered with numerous small spherical particles. These particles are embedded and anchored in the pores of the ceramic membrane, forming a porous, sponge-like structure with high roughness. Following the in-situ reduction of Ag<sup>+</sup> to Ag, as depicted in Fig. 4.6 (c), the composite Ag-TiO<sub>2</sub> particles maintain a spherical and more regular shape, resulting in a porous, loose sponge-like structure. This structure increases the surface area, which is advantageous for photocatalytic degradation. In addition, research suggests that spherical particles, when stacked, tend to form membranes with a more uniform pore size distribution, which could enhance membrane flux (Qin et al., 2020).

The diameter of the Ag-TiO<sub>2</sub> particles on the membrane measured by Nano Measurer (Bian et al., 2024), is approximately 60 nm, larger than the 40 nm TiO<sub>2</sub> particles, as showed in Fig. 4.6 (d). In addition, previous studies have indicated that larger and more regular particles typically form larger pores, potentially improving permeability (Adam et al., 2020; Y. Wang et al., 2020; Wang et al., 2022). Moreover, the noticeable alterations in morphology and porosity on photocatalytic membranes validate the successful immobilization of catalysts on the support.

EDS elemental mapping was used to analyze the composition of the composite materials. Fig. 4.6 (e) and (f) confirm the presence of silver (Ag), titanium (Ti), aluminum

(Al), and oxygen (O), represented by yellow, red, blue, and green colors, respectively. Fig. 4.6 (g) details the weight ratios of these elements: 2.01% Ag, 40.17% Ti, 12.91% Al, and 44.90% O. The indistinct yellow coloration representing the Ag element in Fig. 4.6 (e) aligns with the findings from Fig. 4.6 (f), confirming a minor Ag deposition. It is noted that Fig. 4.6 (g) reveals that the content of Ag in the Ag-TiO<sub>2</sub> nanoparticles exceeds 1%, likely due to Ag covering the surface of the TiO<sub>2</sub> particle. This observation underscores the effective deposition of Ag and immobilization of Ag-TiO<sub>2</sub> on the Al<sub>2</sub>O<sub>3</sub> membrane surface.

Universiti Malaysia

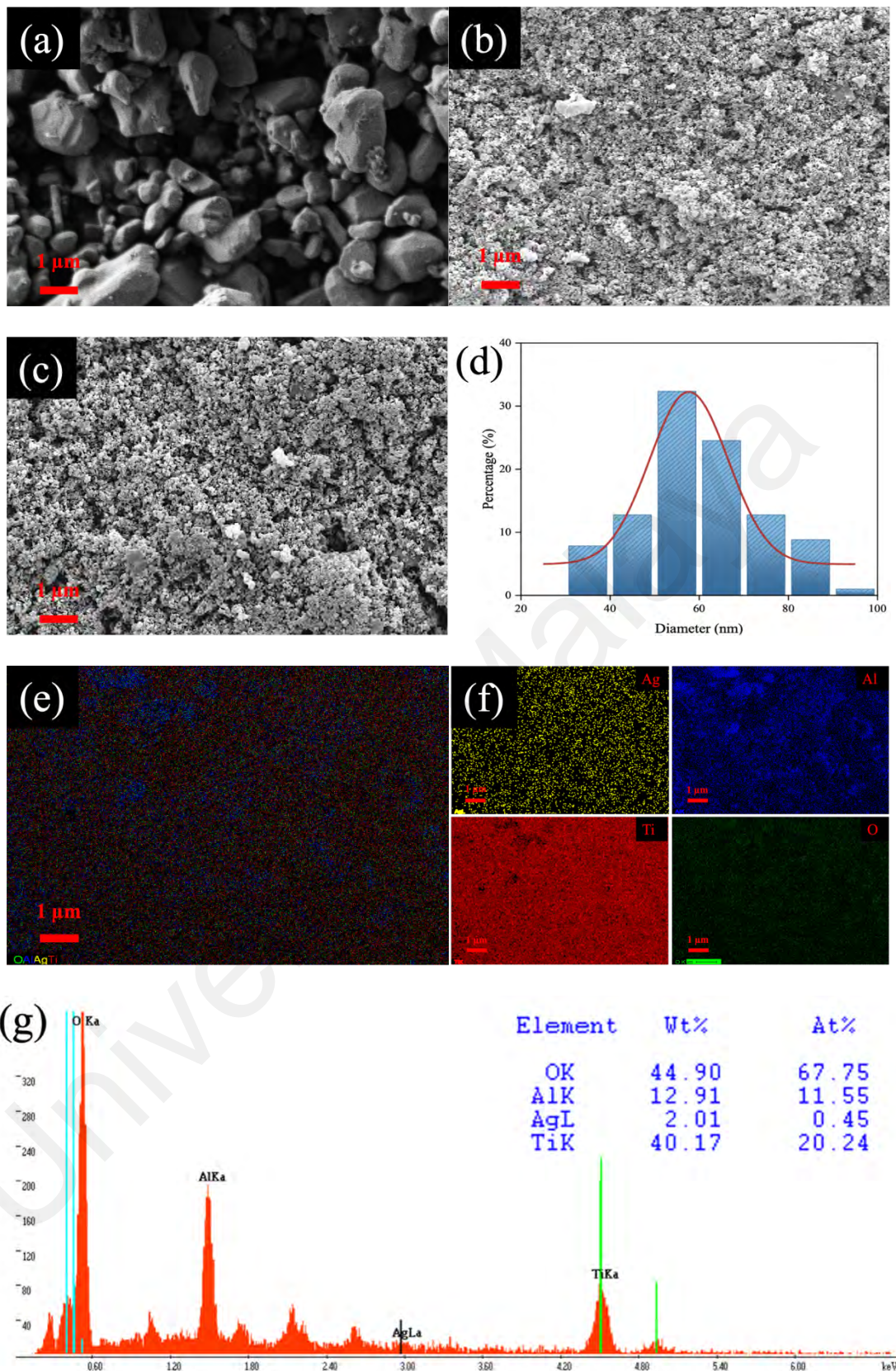


Fig. 4.6. (a) original  $\text{Al}_2\text{O}_3$  ceramic membrane; (b)  $\text{TiO}_2$  catalytic membrane; (c)  $\text{Ag-TiO}_2$  catalytic membrane; (d) diameter of  $\text{Ag-TiO}_2$  particles; (e) and (f) EDS

**element mapping images of Ag, Ti, Al, Ti and O on Ag-TiO<sub>2</sub> membrane; (g) weight ratio results of Ag-TiO<sub>2</sub> membrane.**

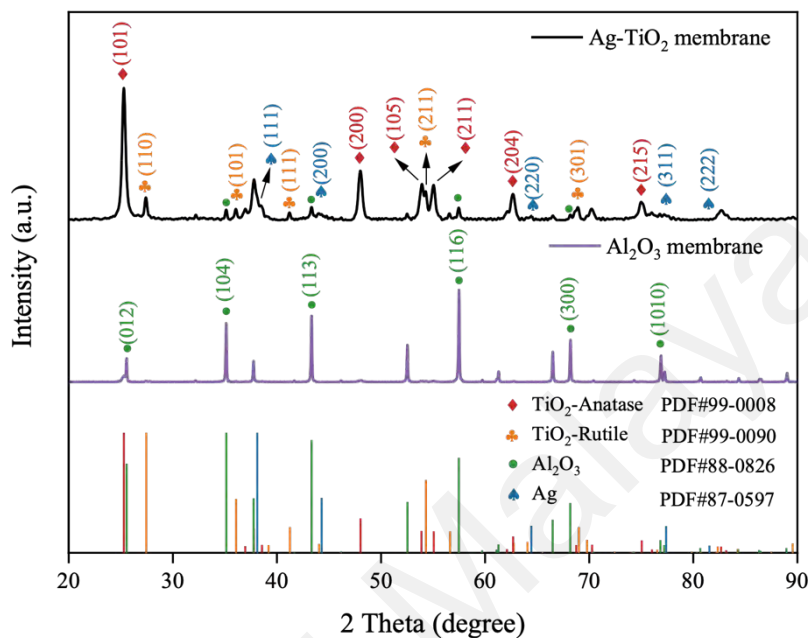
#### **4.4.2 Crystal property of Ag-TiO<sub>2</sub> membranes**

XRD analysis was performed to determine the crystal phase composition and crystallite size of the particles on the membranes. The XRD patterns for the Al<sub>2</sub>O<sub>3</sub> membrane and the Ag-TiO<sub>2</sub> catalytic membrane are shown in Fig. 4.7. For Al<sub>2</sub>O<sub>3</sub>, diffraction peaks are observed at  $2\theta = 35.1^\circ, 43.3^\circ, 57.5^\circ,$  and  $68.2^\circ$ , corresponding to the (104), (113), (116), and (300) crystal planes respectively, as per the Powder Diffraction File (PDF) PDF#88-0826. This peak confirms that the Al<sub>2</sub>O<sub>3</sub> ceramic membrane serves as the substrate for the Ag-TiO<sub>2</sub> catalytic membrane.

The XRD pattern for the Ag- TiO<sub>2</sub> catalytic membrane reveals peaks at  $2\theta=25.3^\circ, 48.0^\circ, 53.9^\circ, 55.1^\circ, 62.7^\circ,$  and  $75.0^\circ$ , corresponding to the (101), (200), (105), (211), (204), and (215) crystal planes of the anatase phase of TiO<sub>2</sub> (PDF#99-0008). The peaks for the anatase phase are more pronounced in area and intensity compared to those for the rutile phase, indicating that the anatase phase is the predominant component in the TiO<sub>2</sub>. The anatase phase is known for its high catalytic efficiency, which is beneficial for photocatalytic applications.

Moreover, the XRD pattern for the Ag-TiO<sub>2</sub> catalytic membrane also shows weak diffraction peaks of silver at  $38.1^\circ, 44.3^\circ, 64.4^\circ, 77.4^\circ,$  and  $81.5^\circ$ , corresponding to the (111), (200), (220), (311), and (222) crystal planes (PDF#87-0597). The presence of these peaks suggests successful incorporation of silver into the TiO<sub>2</sub> matrix. It has been reported that Ag atoms can diffuse into the amorphous TiO<sub>2</sub> structure during thermal annealing, leading to the formation of larger clusters (Mosquera et al., 2016; Viana et al., 2013). Using the Scherrer equation, the average crystallite sizes for the anatase phase TiO<sub>2</sub>, rutile phase TiO<sub>2</sub>, and Ag were calculated to be within the ranges of 20-36 nm, 23-38 nm, and

31-63 nm, respectively. These sizes are consistent with those observed via FESEM, confirming the effective formation and uniform distribution of the crystalline phases in the catalytic membranes.



**Fig. 4.7. XRD pattern of Al<sub>2</sub>O<sub>3</sub> and Ag-TiO<sub>2</sub> membrane.**

#### 4.4.3 Optical property of catalytic membranes

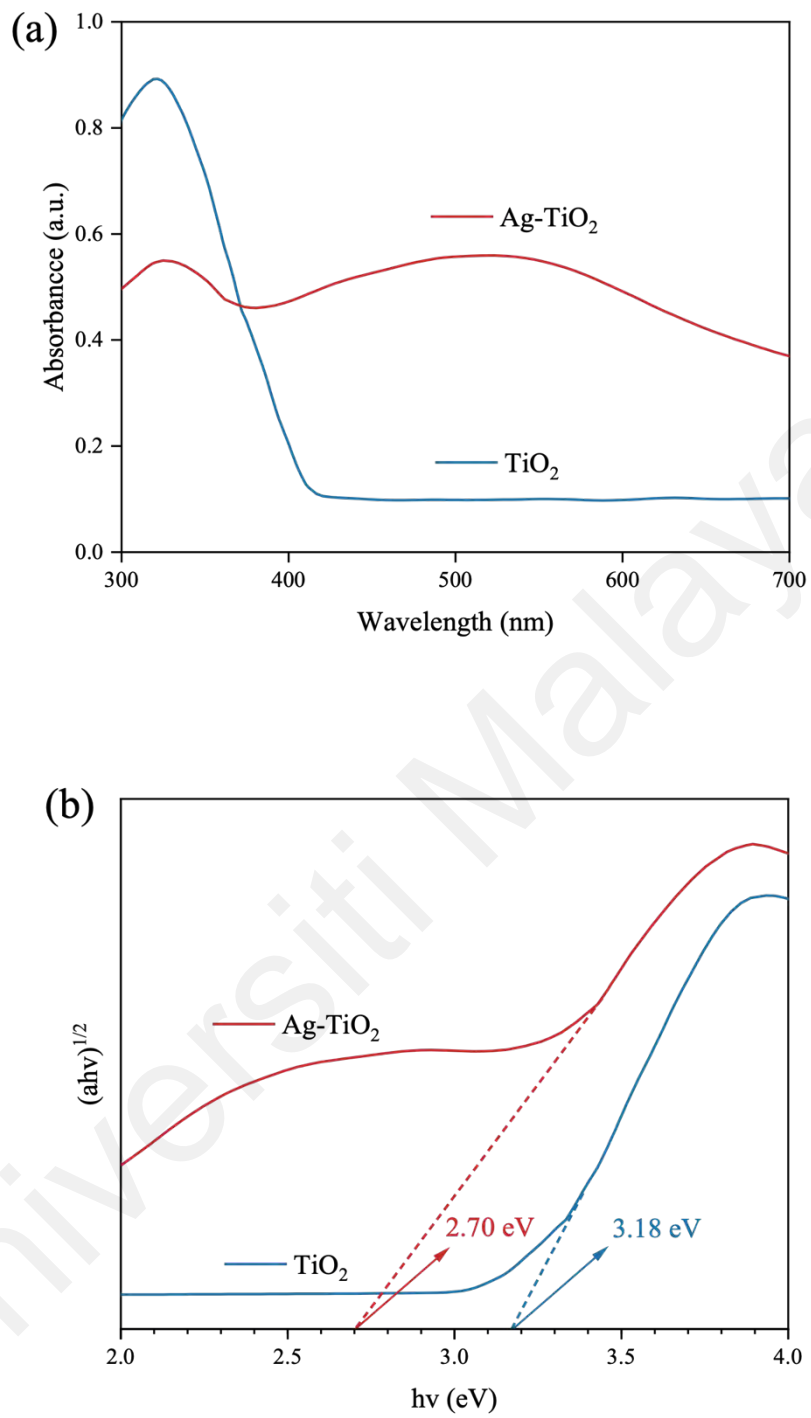
The UV-vis diffuse reflectance spectroscopy (DRS) was employed to analyze the optical properties of TiO<sub>2</sub> and Ag-TiO<sub>2</sub> nanocomposites. The DRS spectra, shown in Fig. 4.8 (a), reveal that both TiO<sub>2</sub> and Ag-TiO<sub>2</sub> nanocomposites exhibit absorption peaks below 400 nm, which is characteristic of the intrinsic band gap absorption of TiO<sub>2</sub> (Zhou et al., 2024). The Ag-TiO<sub>2</sub> nanocomposites show an extended absorption edge into the visible light region compared to pure TiO<sub>2</sub>. This extension indicates enhanced photon absorption capabilities of the Ag-TiO<sub>2</sub> composites, which is beneficial for photocatalytic applications.

To quantify the band gap energy of the photocatalysts, the DRS spectra of TiO<sub>2</sub> and Ag-TiO<sub>2</sub> were converted into Tauc plots using the Kubelka-Munk function, as illustrated

in Fig. 4.8 (b) (Ahmed et al., 2023). By extrapolating the linear portions of these plots, the indirect band gaps were estimated to be approximately 3.18 eV for TiO<sub>2</sub> and 2.70 eV for Ag-TiO<sub>2</sub>. The reduction in the band gap of Ag- TiO<sub>2</sub> by 0.48 eV compared to pure TiO<sub>2</sub> is attributed to the presence of silver clusters or the localized surface plasmon resonance (LSPR) effect. This reduction enhances the photocatalytic activity of Ag- TiO<sub>2</sub> under visible light, making it more effective for photocatalytic processes (Costa et al., 2024; Lincho et al., 2024).

Universiti Malaya





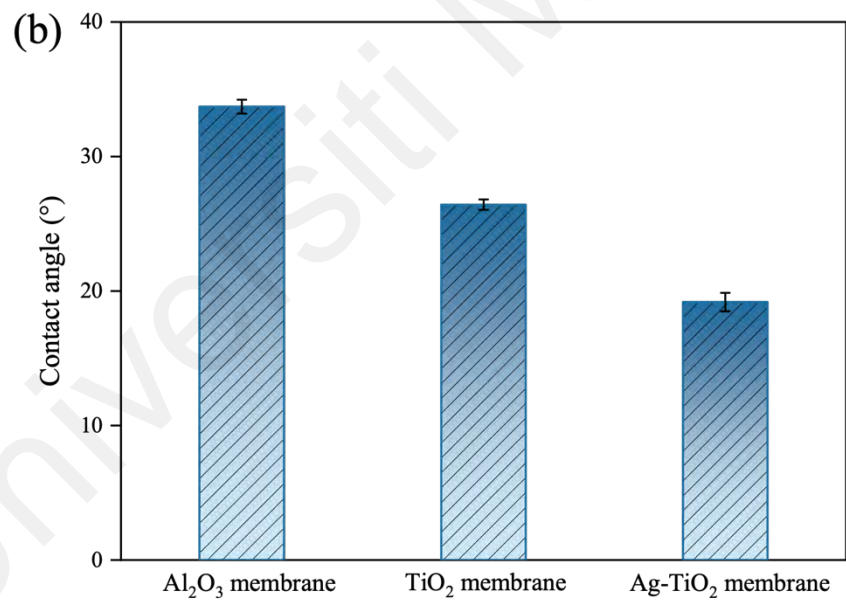
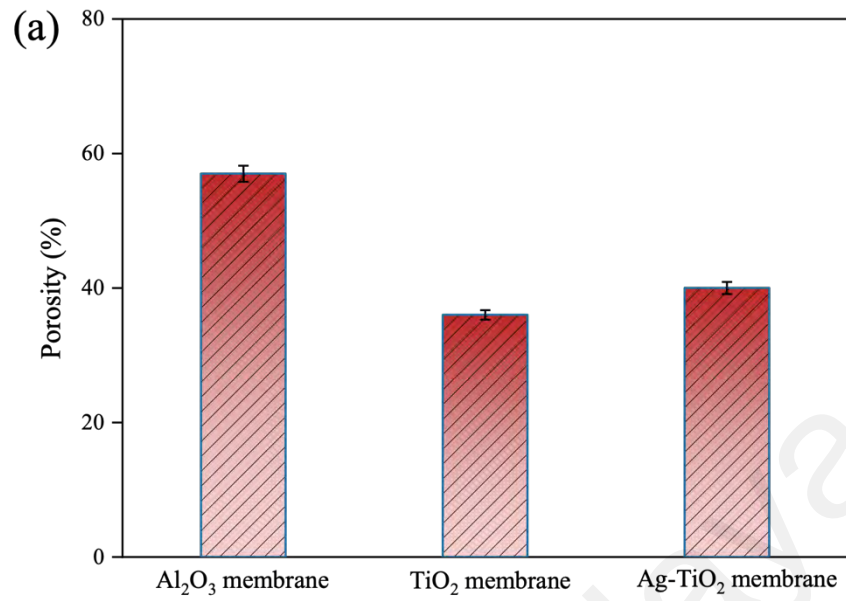
**Fig. 4.8. (a) UV-Vis DRS spectra and (b) Tauc plots for the optical band gap of TiO<sub>2</sub> and Ag-TiO<sub>2</sub> membrane.**

#### 4.4.4 Porosity and pore size of membranes

Porosity and pore size are critical factors in evaluating the membranes performance, as they offer insights into the fouling tendency and separation efficacy. The porosity of the membranes was calculated from the change of dry weight of the membrane and the wet weight after 24 h in distilled water (Kusworo & Puspa, 2024).

Fig. 4.9 (a) indicates that the porosities of  $\text{Al}_2\text{O}_3$  membrane,  $\text{TiO}_2$ -immobilized membrane and Ag- $\text{TiO}_2$ -immobilized membranes are 57 %, 36 %, and 40 %, respectively. The porosity of the catalytic membranes decreased compared to the  $\text{Al}_2\text{O}_3$  membrane. This reduction is likely due to the deposition of photocatalyst nanomaterials, which fill the pores of the membrane and accumulate on its surface. Despite the decrease, the Ag- $\text{TiO}_2$  membrane exhibits slightly higher porosity than the  $\text{TiO}_2$  membrane. This increase can be attributed to the larger size of the Ag-  $\text{TiO}_2$  composite nanoparticles compared to the  $\text{TiO}_2$  particles, which may result in a less dense packing of the particles.

The average pore sizes of the membranes were evaluated using FESEM images (Fig. 4.6 (b) and (c)) (Wang & Wang, 2006). The  $\text{Al}_2\text{O}_3$  membrane had a pore size of 0.1  $\mu\text{m}$ . After the immobilization of  $\text{TiO}_2$  and Ag- $\text{TiO}_2$ , the pore sizes decreased to 0.079  $\mu\text{m}$  and 0.067  $\mu\text{m}$ , respectively. This reduction in pore size suggests that the incorporation of photocatalysts into the membrane structure has narrowed the pores. While this narrowing could enhance the catalytic activity by providing more surface area for reactions, it might also negatively impact membrane flux. This presents a trade-off between improved photocatalytic performance and reduced fluid flow through the membrane.



**Fig. 4.9. (a) Porosity and (b) contact angle value of Al<sub>2</sub>O<sub>3</sub>, TiO<sub>2</sub> and Ag-TiO<sub>2</sub> membrane.**

#### **4.4.5 Contact angle of membranes**

The contact angles of the membranes were measured using deionized water to evaluate the hydrophilicity of their surfaces. Generally, a lower contact angle indicates greater hydrophilicity and enhanced wettability. Hydrophilicity is commonly associated with improved membrane flux and antifouling properties, while wettability is linked to the self-cleaning capabilities of the catalytic layer.

Fig. 4.9 (b) demonstrates the contact angles for the  $\text{Al}_2\text{O}_3$ ,  $\text{TiO}_2$ , and  $\text{Ag-TiO}_2$  membranes are  $33.71^\circ$ ,  $26.42^\circ$ , and  $19.18^\circ$ , respectively. The reduction in contact angles observed for the  $\text{TiO}_2$  and  $\text{Ag-TiO}_2$  membranes compared to the  $\text{Al}_2\text{O}_3$  membrane is attributed to the presence of  $-\text{OH}$ ,  $-\text{O-Ti}$ , and  $-\text{O-Ag}$  functional groups on the surface of the catalysts. These groups enhance surface hydrophilicity by improving interactions with water molecules (Nayeri & Parsa, 2024). The  $\text{Ag-TiO}_2$  membrane, with the lowest contact angle, is expected to provide the best performance in terms of high flux, antifouling properties, and self-cleaning abilities due to its superior hydrophilicity and wettability.

### **4.5 Characterization, elimination, degradation mechanism of PMPF**

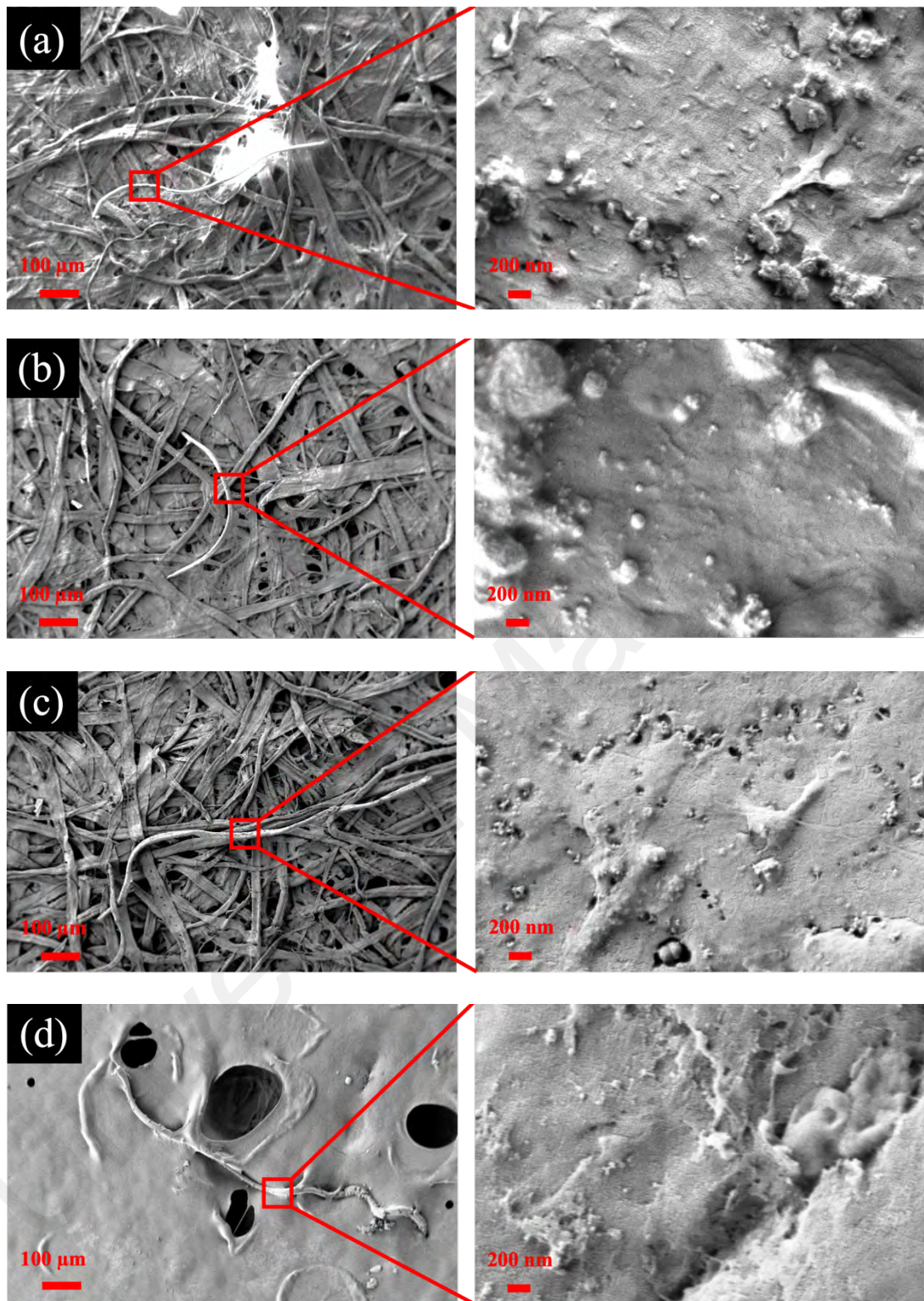
#### **4.5.1 Characterization of PMPF**

##### **4.5.1.1 Morphology analysis of simulated-PMPF**

Fig. 4.10 provides a detailed analysis of the morphology of simulated-PMPF before and after treatment with  $\text{TiO}_2$  and  $\text{Ag-TiO}_2$  catalytic membranes, highlighting the effects of UVC irradiation on fiber structure over time. The initial surface morphology of simulated-PMPF, shown in Fig. 4.10 (a) and (d), reveals a smooth texture with few bulges, typical of polyester fibers with an approximate diameter of  $17\ \mu\text{m}$  and lengths of less than  $1000\ \mu\text{m}$ .

After 24 h of treatment with the  $\text{TiO}_2$  photocatalytic membrane, as depicted in Fig. 4.10 (b), the simulated-PMPF surface exhibits bubble-like protrusions of varying sizes, indicating that the photocatalytic process has started to compromise the fiber's crystal structure. By 48 h, Fig. 4.10 (c) shows that cavities of different sizes have developed on the simulated-PMPF surface, suggesting further degradation. These cavities could allow photo-generated radicals to penetrate deeper into the fibers, accelerating the degradation process.

Similarly, Fig. 4.10 (e) and (f) show the morphology of simulated-PMPF after treatment with the  $\text{Ag-TiO}_2$  catalytic membrane. After 24 h, bubble-like protrusions are present, more pronounced than those observed with  $\text{TiO}_2$ . By 48 h, the surface reveals numerous cavities and cracks, indicating significant morphological changes. These alterations are attributed to the removal of photodegradation products and reorganization of the surface's amorphous content, leading to an increase in the crystalline fraction. This enhanced degradation performance with  $\text{Ag-TiO}_2$  is likely due to the silver's localized surface plasmon resonance (LSPR) effects, which boost photocatalytic activity. Overall, the analysis confirms that both  $\text{TiO}_2$  and  $\text{Ag-TiO}_2$  membranes are effective in degrading simulated-PMPF, with  $\text{Ag-TiO}_2$  showing superior performance.



**Fig. 4.10.** FESEM images of degraded simulated-PMPF by TiO<sub>2</sub> membranes in (a) 0, (b) 24 and (c) 48 h, and by Ag-TiO<sub>2</sub> membranes in (d) 0, (e) 24 and (f) 48 h.

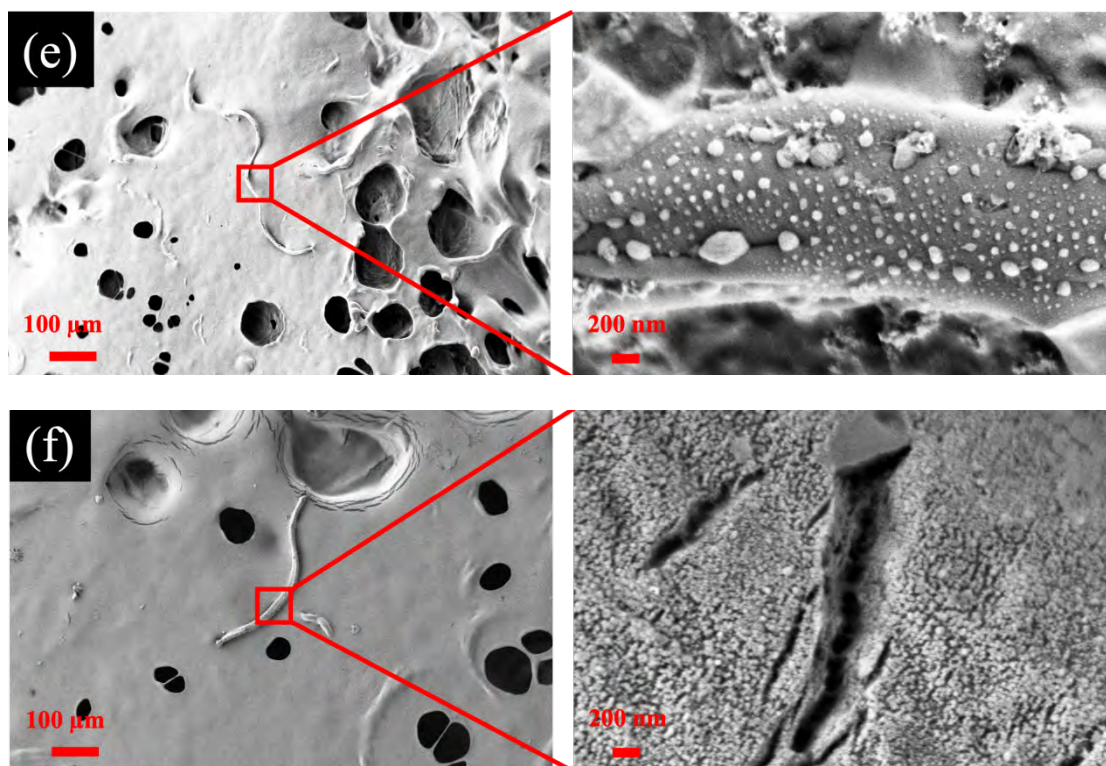


Fig. 4.10, continued.

#### 4.5.1.2 FTIR-ATR spectroscopy for simulated-PMPF

FTIR-ATR is a sensitive and versatile technique for monitoring the early stages of simulated-PMPF photodegradation by detecting changes in chemical structure over time. The comparative FTIR-ATR spectra of simulated-PMPF degradation at various time intervals are illustrated in Fig. 4.11 (a). Initially, at 0 h, the untreated simulated-PMPF displays characteristic absorption peaks at 1720, 1250, and 1100  $\text{cm}^{-1}$ , corresponding to the C=O stretching of amorphous ester carbonyls, C-O-C stretching of ester groups, and C-O stretching vibrations of aliphatic esters, respectively. This result aligns with the FTIR peaks of polyester reported in previous studies (Pasichnyk et al., 2022). Additional absorption peaks at 3350, 2970, and 720  $\text{cm}^{-1}$  are associated with the O-H stretching vibration of alcohols, CH<sub>2</sub> stretching vibration of amorphous aliphatic, and C-H stretching vibrations of aromatic compounds.

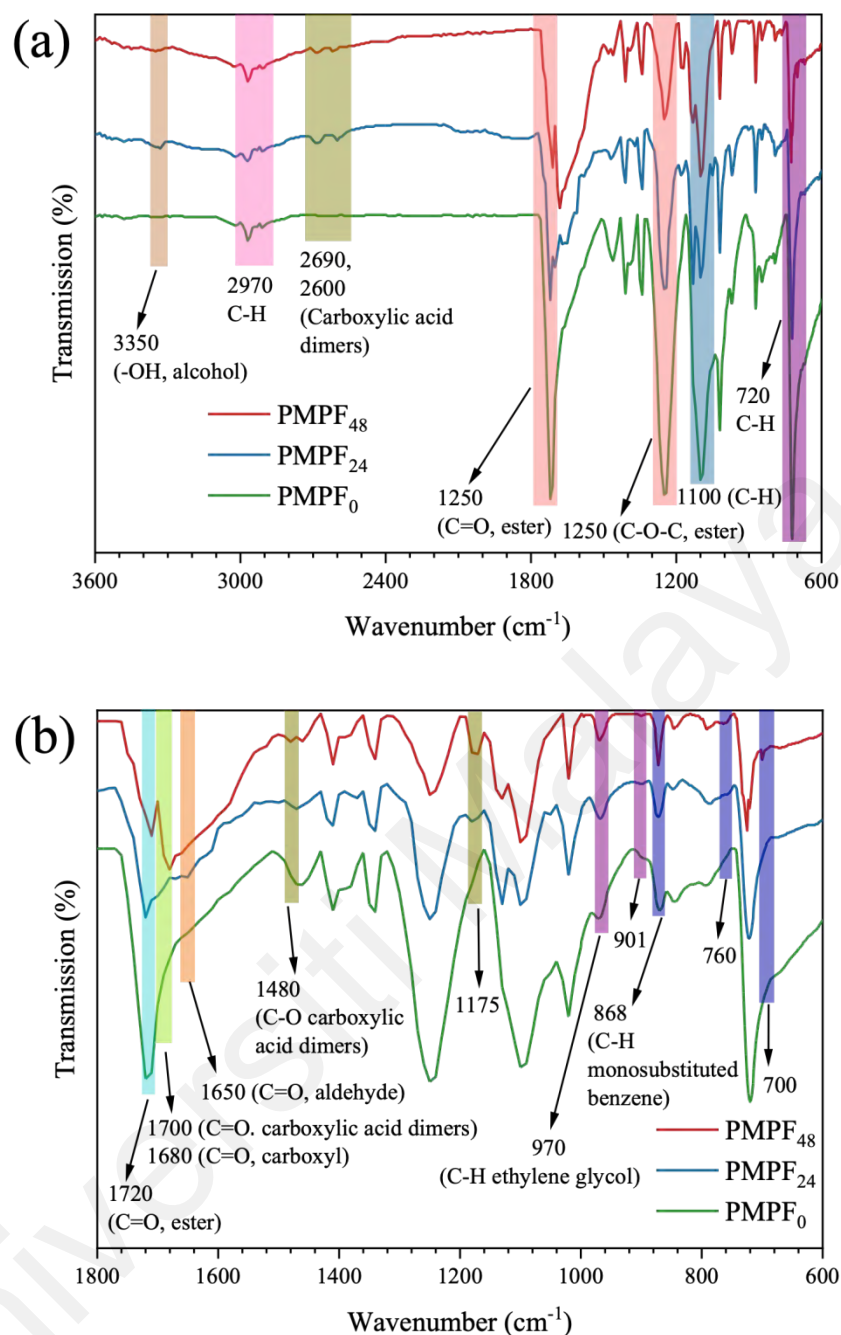
As the photodegradation progresses, significant changes in the FTIR-ATR spectra are observed. In the 3600-1800  $\text{cm}^{-1}$  region, there is an increase in absorbance, especially in

the O-H stretching region, indicating the formation of O-H end groups from alcohols and carboxylic acid dimers. Detailed analysis of the 1800-600  $\text{cm}^{-1}$  region (Fig. 4.11 (b)) reveals a notable increase in absorbance across most regions, with a decrease around 1720  $\text{cm}^{-1}$ , reflecting alterations in C=O groups. The region between 1500-700  $\text{cm}^{-1}$  shows a general decrease in absorbance, with some areas exhibiting new or increased peaks, suggesting variations in the concentration of functional groups such as C-H.

Specifically, the peaks at 3350  $\text{cm}^{-1}$ , 970  $\text{cm}^{-1}$ , and 901  $\text{cm}^{-1}$  become more pronounced, related to the O-H stretch from alcohols and C-H stretches from ethylene glycol isomers. Conversely, the peaks around 1720  $\text{cm}^{-1}$ , linked to ester C=O stretches, gradually diminish, indicating chain scission of ester groups under photo-oxidation and photocatalysis. This degradation leads to the formation of terephthalic acid and ethylene glycol monomers. The peak at 868  $\text{cm}^{-1}$ , reflecting C-H deformation adjacent to benzene rings, decreases slightly, while new peaks at 760  $\text{cm}^{-1}$  and 700  $\text{cm}^{-1}$  suggest substitution reactions on the benzene rings, highlighting complex degradation pathways.

Further analysis reveals significant changes in carbonyl groups, particularly carboxyl groups. There is an increase in absorption bands at 1680  $\text{cm}^{-1}$ , associated with carboxyl C=O stretching vibrations. New peaks and increased absorbance at 2690  $\text{cm}^{-1}$ , 2600  $\text{cm}^{-1}$ , 1700  $\text{cm}^{-1}$ , 1480  $\text{cm}^{-1}$ , and 1175  $\text{cm}^{-1}$  indicate the presence of carboxylic acid dimers. The appearance of C=O stretching vibrations at 1695  $\text{cm}^{-1}$ , linked to aldehyde groups, confirms ongoing degradation. These spectral changes, including the formation of carboxylic acid dimers, suggest that the polyester is likely undergoing dehydration to anhydrides, driven by photo-oxidation, photocatalysis, and ester bond scission mechanisms such as Norrish Type I and II reactions.





**Fig. 4.11. (a) FTIR-ATR spectra of degraded simulated-PMPF by Ag-TiO<sub>2</sub> membranes in 0, 24 and 48 h with enlarged region between (b) 1800-600 cm<sup>-1</sup>.**

#### 4.5.1.3 Photodegradation by-products of simulated-PMPF via GC/MS

GC/MS analysis has provided a comprehensive profile of the by-products generated from the photodegradation of simulated-PMPF, illustrating the efficacy of the photocatalytic treatment. Table. 4.2 details the primary by-products detected, including

their molecular formulas and mass-to-charge ratios ( $m/z$ ). The analysis identified several key compounds resulting from the degradation process.

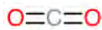
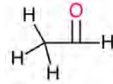

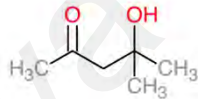
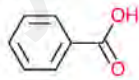
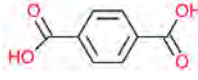
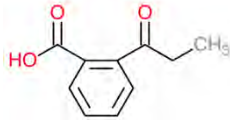
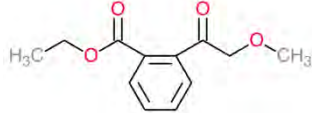
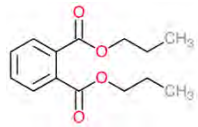
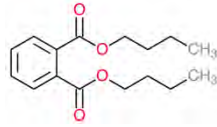
Carbon dioxide and acetaldehyde emerged as simple volatile products, signaling the breakdown of the polymer's carbon chain. The presence of ethylene glycol indicates that the ester bonds within the polyester molecules have been cleaved, resulting in smaller diol molecules. Diacetone alcohol was also detected, a product of the oxidation and cleavage of more complex organic molecules, suggesting that multi-step oxidation reactions are occurring.

Benzoic acid and terephthalic acid were identified as degradation products of the aromatic components of the simulated-PMPF, indicating partial oxidation and decomposition of the aromatic ring structure. Additionally, 4-Propionylbenzoic acid, a further oxidation product of benzoic acid derivatives, reflects more extensive degradation of the aromatic compounds.

Complex ester compounds, such as diethyl phthalate, dipropyl 1,2-phthalate, and bis(2-methylpropyl) 1,2-phthalate, were also observed. These suggest the formation of various esterification products during the degradation process. The variety of detected by-products indicates that multiple chemical reactions—including oxidation, hydrolysis, and free radical-driven processes—are involved in the degradation of simulated-PMPF.

While the detection of simple molecules like carbon dioxide confirms the effectiveness of the photocatalytic process, the presence of complex organic compounds, particularly phthalates and aromatic derivatives, highlights the need for additional treatment steps. Ensuring complete mineralization and evaluating the potential toxicity of these by-products are essential for assessing the overall environmental impact and safety of the photocatalytic degradation process.

**Table. 4.2. The information of the possible intermediate products.**

Chemical name	Formula	m/z	Possible structure
Carbon dioxide	CO <sub>2</sub>	44	
Acetaldehyde	C <sub>2</sub> H <sub>4</sub> O	44	
Ethylene Glycol	C <sub>2</sub> H <sub>6</sub> O <sub>2</sub>	62	
2-Pentanone, 4-hydroxy-4-methyl	C <sub>6</sub> H <sub>12</sub> O <sub>2</sub>	116	
Benzoic acid	C <sub>7</sub> H <sub>6</sub> O <sub>2</sub>	122	
Terephthalic Acid	C <sub>8</sub> H <sub>6</sub> O <sub>4</sub>	166	
4-propionylbenzoic acid	C <sub>10</sub> H <sub>10</sub> O <sub>3</sub>	178	
Diethyl phthalate	C <sub>12</sub> H <sub>12</sub> O <sub>4</sub>	222	
1,2-Benzenedicarboxylic acid, dipropyl ester	C <sub>14</sub> H <sub>18</sub> O <sub>4</sub>	250	
1,2-Benzenedicarboxylic acid, bis(2-methylpropyl) ester	C <sub>16</sub> H <sub>22</sub> O <sub>4</sub>	278	

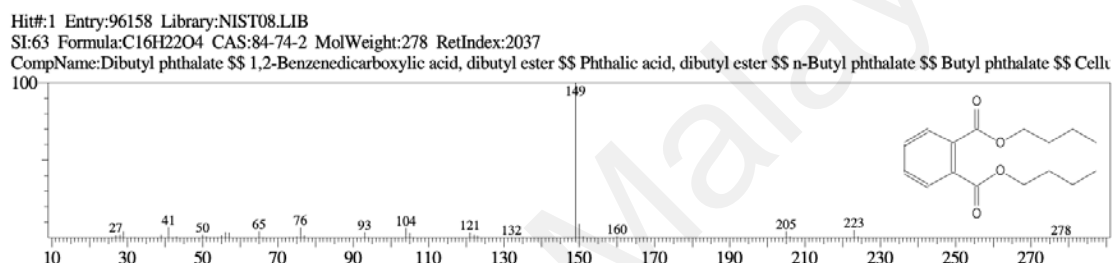
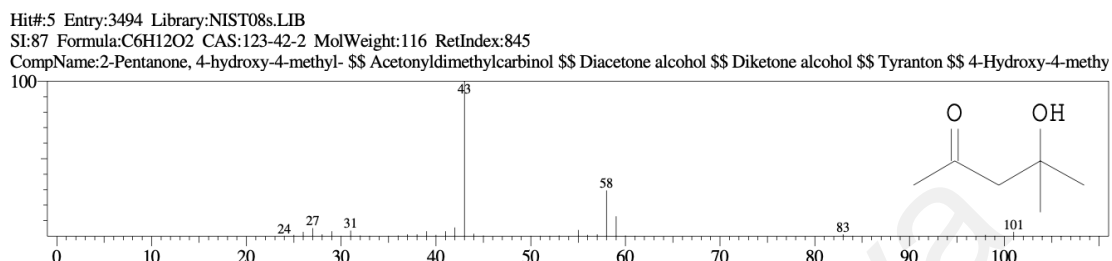
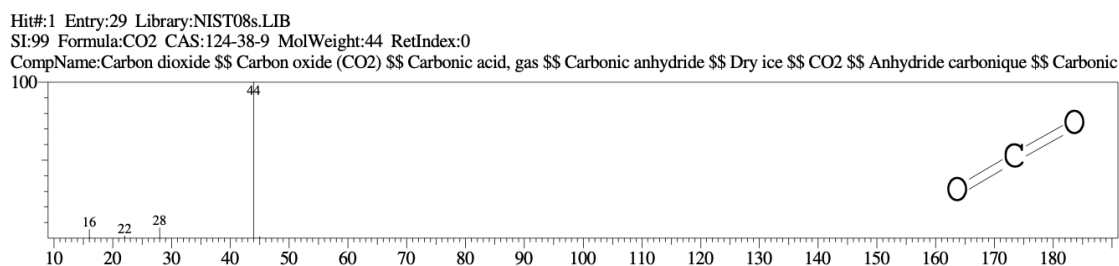


Fig. 4.12. Major possible intermediate products by GC/MS.

## 4.5.2 Membranes performance for PMPF rejection and degradation

### 4.5.2.1 Simulated-PMPF rejection via membranes

The study initially observed that a significant portion of the simulated-PMPF accumulates on the membrane surface due to concentration polarization, complicating the accurate measurement of its concentration in the feed solution. To address this issue, backwashing for the membrane after the experiment was implemented to ensure precise measurements of simulated-PMPF in the feed. The simulated-PMPF was subjected to photocatalytic reactions for varying durations (12, 24, 36, and 48 h) to evaluate the membranes' effectiveness in rejecting and degrading the simulated-PMPF under different photoreaction times. Each test was conducted after the system reached adsorption/desorption equilibrium, using 10 mg of simulated-PMPF per experiment unless otherwise specified.

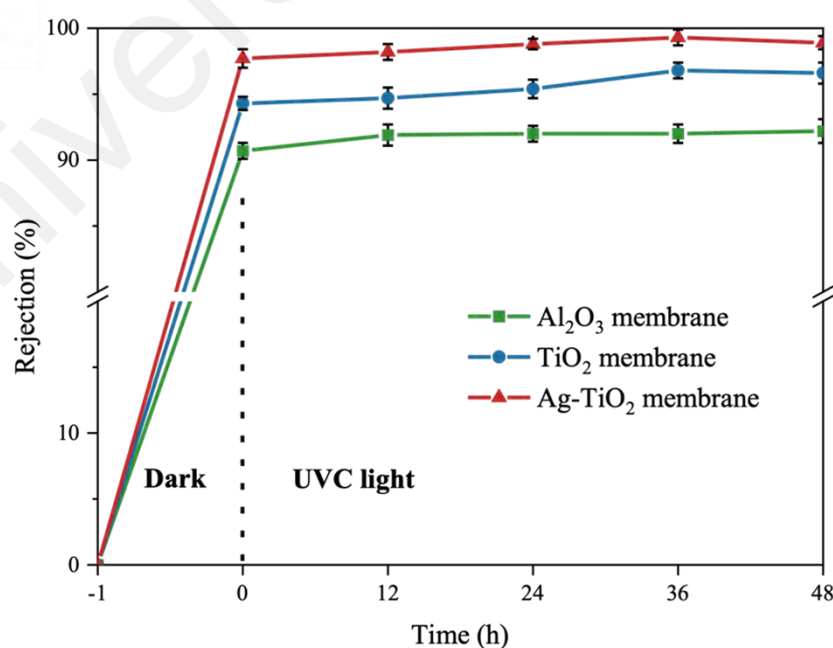
Fig. 4.13 illustrates that after 1 h in the dark, all membranes exhibited high rejection rates for simulated-PMPF, exceeding 90%. This efficiency is attributed to the size screening effect of the membranes, where the pores are smaller than the length of the simulated-PMPF fibers but larger than their diameter, allowing only a few fibers on the membrane surface to pass through longitudinally due to transmembrane pressure differences.

Between 0 and 36 hours of UVC irradiation, the rejection rates for simulated-PMPF increased for all membranes: Al<sub>2</sub>O<sub>3</sub>, TiO<sub>2</sub>, and Ag-TiO<sub>2</sub>, reaching  $90.4 \pm 0.8\%$ ,  $96.8 \pm 1.1\%$ , and  $99.3 \pm 0.6\%$ , respectively. This increase is primarily due to the enhanced hydrophilicity of the membrane surfaces under UVC radiation, which reduces the accumulation of hydrophobic simulated-PMPF. Additionally, the photoactive groups on the Al<sub>2</sub>O<sub>3</sub>, TiO<sub>2</sub>, and Ag-TiO<sub>2</sub> catalytic membranes actively degrade the simulated-PMPF on the membrane surface, thereby minimizing the chances of fibers passing through the membrane longitudinally. Consequently, the rejection performance of the catalytic membranes improves with extended photocatalytic exposure. These results highlight that the high rejection rates achieved by the photocatalytic membranes are due to the combined effects of membrane separation and photocatalysis.

From 0 to 36 h, the rejection rates of the Al<sub>2</sub>O<sub>3</sub>, TiO<sub>2</sub>, and Ag-TiO<sub>2</sub> membranes for simulated-PMPF showed a gradual increase, reaching  $90.4 \pm 0.8\%$ ,  $96.8 \pm 1.1\%$ , and  $99.3 \pm 0.6\%$ , respectively. This progressive improvement is primarily attributed to the enhanced hydrophilicity of the membrane surfaces under UVC radiation, which effectively reduces the accumulation of hydrophobic simulated-PMPF. Moreover, the photoactive groups generated by the TiO<sub>2</sub> and Ag-TiO<sub>2</sub> catalytic membranes actively degrade the simulated-PMPF attached on the membrane surface, reducing the possibility of simulated-PMPF fibers passing through the membrane longitudinally. Consequently,

the rejection performance of the catalytic membranes continues to improve with extended photocatalytic exposure. These findings indicate that the high rejection of the photocatalytic membranes is achieved through the synergistic effects of membrane separation and photocatalysis.

After 36 h there was a slight decrease in the rejection rates of the photocatalytic membranes for simulated-PMPF, while the performance of the  $\text{Al}_2\text{O}_3$  membrane remained relatively stable. This reduction is likely due to the photodegradation of the simulated-PMPF into smaller fragments, which are more likely to pass through the membrane pores. Studies also suggest that smaller microplastics increase turbidity, which could lead to higher turbidity values in the permeate and thus lower rejection rates (Bayarkhuu & Byun, 2022). Overall, the photocatalytic membranes demonstrated superior performance compared to the  $\text{Al}_2\text{O}_3$  membrane, due to their enhanced hydrophilicity and photocatalytic properties that prevent simulated-PMPF adherence and effectively degrade the fibers that do attach.



**Fig. 4.13. Rejection of simulated-PMPF.**

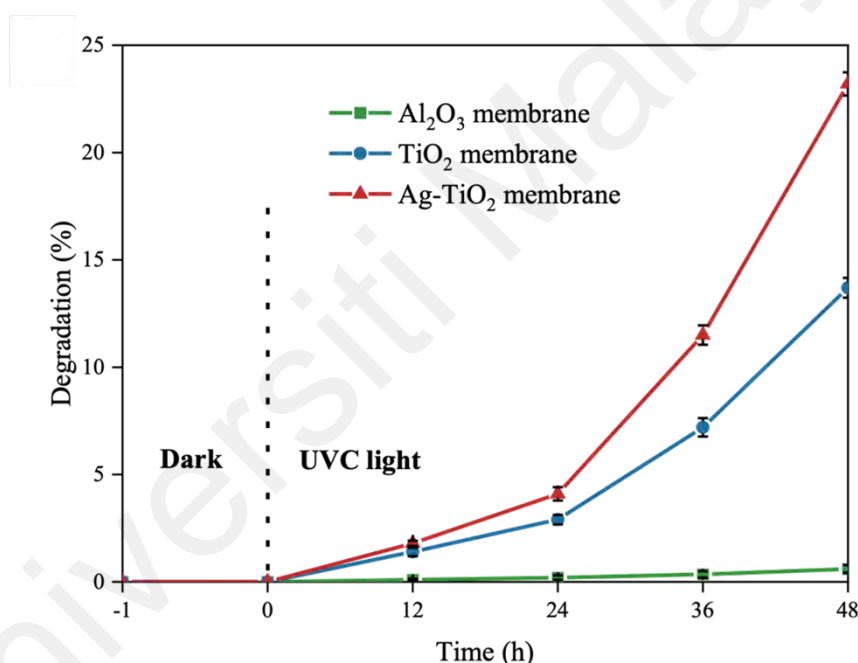
#### 4.5.2.2 Simulated-PMPF degradation via membranes

Fig. 4.14 shows the degradation rates of simulated-PMPF by the  $\text{Al}_2\text{O}_3$ ,  $\text{TiO}_2$ , and Ag- $\text{TiO}_2$  membranes. The Ag- $\text{TiO}_2$  membrane exhibited the highest degradation rate at 23.2 %, followed by 13.7 % for the  $\text{TiO}_2$  membrane and 0.6 % for the  $\text{Al}_2\text{O}_3$  membrane after 48 h. The degradation rate increased with the duration of photocatalytic exposure, supported by FESEM and FTIR analysis, highlighting the destruction of PMPF crystal structure and the formation of oxidation cracks and voids on the surface. In addition, these cracks and voids on the simulated-PMPF further expanded the photocatalytic reaction area. Furthermore, the degradation of simulated-PMPF by all membranes under dark conditions is near zero. The degradation rate of simulated PMPF by  $\text{Al}_2\text{O}_3$  membrane under 48 h UVC irradiation was also less than 1 %. These results confirm that the effective photocatalytic degradation of simulated-PMPF requires the combined action of photocatalyst and UVC light.

Fig. 4.14 presents the degradation rates of simulated-PMPF for the  $\text{Al}_2\text{O}_3$ ,  $\text{TiO}_2$ , and Ag- $\text{TiO}_2$  membranes over a 48-h period. Among these, the Ag- $\text{TiO}_2$  membrane demonstrated the highest degradation rate at 23.2%, significantly outperforming the  $\text{TiO}_2$  membrane, which achieved a degradation rate of 13.7%. In contrast, the  $\text{Al}_2\text{O}_3$  membrane exhibited a minimal degradation rate of 0.6% after the same duration. These results indicate that the presence of silver in the Ag- $\text{TiO}_2$  membrane notably enhances its photocatalytic activity.

The degradation rates increased with the duration of photocatalytic exposure, as evidenced by the FESEM and FTIR analyses. These analyses reveal the destruction of the simulated-PMPF crystal structure, characterized by the development of oxidation cracks and voids on the surface. Such structural changes expand the surface area available for photocatalytic reactions, thereby improving degradation efficiency.

Under dark conditions, the degradation of simulated-PMPF by all membranes was negligible, with the Al<sub>2</sub>O<sub>3</sub> membrane showing less than 1% degradation even after 48 h of UVC irradiation. This underscores that effective photocatalytic degradation of simulated-PMPF necessitates the combined action of a photocatalyst and UVC light. The results confirm that the catalytic membranes' ability to degrade simulated-PMPF is significantly enhanced when both photocatalytic material and UV light are present, with the Ag-TiO<sub>2</sub> membrane being particularly effective due to its superior photocatalytic properties.



**Fig. 14. Degradation of simulated-PMPF.**

#### 4.5.2.3 Performance comparison of immobilized-PMR and other studies

Currently, studies on the elimination of fibrous polyester microplastics using immobilized-PMR are relatively limited. Therefore, Table. 4.3 provides a comparative overview of this study's findings with other research focused on photocatalytic degradation of polyester or polyethylene terephthalate (PET).



Generally, the degradation rates of polyester reported in existing studies are not high, and the effectiveness of different catalysts often hinges on specific experimental conditions, such as pH and light sources. While the Ag-TiO<sub>2</sub> catalytic membrane used in this study does not exhibit the highest polyester degradation rates reported in this table, it demonstrates a significant advantage in practical applications. Specifically, the immobilized-PMR approach employed here achieves substantial degradation rates without the need for extensive pretreatment of polyester or PET materials.

In contrast, approaches such as those by Poerio et al., which involve suspended-PMR systems, achieve similar degradation rates but require frequent membrane cleaning and maintenance (Poerio et al., 2024). The immobilized-PMR technique used in this study not only simplifies the operational setup but also enhances the degradation and separation rate of polyester fibers. This approach minimizes the risk of membrane contamination and operational complexities, offering a more streamlined and effective solution compared to other photocatalytic methods. Thus, while the Ag-TiO<sub>2</sub> membrane may not lead the field in terms of maximum degradation rates, the immobilized-PMR has practical benefits in terms of operational simplicity and effectiveness in degrading and separating polyester fibers are notable.

**Table. 4.3. Comparison of the polyester microplastic degradation in this study and other research.**

<b>Polyester shape</b>	<b>Degradation method</b>	<b>Catalyst</b>	<b>Experiment condition</b>	<b>Degradation rate (%)</b>	<b>Ref</b>
fiber	Photocatalysis + membrane separation	TiO <sub>2</sub> and	pH = 7;	13.7	This study
		Ag-TiO <sub>2</sub> membrane	React time = 48 h; Catalyst = 50 mg;	23.2	
fragment	Photocatalysis	TiO <sub>2</sub> /MIL-100 (Fe) in fine mesh	PET = 10 mg; pH = 3; React time = 5 h; Catalyst = 200 mg;	-	(Rojas - Guerrero et al., 2023)
fiber	Photocatalysis	Ni <sub>5</sub> P <sub>4</sub> /TiO <sub>2</sub> /C nanofilm	PET = 100 mg/L; React time = 12 h;	6.23	(Peng et al., 2023)
fiber	Photocatalysis	Bi <sub>2</sub> O <sub>3</sub> @N-TiO <sub>2</sub> powder	pH = 9; React time = 48 h; Catalyst = 50 mg;	10.23	(Zhou, Wang, et al., 2022)
fiber	Photocatalysis + membrane separation	TiO <sub>2</sub> + MF/UF membrane	PET = 10 mg/L; pH = 3 React time = 48h; Catalyst = 500 mg;	13.52	(Poerio et al., 2024)
-	Photocatalysis	Fe <sub>3</sub> O <sub>4</sub> @SiO <sub>2</sub> powder	PET = 100 mg/L; Additive = peroxymonosulfat; React time = 192 h; Catalyst = 91 mg; PET = 900 mg;	13.65	(Blanco-Gutiérrez et al., 2022)

**Table. 4.3 continued**

powder	Photocatalysis	C,N-TiO <sub>2</sub> /SiO <sub>2</sub> powder	pH = 6; React time = 120 h; Catalyst = 200 mg;	16.22	(Ariza - Tarazona et al., 2023)
fiber	Photocatalysis	Pt@N-TiO <sub>2</sub> -1.5% powder	PET = 200 mg; A hydrothermal pre-treatment = (180 °C/12h) React time = 48 h; Catalyst = 20 mg; PET = 100 mg/L;	28.96	(Zhou, Luo, et al., 2022)

#### 4.5.2.4 Pure water flux and anti-fouling performance

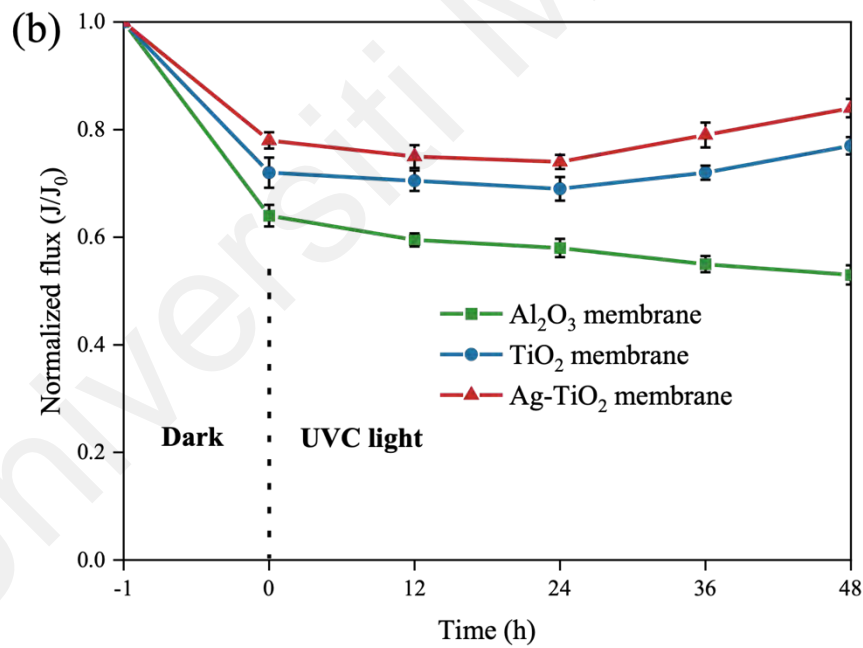
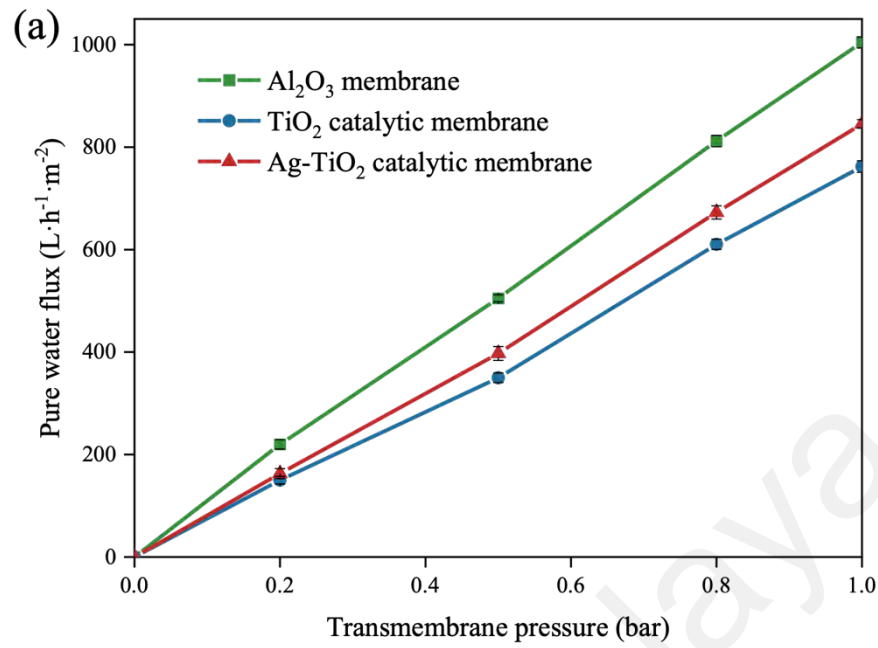
To comprehensively evaluate the performance of the membranes beyond rejection and degradation rates, their pure water flux and anti-fouling properties were examined. The flux of  $\text{Al}_2\text{O}_3$ ,  $\text{TiO}_2$ , and  $\text{Ag-TiO}_2$  membranes was assessed under two conditions: 1 h in darkness and 48 h of continuous UVC illumination. As illustrated in Fig. 4.15 (a), the pure water flux for  $\text{TiO}_2$  and  $\text{Ag-TiO}_2$  membranes decreased by 24.1% and 15.8%, respectively, compared to the  $\text{Al}_2\text{O}_3$  membrane. This reduction is largely attributed to the presence of catalyst particles, which can obstruct the membrane pores. Despite these reductions, the benefits of the added photocatalytic functionalities are considered to outweigh the decrease in flux.

The anti-fouling performance was assessed by measuring the normalized permeate flux ( $J/J_0$ ) during filtration of simulated-PMPF. Fig. 4.15 (b) shows the flux decline over a 1 h dark period followed by 48 h of UVC irradiation. Initially, the  $\text{Al}_2\text{O}_3$  membrane experienced a 36% reduction in flux. In contrast, the  $\text{TiO}_2$  and  $\text{Ag-TiO}_2$  membranes exhibited lower reductions of 28% and 22%, respectively. Upon UVC exposure duration, the flux decline for the  $\text{Al}_2\text{O}_3$  membrane further increased to 47%, while the reductions for the  $\text{TiO}_2$  and  $\text{Ag-TiO}_2$  membranes improved to 23% and 16%, respectively. These results indicate that the photocatalytic membranes, particularly those with  $\text{TiO}_2$  and  $\text{Ag-TiO}_2$ , exhibit enhanced anti-fouling properties. This improvement is attributed to the increased hydrophilicity and the self-cleaning effect induced by photocatalytic activity under UVC light.

The observed improvement in flux stability for  $\text{TiO}_2$  and  $\text{Ag-TiO}_2$  membranes, compared to the  $\text{Al}_2\text{O}_3$  membrane, aligns with their enhanced hydrophilicity, as confirmed by contact angle measurements. The UVC irradiation further enhances the hydrophilicity of these membranes, leading to higher water flux and reduced adherence

of hydrophobic simulated-PMPF. This synergy between photocatalytic activity and increased hydrophilicity demonstrates the effectiveness of these membranes in maintaining performance and mitigating fouling, even under demanding conditions (Chen et al., 2024; Farahbakhsh et al., 2024).

Universiti Malaya



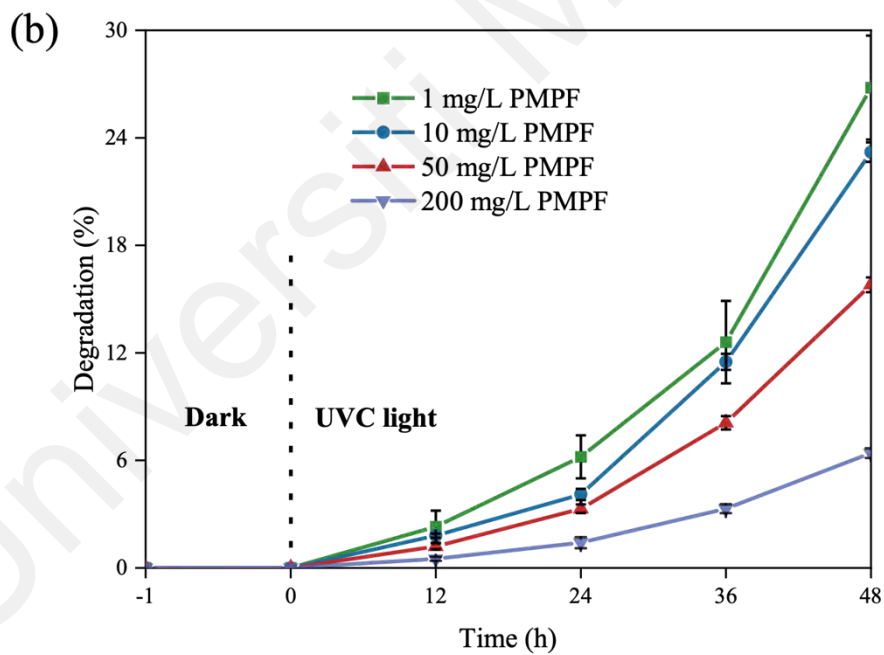
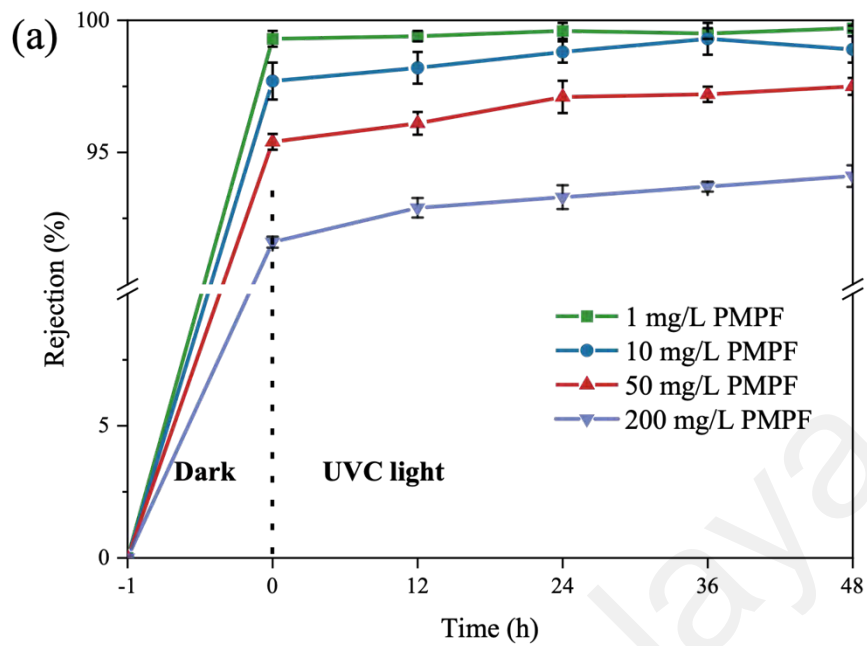
**Fig. 4.15. (a) Pure water flux under different TMP; (b) normalized permeate flux of all membranes.**

#### 4.5.2.5 Effect of concentration for simulated-PMPF removal

The impact of simulated-PMPF concentration on membrane performance was evaluated by measuring rejection and degradation rates across different concentrations ranging from 1 to 200 mg/L. As depicted in Fig. 4.16 (a), the rejection rates for the Al<sub>2</sub>O<sub>3</sub>, TiO<sub>2</sub>, and Ag-TiO<sub>2</sub> membranes decreased as the concentration of simulated-PMPF increased. Specifically, the rejection rates were 99.2%, 98.9%, 97.5%, and 94.1% at concentrations of 1, 10, 50, and 200 mg/L, respectively. This decline in rejection rate is attributed to the increased concentration of simulated-PMPF accumulating in the filter cake layer, which raises the likelihood of fibers passing the membrane longitudinally.

In parallel, Fig. 4.16 (b) illustrates a reduction in the degradation rate of simulated-PMPF with increasing concentration. At the highest tested concentration of 200 mg/L, the degradation rate fell to 6.4%. This substantial decrease is primarily due to the formation of a thick filter cake layer on the membrane surface, which impedes the effective activation of the photocatalyst by UVC light. The large error bar associated with the 1 mg/L concentration suggests potential inaccuracies in measuring very low degradation rates, possibly due to the experimental challenges of handling low concentrations.

These findings underscore the difficulties associated with treating high concentrations of simulated-PMPF. The results highlight the need for optimizing operational parameters, such as membrane flux and catalyst loading, to improve both rejection and degradation performance under varying pollutant loads.



**Fig. 4.16. The (a) rejection and (b) degradation of Ag-TiO<sub>2</sub> membrane for simulated-PMPF with different concentrations.**



#### 4.5.2.6 Removal of real-PMPF in actual laundry wastewater

To validate the immobilized-PMR performance in practical application, evaluating the membrane flux and rejection rate in the real-PMPF treatment process. The laundry wastewater, sourced from washing polyester garments with tap water at Universiti Malaya, was characterized by a pH of 6.7, a conductivity of 1.956 mg/L, a total nitrogen content of 53.6  $\mu\text{S}/\text{cm}$ , and a turbidity of 71 NTU. In contrast, tap water had a pH of 6.5, conductivity of 1.254 mg/L, total nitrogen content of 11.3  $\mu\text{S}/\text{cm}$ , and a turbidity of 8.2 NTU. In addition, the real-PMPF concentration in the wastewater after the fifth wash ranged from 3.57 to 178 mg per washing.

As shown in Fig. 4.17 (a), the permeate flux through the membranes was significantly reduced when filtering real-PMPF compared to simulated-PMPF. The final normalized permeate flux values for the  $\text{Al}_2\text{O}_3$ ,  $\text{TiO}_2$ , and  $\text{Ag-TiO}_2$  membranes were 0.35, 0.57, and 0.65, respectively. This reduction is attributed to the formation of a dense filter cake layer on the membrane surface, composed of real-PMPF and other organic and inorganic substances present in the wastewater. This layer significantly decreases permeate flux and impedes UVC light from effectively activating the photocatalytic layer, leading to reduced flux performance. Similar reductions of membrane flux due to membrane fouling from organic and inorganic materials have been reported in previous studies (Wols & Hofman-Caris, 2012; Zakria et al., 2024).

Fig. 4.17 (b) illustrates that the rejection rates for real-PMPF by all three membranes exceeded 95%, with the  $\text{Ag-TiO}_2$  membrane achieving the highest performance, producing permeate with near-zero turbidity. This enhanced performance is attributed to the smaller pore size resulting from the  $\text{Ag-TiO}_2$  catalyst immobilization, which improves real-PMPF rejection rate. Although the rejection rates for real wastewater were notably higher than those for simulated wastewater, the presence of real-PMPF adsorbed onto

larger particulates might negatively affect the degradation rate. This analysis underscores the complexities involved in treating real wastewater and highlights the advanced capabilities of photocatalytic membranes, particularly those incorporating Ag-TiO<sub>2</sub>, in effectively addressing such challenging conditions.

Universiti Malaya

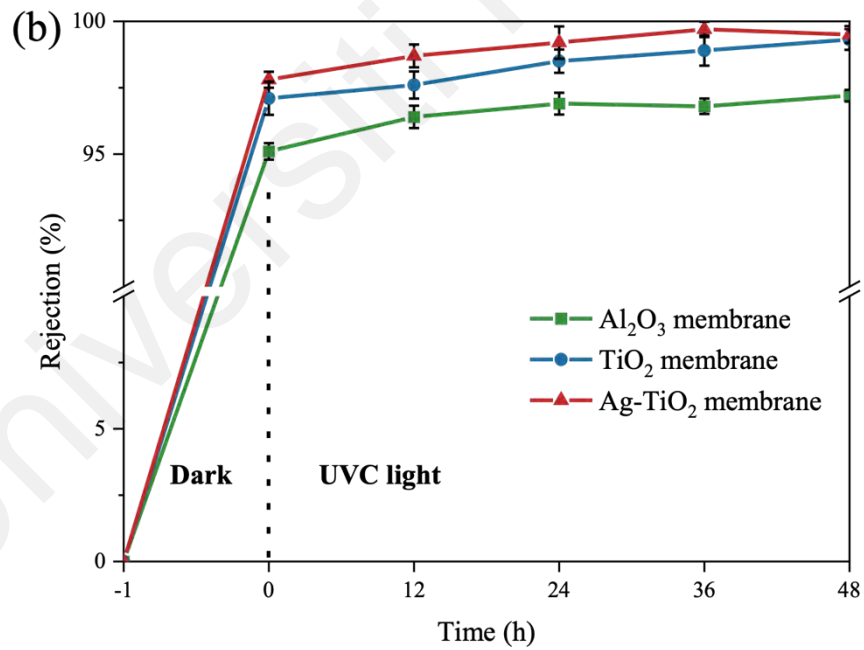
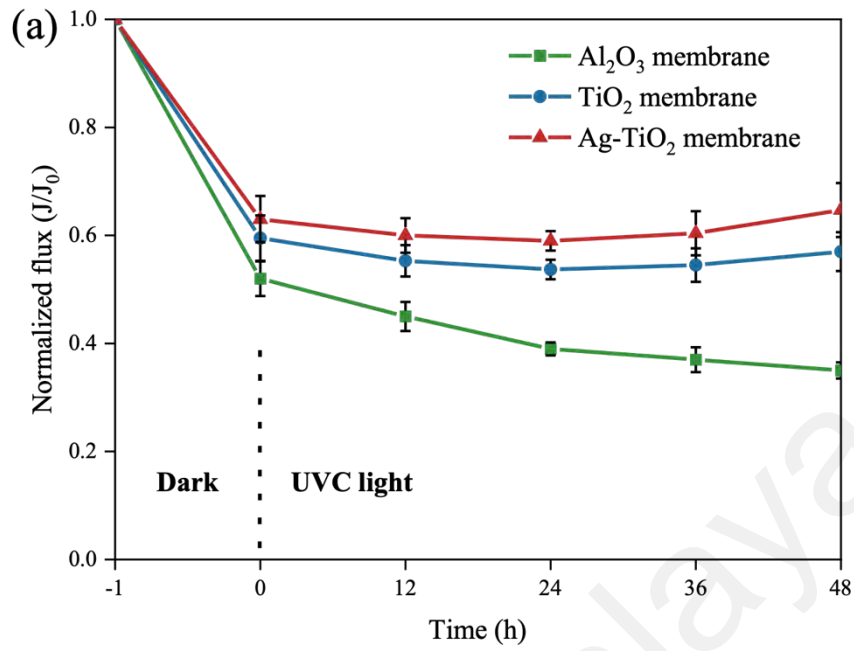


Fig. 4.17. (a) Normalized permeate flux; (b) rejection of real-PMPF.

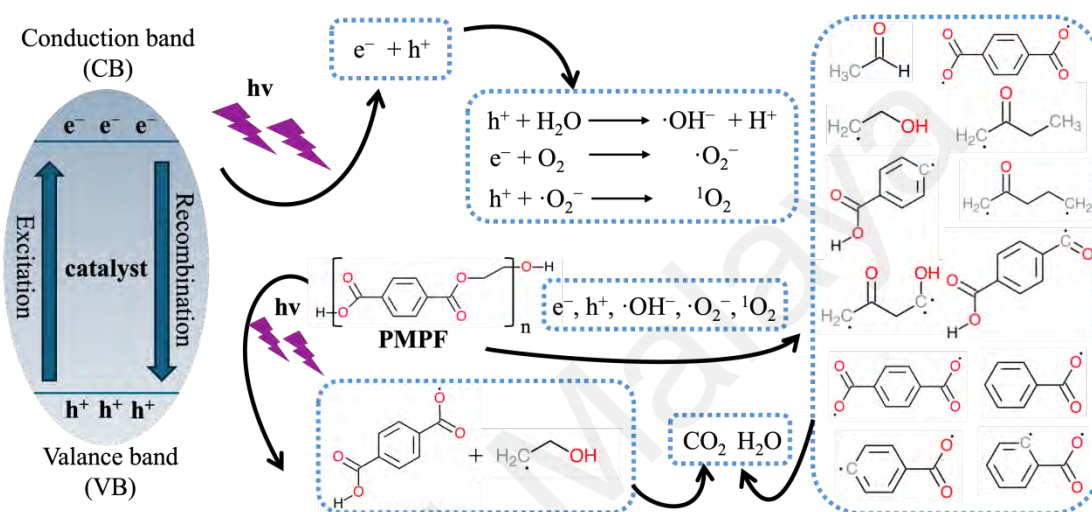
### 4.5.3 Possible degradation mechanism of simulated-PMPF

The degradation of simulated-PMPF under photocatalytic conditions is driven by a combination of photooxidation and photocatalytic oxidation processes. Photooxidation primarily causes chain scission within the simulated-PMPF, notably breaking ester bonds. This bond cleavage leads to a decrease in polymer molecular weight and the formation of carboxyl end groups, as detailed by previous studies (Hurley & Leggett, 2009; Sang et al., 2020).

Photocatalytic oxidation involves the generation of electron-hole ( $e^-$ - $h^+$ ) pairs when  $TiO_2$  and Ag- $TiO_2$  catalytic membranes are irradiated with UVC light. In this process, electrons transition from the valence band to the conduction band of the photocatalyst, creating electron-hole pairs. Notably, the Ag- $TiO_2$  membranes exhibit a lower recombination rate of these electron-hole pairs compared to  $TiO_2$  membranes, owing to Ag's role as an electron acceptor. This enhancement in photocatalytic efficiency is crucial for the process. The unrecombined electrons can interact directly with simulated-PMPF or react with water and oxygen to produce reactive oxygen species (ROS), such as hydroxyl radicals ( $\cdot OH$ ), superoxide anions ( $\cdot O_2^-$ ), and singlet oxygen ( $^1O_2$ ). These ROS are highly reactive and play a significant role in the degradation of simulated-PMPF molecules.

Based on the analysis presented, the inferred mechanism for the degradation of simulated-PMPF is detailed in Fig. 4.18. Research suggests that ROS, such as  $\cdot OH$ ,  $\cdot O_2^-$ , and  $^1O_2$ , play a crucial role in this process through mechanisms such as free radical adduct formation, hydrogen atom extraction, and electron transfer (Qiu et al., 2023; Shi et al., 2022). The  $\cdot OH$ , known for its high redox potential, is particularly significant in the breakdown of simulated-PMPF. This radical engages in reactions with aliphatic carboxylic acids to form highly reactive carbon-centered free radicals by extracting

hydrogen atoms. It can also hydroxylate aromatic carboxylic acids, further contributing to the degradation process. Additionally, the  $\cdot\text{O}_2^-$  interacts with simulated-PMPF to generate carbon-based free radicals and additional carboxylic acids, while  $^1\text{O}_2$  selectively oxidizes alcohols. These reactive intermediates eventually decompose into water and carbon dioxide, completing the degradation pathway.



**Fig. 4.18. Diagram of possible mechanism of simulated-PMPF degradation.**

## CHAPTER 5: CONCLUSION

This study investigates the effectiveness of an innovative TiO<sub>2</sub>-based immobilized-PMR for eliminating simulated- and real- PMPF from laundry wastewater. Comprehensive analyses, including morphological and structural assessments, confirmed the successful immobilization of TiO<sub>2</sub> and Ag-TiO<sub>2</sub> on Al<sub>2</sub>O<sub>3</sub> ceramic membranes, which exhibited significantly enhanced hydrophilicity and photocatalytic properties. Among the tested membranes, the Ag-TiO<sub>2</sub> membrane demonstrated superior performance, achieving up to 99% rejection of simulated- and real- PMPF, with a degradation rate of 23.2% for simulated-PMPF under UVC irradiation.

This study also confirmed the real-world applicability of the photocatalytic membranes by testing them with actual laundry wastewater. The Ag-TiO<sub>2</sub> membrane showed excellent flux stability and high rejection rates for real-PMPF, demonstrating its practical utility in wastewater treatment. FTIR and GC/MS analyses of the degradation mechanism revealed that ROS play a critical role in breaking down polyester fibers. These ROS facilitate the conversion of larger polymer structures into smaller fragments, eventually mineralizing them into water and carbon dioxide. This understanding underscores the potential of photocatalytic membranes in addressing MPs pollution effectively.

Overall, the immobilized-PMR offers a promising, efficient, and practical solution for the removal of polyester fiber from laundry wastewater. The synergy between photocatalysis and membrane filtration, particularly with Ag-TiO<sub>2</sub> catalysts, presents a robust framework for developing advanced wastewater treatment technologies aimed at tackling fibrous MPs pollution.

## REFERENCES

- Adam, M. R., Othman, M. H. D., Sheikh Abdul Kadir, S. H., Mohd Sokri, M. N., Tai, Z. S., Iwamoto, Y., Tanemura, M., Honda, S., Puteh, M. H., & Rahman, M. A. (2020). Influence of the natural zeolite particle size toward the ammonia adsorption activity in ceramic hollow fiber membrane. *Membranes*, *10*(4), 63.
- Ahmad, I., Shukrullah, S., Naz, M. Y., Ahmed, E., Ahmad, M., Obaidullah, A. J., Alkhouri, A., Mahal, A., & Ghadi, Y. Y. (2024). An aimed review of current advances, challenges, and future perspectives of TiO<sub>2</sub>-based S-scheme heterojunction photocatalysts. *Materials Science in Semiconductor Processing*, *172*, 108088.
- Ahmad, R., Lee, C. S., Kim, J. H., & Kim, J. (2020). Partially coated TiO<sub>2</sub> on Al<sub>2</sub>O<sub>3</sub> membrane for high water flux and photodegradation by novel filtration strategy in photocatalytic membrane reactors. *Chemical Engineering Research and Design*, *163*, 138-148.
- Ahmed, D. S., Al-Baidhani, M., Adil, H., Bufaroosha, M., Rashad, A. A., Zainulabdeen, K., & Yousif, E. (2023). Recent study of PF/ZnO nanocomposites: Synthesis, characterization and optical properties. *Materials Science for Energy Technologies*, *6*, 29-34.
- Ahmed, S. (2011). *Development of heterogeneous photocatalytic water purification technology for storm and wastewater reuse* [CQUUniversity].
- Al Mamun, A., Prasetya, T. A. E., Dewi, I. R., & Ahmad, M. (2023). Microplastics in human food chains: Food becoming a threat to health safety. *Science of the Total Environment*, *858*, 159834.
- Alabi, O. A., Ologbonjaye, K. I., Awosolu, O., & Alalade, O. E. (2019). Public and environmental health effects of plastic wastes disposal: a review. *J Toxicol Risk Assess*, *5*(021), 1-13.
- Alem, A., Sarpoolaky, H., & Keshmiri, M. (2009). Sol-gel preparation of titania multilayer membrane for photocatalytic applications. *Ceramics International*, *35*(5), 1837-1843.
- Ali, H., Kim, K. W., Bang, S. G., Chae, H. B., Shin, S. W., & Park, C. W. (2019). Numerical modeling of fluid-structure interaction between sewage water flow and bar screen to improve the screening process. *Water and Environment Journal*, *33*(4), 560-573.
- Ali, I., Ding, T., Peng, C., Naz, I., Sun, H., Li, J., & Liu, J. (2021). Micro-and nanoplastics in wastewater treatment plants: occurrence, removal, fate, impacts and remediation technologies—a critical review. *Chemical Engineering Journal*, *423*, 130205.
- Alvim, C. B., Mendoza-Roca, J. A., & Bes-Piá, A. (2020). Wastewater treatment plant as microplastics release source—quantification and identification techniques. *Journal of Environmental Management*, *255*, 109739.

- Anan, N. S. M., Jaafar, J., Sato, S., & Mohamud, R. (2021). Titanium dioxide incorporated polyamide thin film composite photocatalytic membrane for bisphenol A removal. *IOP Conference Series: Materials Science and Engineering*,
- Anbumani, S., & Kakkar, P. (2018). Ecotoxicological effects of microplastics on biota: a review. *Environmental Science and Pollution Research*, *25*, 14373-14396.
- Arenas-Guerrero, P., Delgado, Á. V., Donovan, K. J., Scott, K., Bellini, T., Mantegazza, F., & Jiménez, M. L. (2018). Determination of the size distribution of non-spherical nanoparticles by electric birefringence-based methods. *Scientific reports*, *8*(1), 1-10.
- Ariza-Tarazona, M. C., Siligardi, C., Carreón-López, H. A., Valdéz-Cerda, J. E., Pozzi, P., Kaushik, G., Villarreal-Chiu, J. F., & Cedillo-González, E. I. (2023). Low environmental impact remediation of microplastics: Visible-light photocatalytic degradation of PET microplastics using bio-inspired C, N-TiO<sub>2</sub>/SiO<sub>2</sub> photocatalysts. *Marine pollution bulletin*, *193*, 115206.
- Arslan, E., Demir, T., Üstünyıldız, B., & Pakdil, N. B. (2023). Operational issues and proposed solutions in wastewater treatment plants in the Western Black Sea basin of Turkey. *Materials Today: Proceedings*.
- Banerjee, S., Dionysiou, D. D., & Pillai, S. C. (2015). Self-cleaning applications of TiO<sub>2</sub> by photo-induced hydrophilicity and photocatalysis. *Applied Catalysis B: Environmental*, *176*, 396-428.
- Bao, R., Wang, Z., Qi, H., Mehmood, T., Cai, M., Zhang, Y., Yang, R., Peng, L., & Liu, F. (2022). Occurrence and distribution of microplastics in wastewater treatment plant in a tropical region of China. *Journal of Cleaner Production*, *349*, 131454.
- Baresel, C., Harding, M., & Fang, J. (2019). Ultrafiltration/granulated active carbon-biofilter: efficient removal of a broad range of micropollutants. *Applied Sciences*, *9*(4), 710.
- Batool, A., & Valiyaveetil, S. (2021). Surface functionalized cellulose fibers—A renewable adsorbent for removal of plastic nanoparticles from water. *Journal of Hazardous Materials*, *413*, 125301.
- Bayarkhuu, B., & Byun, J. (2022). Optimization of coagulation and sedimentation conditions by turbidity measurement for nano-and microplastic removal. *Chemosphere*, *306*, 135572.
- Bayo, J., Olmos, S., & López-Castellanos, J. (2020). Microplastics in an urban wastewater treatment plant: The influence of physicochemical parameters and environmental factors. *Chemosphere*, *238*, 124593.
- Bet-Moushoul, E., Mansourpanah, Y., Farhadi, K., & Tabatabaei, M. (2016). TiO<sub>2</sub> nanocomposite based polymeric membranes: a review on performance improvement for various applications in chemical engineering processes. *Chemical Engineering Journal*, *283*, 29-46.



- Bian, J., Wang, X., Feng, Y., Tong, H., Zu, H., Yu, Y., Wang, S., Zu, J., Zhang, H., & Liu, H. (2024). Crystal structural, magnetic, and dielectric properties of Cobalt-doped breathing pyrochlore  $\text{LiInCr}_{4-x}\text{Co}_x\text{O}_8$ . *Materials Research Express*, *11*(1), 016101.
- Biao, W., Hashim, N. A., Rabuni, M. F. B., Lide, O., & Ullah, A. (2024). Microplastics in aquatic systems: an in-depth review of current and potential water treatment processes. *Chemosphere*, 142546.
- Binazadeh, M., Rasouli, J., Sabbaghi, S., Mousavi, S. M., Hashemi, S. A., & Lai, C. W. (2023). An Overview of Photocatalytic Membrane Degradation Development. *Materials*, *16*(9), 3526.
- Blackburn, K., & Green, D. (2022). The potential effects of microplastics on human health: What is known and what is unknown. *Ambio*, *51*(3), 518-530.
- Blair, R. M., Waldron, S., & Gauchotte-Lindsay, C. (2019). Average daily flow of microplastics through a tertiary wastewater treatment plant over a ten-month period. *Water Research*, *163*, 114909.
- Blanco-Gutiérrez, V., Li, P., Berzal-Cabetas, R., & Dos santos-García, A. (2022). Exploring the photocatalytic activity of nanometric magnetite for PET materials degradation under UV light. *Journal of Solid State Chemistry*, *316*, 123509.
- Blettler, M. C., Ulla, M. A., Rabuffetti, A. P., & Garello, N. (2017). Plastic pollution in freshwater ecosystems: macro-, meso-, and microplastic debris in a floodplain lake. *Environmental monitoring and assessment*, *189*, 1-13.
- Boucher, J., & Friot, D. (2017). *Primary microplastics in the oceans: a global evaluation of sources* (Vol. 43). Iucn Gland, Switzerland.
- Cabernard, L., Roscher, L., Lorenz, C., Gerdt, G., & Primpke, S. (2018). Comparison of Raman and Fourier transform infrared spectroscopy for the quantification of microplastics in the aquatic environment. *Environmental science & technology*, *52*(22), 13279-13288.
- Caputo, F., Vogel, R., Savage, J., Vella, G., Law, A., Della Camera, G., Hannon, G., Peacock, B., Mehn, D., & Ponti, J. (2021). Measuring particle size distribution and mass concentration of nanoplastics and microplastics: addressing some analytical challenges in the sub-micron size range. *Journal of Colloid and Interface Science*, *588*, 401-417.
- Carmichael, A. (2015). Man-made fibers continue to grow. *Textile World*, *165*(705), 20-22.
- Carr, B., & Wright, M. (2008). Nanoparticle tracking analysis. *Innovations in Pharmaceutical Technology*, *26*, 38-40.
- Cesa, F. S., Turra, A., Checon, H. H., Leonardi, B., & Baroque-Ramos, J. (2020). Laundering and textile parameters influence fibers release in household washings. *Environmental Pollution*, *257*, 113553.

- Chen, D., Li, F., & Ray, A. K. (2001). External and internal mass transfer effect on photocatalytic degradation. *Catalysis Today*, 66(2-4), 475-485.
- Chen, H., Chen, H., Nan, S., Liu, H., Chen, L., & Yu, L. (2022). Investigation of Microplastics in Digestion System: Effect on Surface Microstructures and Probiotics. *Bulletin of Environmental Contamination and Toxicology*, 109(5), 882-892.
- Chen, J., Qiu, F., Xu, W., Cao, S., & Zhu, H. (2015). Recent progress in enhancing photocatalytic efficiency of TiO<sub>2</sub>-based materials. *Applied Catalysis A: General*, 495, 131-140.
- Chen, L., Xu, P., & Wang, H. (2022). Photocatalytic membrane reactors for produced water treatment and reuse: Fundamentals, affecting factors, rational design, and evaluation metrics. *Journal of Hazardous Materials*, 424, 127493.
- Chen, R., Hu, L., Zhang, H., Lin, D., Wang, J., Xu, D., Gong, W., & Liang, H. (2022). Toward emerging contaminants removal using acclimated activated sludge in the gravity-driven membrane filtration system. *Journal of Hazardous Materials*, 438, 129541.
- Chen, S.-y., Li, L., Feng, M., Huang, T., Zhang, N., & Wang, Y. (2024). UV-activated superwetting ability of electrospun polysulfone/titanium dioxide membranes toward highly efficient methylene blue removal and oil/water separation. *Journal of Membrane Science*, 695, 122450.
- Cheng, Y. L., Kim, J.-G., Kim, H.-B., Choi, J. H., Tsang, Y. F., & Baek, K. (2021). Occurrence and removal of microplastics in wastewater treatment plants and drinking water purification facilities: A review. *Chemical Engineering Journal*, 410, 128381.
- Cole, M. (2016). A novel method for preparing microplastic fibers. *Scientific Reports*, 6(1), 1-7.
- Conley, K., Clum, A., Deepe, J., Lane, H., & Beckingham, B. (2019). Wastewater treatment plants as a source of microplastics to an urban estuary: Removal efficiencies and loading per capita over one year. *Water research X*, 3, 100030.
- Corami, F., Rosso, B., Bravo, B., Gambaro, A., & Barbante, C. (2020). A novel method for purification, quantitative analysis and characterization of microplastic fibers using Micro-FTIR. *Chemosphere*, 238, 124564.
- Costa, D., Rodrigues, M. S., Roiban, L., Borges, J., Steyer, P., & Vaz, F. (2024). Transmission electron microscopy reveals clusters of Au–Ag nanoparticles formed in TiO<sub>2</sub> thin film, with enhanced plasmonic response. *Journal of Physics D: Applied Physics*, 57(23), 235304.
- Coyle, R., Hardiman, G., & O'Driscoll, K. (2020). Microplastics in the marine environment: A review of their sources, distribution processes, uptake and exchange in ecosystems. *Case Studies in Chemical and Environmental Engineering*, 2, 100010.

- Crawford, C. B., & Quinn, B. (2017). The interactions of microplastics and chemical pollutants. *Microplastic pollutants*, 131-157.
- Cristaldi, A., Fiore, M., Zuccarello, P., Oliveri Conti, G., Grasso, A., Nicolosi, I., Copat, C., & Ferrante, M. (2020). Efficiency of wastewater treatment plants (WWTPs) for microplastic removal: A systematic review. *International journal of environmental research and public health*, 17(21), 8014.
- Danfá, S., Martins, R. C., Quina, M. J., & Gomes, J. (2021). Supported TiO<sub>2</sub> in ceramic materials for the photocatalytic degradation of contaminants of emerging concern in liquid effluents: A Review. *Molecules*, 26(17), 5363.
- De Falco, F., Cocca, M., Guarino, V., Gentile, G., Ambrogio, V., Ambrosio, L., & Avella, M. (2019). Novel finishing treatments of polyamide fabrics by electrofluidodynamic process to reduce microplastic release during washings. *Polymer Degradation and Stability*, 165, 110-116.
- De Falco, F., Di Pace, E., Cocca, M., & Avella, M. (2019). The contribution of washing processes of synthetic clothes to microplastic pollution. *Scientific reports*, 9(1), 1-11.
- de Oliveira, C. R. S., da Silva Júnior, A. H., Mulinari, J., Ferreira, A. J. S., & da Silva, A. (2023). Fibrous microplastics released from textiles: Occurrence, fate, and remediation strategies. *Journal of Contaminant Hydrology*, 104169.
- Deba, S. A. H., Wols, B. A., Yntema, D. R., & Lammertink, R. G. (2023). Advanced ceramics in radical filtration: TiO<sub>2</sub> layer thickness effect on the photocatalytic membrane performance. *Journal of Membrane Science*, 672, 121423.
- Deepracha, S., Atfane, L., Ayrál, A., & Ogawa, M. (2021). Simple and efficient method for functionalizing photocatalytic ceramic membranes and assessment of its applicability for wastewater treatment in up-scalable membrane reactors. *Separation and purification technology*, 262, 118307.
- Deng, Y., Zhang, Y., Qiao, R., Bonilla, M. M., Yang, X., Ren, H., & Lemos, B. (2018). Evidence that microplastics aggravate the toxicity of organophosphorus flame retardants in mice (*Mus musculus*). *Journal of hazardous materials*, 357, 348-354.
- Détrée, C., & Gallardo-Escárate, C. (2018). Single and repetitive microplastics exposures induce immune system modulation and homeostasis alteration in the edible mussel *Mytilus galloprovincialis*. *Fish & shellfish immunology*, 83, 52-60.
- Domínguez-Jaimes, L. P., Cedillo-González, E. I., Luévano-Hipólito, E., Acuña-Bedoya, J. D., & Hernández-López, J. M. (2021). Degradation of primary nanoplastics by photocatalysis using different anodized TiO<sub>2</sub> structures. *Journal of hazardous materials*, 413, 125452.
- Dong, S., Gao, P., Li, B., Feng, L., Liu, Y., Du, Z., & Zhang, L. (2022). Occurrence and migration of microplastics and plasticizers in different wastewater and sludge treatment units in municipal wastewater treatment plant. *Frontiers of Environmental Science & Engineering*, 16(11), 142.

- Edo, C., González-Pleiter, M., Leganés, F., Fernández-Piñas, F., & Rosal, R. (2020). Fate of microplastics in wastewater treatment plants and their environmental dispersion with effluent and sludge. *Environmental Pollution*, 259, 113837.
- Estahbanati, M. K., Feilizadeh, M., Avazpour, S., Kavand, M., Drogui, P., & Tyagi, R. (2023). Physical and physicochemical separation of microplastics and nanoplastics from water. In *Current Developments in Biotechnology and Bioengineering* (pp. 269-292). Elsevier.
- Exchange, T. (2019). Preferred fiber & materials market report 2019. *Textile Exchange: Lamesa, TX, USA*.
- Exchange, T. (2023). *Materials Market Report 2023*. Retrieved December from <https://textileexchange.org/knowledge-center/reports/materials-market-report-2023/>
- Falås, P., Longrée, P., la Cour Jansen, J., Siegrist, H., Hollender, J., & Joss, A. (2013). Micropollutant removal by attached and suspended growth in a hybrid biofilm-activated sludge process. *Water research*, 47(13), 4498-4506.
- Fan, C., Huang, Y.-Z., Lin, J.-N., & Li, J. (2022). Microplastic quantification of nylon and polyethylene terephthalate by chromic acid wet oxidation and ultraviolet spectrometry. *Environmental Technology & Innovation*, 28, 102683.
- Fan, Q., McQuillin, B., Ray, A., Turner, M., & Seddon, A. (2000). High density, non-porous anatase titania thin films for device applications. *Journal of Physics D: Applied Physics*, 33(21), 2683.
- Farahbakhsh, J., Gholi, M., Khiadani, M., Razmjou, A., & Zargar, M. (2024). Microplastics fouling mitigation in forward osmosis membranes by the molecular assembly of sulfobetaine zwitterion. *Desalination*, 575, 117300.
- Foundation, C. M. (2021). Synthetics anonymous–fashion brands’ addiction to fossil fuels. In: Changing Markets Foundation.
- Fraser, M. A., Chen, L., Ashar, M., Huang, W., Zeng, J., Zhang, C., & Zhang, D. (2020). Occurrence and distribution of microplastics and polychlorinated biphenyls in sediments from the Qiantang River and Hangzhou Bay, China. *Ecotoxicology and Environmental Safety*, 196, 110536.
- Furukuma, S., & Fujii, N. (2016). In vitro cytotoxicity evaluation of plastic marine debris by colony-forming assay. *Japanese Journal of Environmental Toxicology*, 19(2), 71-81.
- Gao, W., Zhang, Y., Mo, A., Jiang, J., Liang, Y., Cao, X., & He, D. (2022). Removal of microplastics in water: Technology progress and green strategies. *Green Analytical Chemistry*, 100042.
- Ge, J., Zhang, Z., Ouyang, Z., Shang, M., Liu, P., Li, H., & Guo, X. (2022). Photocatalytic degradation of (micro) plastics using TiO<sub>2</sub>-based and other catalysts: Properties, influencing factor, and mechanism. *Environmental Research*, 209, 112729.

- Gies, E. A., LeNoble, J. L., Noël, M., Etemadifar, A., Bishay, F., Hall, E. R., & Ross, P. S. (2018). Retention of microplastics in a major secondary wastewater treatment plant in Vancouver, Canada. *Marine pollution bulletin*, 133, 553-561.
- Gillibert, R., Balakrishnan, G., Deshoules, Q., Tardivel, M., Magazzù, A., Donato, M. G., Maragò, O. M., Lamy de La Chapelle, M., Colas, F., & Lagarde, F. (2019). Raman tweezers for small microplastics and nanoplastics identification in seawater. *Environmental science & technology*, 53(15), 9003-9013.
- Gong, J., & Xie, P. (2020). Research progress in sources, analytical methods, eco-environmental effects, and control measures of microplastics. *Chemosphere*, 254, 126790.
- Gu, Y., Zhao, J., & Johnson, J. A. (2020). Polymer networks: from plastics and gels to porous frameworks. *Angewandte Chemie International Edition*, 59(13), 5022-5049.
- Guan, J., Qi, K., Wang, J., Wang, W., Wang, Z., Lu, N., & Qu, J. (2020). Microplastics as an emerging anthropogenic vector of trace metals in freshwater: Significance of biofilms and comparison with natural substrates. *Water research*, 184, 116205.
- Gülay, A., Musovic, S., Albrechtsen, H.-J., Al-Soud, W. A., Sørensen, S. J., & Smets, B. F. (2016). Ecological patterns, diversity and core taxa of microbial communities in groundwater-fed rapid gravity filters. *The ISME journal*, 10(9), 2209-2222.
- Hamidian, A. H., Ozumchelouei, E. J., Feizi, F., Wu, C., Zhang, Y., & Yang, M. (2021). A review on the characteristics of microplastics in wastewater treatment plants: a source for toxic chemicals. *Journal of Cleaner Production*, 295, 126480.
- Hanvey, J. S., Lewis, P. J., Lavers, J. L., Crosbie, N. D., Pozo, K., & Clarke, B. O. (2017). A review of analytical techniques for quantifying microplastics in sediments. *Analytical Methods*, 9(9), 1369-1383.
- He, W., Liu, S., Zhang, W., Yi, K., Zhang, C., Pang, H., Huang, D., Huang, J., & Li, X. (2023). Recent advances on microplastic aging: Identification, mechanism, influence factors, and additives release. *Science of The Total Environment*, 164035.
- Heris, S. Z., Etemadi, M., Mousavi, S. B., Mohammadpourfard, M., & Ramavandi, B. (2023). Preparation and characterizations of TiO<sub>2</sub>/ZnO nanohybrid and its application in photocatalytic degradation of tetracycline in wastewater. *Journal of Photochemistry and Photobiology A: Chemistry*, 114893.
- Hidayaturrahman, H., & Lee, T.-G. (2019). A study on characteristics of microplastic in wastewater of South Korea: Identification, quantification, and fate of microplastics during treatment process. *Marine Pollution Bulletin*, 146, 696-702.
- Horovitz, I., Gitis, V., Avisar, D., & Mamane, H. (2020). Ceramic-based photocatalytic membrane reactors for water treatment—where to next? *Reviews in Chemical Engineering*, 36(5), 593-622.

- Hou, L., Kumar, D., Yoo, C. G., Gitsov, I., & Majumder, E. L.-W. (2021). Conversion and removal strategies for microplastics in wastewater treatment plants and landfills. *Chemical Engineering Journal*, 406, 126715.
- Hurley, C. R., & Leggett, G. J. (2009). Quantitative investigation of the photodegradation of polyethylene terephthalate film by friction force microscopy, contact-angle goniometry, and X-ray photoelectron spectroscopy. *ACS applied materials & interfaces*, 1(8), 1688-1697.
- Imhof, H. K., Laforsch, C., Wiesheu, A. C., Schmid, J., Anger, P. M., Niessner, R., & Ivleva, N. P. (2016). Pigments and plastic in limnetic ecosystems: A qualitative and quantitative study on microparticles of different size classes. *Water research*, 98, 64-74.
- Iyare, P. U., Ouki, S. K., & Bond, T. (2020). Microplastics removal in wastewater treatment plants: a critical review. *Environmental Science: Water Research & Technology*, 6(10), 2664-2675.
- Ji, J., Wu, X., Li, X., & Zhu, Y. (2023). Effects of microplastics in aquatic environments on inflammatory bowel disease. *Environmental Research*, 115974.
- Jiang, J., Wang, X., Ren, H., Cao, G., Xie, G., Xing, D., & Liu, B. (2020). Investigation and fate of microplastics in wastewater and sludge filter cake from a wastewater treatment plant in China. *Science of the Total Environment*, 746, 141378.
- Jiang, L., Chen, M., Huang, Y., Peng, J., Zhao, J., Chan, F., & Yu, X. (2022). Effects of different treatment processes in four municipal wastewater treatment plants on the transport and fate of microplastics. *Science of The Total Environment*, 831, 154946.
- Jose, L. M., George, N. S., Kadam, S. A., Athira, S., Kripa, A., Aravind, A., Ma, Y.-R., & Chen, Y.-R. (2023). Insight into the adsorption, photocatalytic and magnetic properties of bandgap tailored hydrothermally grown SnO<sub>2</sub>: Ni/Cu nanostructures. *Optical Materials*, 135, 113348.
- Kamalian, P., Khorasani, S. N., Abdolmaleki, A., Karevan, M., Khalili, S., Shirani, M., & Neisiany, R. E. (2020). Toward the development of polyethylene photocatalytic degradation. *Journal of Polymer Engineering*, 40(2), 181-191.
- Kanakaraju, D., & Chandrasekaran, A. (2023). Recent advances in TiO<sub>2</sub>/ZnS-based binary and ternary photocatalysts for the degradation of organic pollutants. *Science of the Total Environment*, 868, 161525.
- Käppler, A., Fischer, D., Oberbeckmann, S., Schernewski, G., Labrenz, M., Eichhorn, K.-J., & Voit, B. (2016). Analysis of environmental microplastics by vibrational microspectroscopy: FTIR, Raman or both? *Analytical and bioanalytical chemistry*, 408(29), 8377-8391.
- Katsumata, K.-i., Machida, S., Nakata, K., & Ogawa, M. (2023). Photoinduced Hydrophilicity and Antimicrobial Activity by Photocatalysis. In *Photo-switched Biodegradation of Bioplastics in Marine Environments* (pp. 77-88). Springer.

- Kernchen, S., Löder, M. G., Fischer, F., Fischer, D., Moses, S. R., Georgi, C., Nölscher, A. C., Held, A., & Laforsch, C. (2022). Airborne microplastic concentrations and deposition across the Weser River catchment. *Science of The Total Environment*, *818*, 151812.
- Khan, H., & Shah, M. U. H. (2023). Modification Strategies of TiO<sub>2</sub> Based Photocatalysts for Enhanced Visible Light Activity and Energy Storage Ability: A Review. *Journal of Environmental Chemical Engineering*, 111532.
- Kim, D., Kim, H., & An, Y.-J. (2023). Species sensitivity distributions of micro- and nanoplastics in soil based on particle characteristics. *Journal of hazardous materials*, *452*, 131229.
- Kim, S., Hyeon, Y., Rho, H., & Park, C. (2024). Ceramic membranes as a potential high-performance alternative to microplastic filters for household washing machines. *Separation and Purification Technology*, *344*, 127278.
- Kirstein, I. V., Kirmizi, S., Wichels, A., Garin-Fernandez, A., Erler, R., Löder, M., & Gerdt, G. (2016). Dangerous hitchhikers? Evidence for potentially pathogenic *Vibrio* spp. on microplastic particles. *Marine environmental research*, *120*, 1-8.
- Kökkılıç, O., Mohammadi-Jam, S., Chu, P., Marion, C., Yang, Y., & Waters, K. E. (2022). Separation of plastic wastes using froth flotation—an overview. *Advances in Colloid and Interface Science*, 102769.
- Kosek, K., Luczkiewicz, A., Fudala-Ksiazek, S., Jankowska, K., Szopinska, M., Svahn, O., Tranckner, J., Kaiser, A., Langas, V., & Bjorklund, E. (2020). Implementation of advanced micropollutants removal technologies in wastewater treatment plants (WWTPs) - Examples and challenges based on selected EU countries. *Environmental Science & Policy*, *112*, 213-226. <https://doi.org/10.1016/j.envsci.2020.06.011>
- Krishnan, R. Y., Manikandan, S., Subbaiya, R., Karmegam, N., Kim, W., & Govarthan, M. (2023). Recent approaches and advanced wastewater treatment technologies for mitigating emerging microplastics contamination—A critical review. *Science of The Total Environment*, *858*, 159681.
- Kumar, A., Choudhary, P., Kumar, A., Camargo, P. H., & Krishnan, V. (2022). Recent advances in plasmonic photocatalysis based on TiO<sub>2</sub> and noble metal nanoparticles for energy conversion, environmental remediation, and organic synthesis. *Small*, *18*(1), 2101638.
- Kumar, V., Singh, E., Singh, S., Pandey, A., & Bhargava, P. C. (2023). Micro- and nanoplastics (MNPs) as emerging pollutant in ground water: Environmental impact, potential risks, limitations and way forward towards sustainable management. *Chemical Engineering Journal*, *459*, 141568.
- Kurniawan, T. A., Haider, A., Ahmad, H. M., Mohyuddin, A., Aslam, H. M. U., Nadeem, S., Javed, M., Othman, M. H. D., Goh, H. H., & Chew, K. W. (2023). Source, occurrence, distribution, fate, and implications of microplastic pollutants in freshwater on environment: A critical review and way forward. *Chemosphere*, 138367.

- Kusworo, T. D., Kumoro, A. C., & Utomo, D. P. (2022). Photocatalytic nanohybrid membranes for highly efficient wastewater treatment: A comprehensive review. *Journal of Environmental Management*, 317, 115357.
- Kusworo, T. D., & Puspa, M. B. (2024). Performance of PVDF-La dope TiO<sub>2</sub> Membrane Photocatalytic Under Visible Light Irradiation for Produced Water Treatment. E3S Web of Conferences,
- Kutralam-Muniasamy, G., Pérez-Guevara, F., Elizalde-Martínez, I., & Shruti, V. (2020). An overview of recent advances in micro/nano beads and microfibers research: Critical assessment and promoting the less known. *Science of the Total Environment*, 740, 139991.
- Lares, M., Ncibi, M. C., Sillanpää, M., & Sillanpää, M. (2018). Occurrence, identification and removal of microplastic particles and fibers in conventional activated sludge process and advanced MBR technology. *Water research*, 133, 236-246.
- Lee, H., & Kim, Y. (2018). Treatment characteristics of microplastics at biological sewage treatment facilities in Korea. *Marine pollution bulletin*, 137, 1-8.
- Lee, J.-M., Busquets, R., Choi, I.-C., Lee, S.-H., Kim, J.-K., & Campos, L. C. (2020). Photocatalytic degradation of polyamide 66; evaluating the feasibility of photocatalysis as a microfibre-targeting technology. *Water*, 12(12), 3551.
- Leong, K. H., Gan, B. L., Ibrahim, S., & Saravanan, P. (2014). Synthesis of surface plasmon resonance (SPR) triggered Ag/TiO<sub>2</sub> photocatalyst for degradation of endocrine disturbing compounds. *Applied Surface Science*, 319, 128-135.
- Leslie, H., Brandsma, S., Van Velzen, M., & Vethaak, A. (2017). Microplastics en route: Field measurements in the Dutch river delta and Amsterdam canals, wastewater treatment plants, North Sea sediments and biota. *Environment International*, 101, 133-142.
- Leslie, H. A., Van Velzen, M. J., Brandsma, S. H., Vethaak, A. D., Garcia-Vallejo, J. J., & Lamoree, M. H. (2022). Discovery and quantification of plastic particle pollution in human blood. *Environment international*, 163, 107199.
- Li, J., Duan, Y., Wang, L., & Ma, J. (2024). Preparation of core-shell structure Ag@TiO<sub>2</sub> plasma photocatalysts and reduction of Cr (VI): Size dependent and LSPR effect. *Environmental Research*, 248, 118265.
- Li, J., Liu, H., & Chen, J. P. (2018). Microplastics in freshwater systems: A review on occurrence, environmental effects, and methods for microplastics detection. *Water Research*, 137, 362-374.
- Li, L., Geng, S., Li, Z., & Song, K. (2020). Effect of microplastic on anaerobic digestion of wasted activated sludge. *Chemosphere*, 247, 125874.
- Li, L., Xu, G., & Yu, H. (2018). Dynamic membrane filtration: formation, filtration, cleaning, and applications. *Chemical Engineering & Technology*, 41(1), 7-18.



- Li, N., Tian, Y., Zhang, J., Sun, Z., Zhao, J., Zhang, J., & Zuo, W. (2017). Precisely-controlled modification of PVDF membranes with 3D TiO<sub>2</sub>/ZnO nanolayer: enhanced anti-fouling performance by changing hydrophilicity and photocatalysis under visible light irradiation. *Journal of Membrane Science*, *528*, 359-368.
- Li, Q., Jia, R., Shao, J., & He, Y. (2019). Photocatalytic degradation of amoxicillin via TiO<sub>2</sub> nanoparticle coupling with a novel submerged porous ceramic membrane reactor. *Journal of Cleaner Production*, *209*, 755-761.
- Li, W. C. (2018). The occurrence, fate, and effects of microplastics in the marine environment. In *Microplastic Contamination in Aquatic Environments* (pp. 133-173). Elsevier.
- Li, Y., Wan, S., Lin, C., Gao, Y., Lu, Y., Wang, L., & Zhang, K. (2021). Engineering of 2D/2D MoS<sub>2</sub>/Cd<sub>x</sub>Zn<sub>1-x</sub>S photocatalyst for solar H<sub>2</sub> evolution coupled with degradation of plastic in alkaline solution. *Solar RRL*, *5*(6), 2000427.
- Li, Y., Xiao, P., Donnici, S., Cheng, J., & Tang, C. (2023). Spatial and seasonal distribution of microplastics in various environmental compartments around Sishili Bay of North Yellow Sea, China. *Marine Pollution Bulletin*, *186*, 114372.
- Lincho, J., Mazierski, P., Klimczuk, T., Martins, R. C., Gomes, J., & Zaleska-Medynska, A. (2024). TiO<sub>2</sub> nanotubes modification by photodeposition with noble metals: Characterization, optimization, photocatalytic activity, and by-products analysis. *Journal of Environmental Chemical Engineering*, 112990.
- Liu, J., Liang, J., Ding, J., Zhang, G., Zeng, X., Yang, Q., Zhu, B., & Gao, W. (2021). Microfiber pollution: an ongoing major environmental issue related to the sustainable development of textile and clothing industry. *Environment, Development and Sustainability*, *23*, 11240-11256.
- Liu, L., Xu, M., Ye, Y., & Zhang, B. (2022). On the degradation of (micro) plastics: Degradation methods, influencing factors, environmental impacts. *Science of the Total Environment*, *806*, 151312.
- Liu, X., Yuan, W., Di, M., Li, Z., & Wang, J. (2019). Transfer and fate of microplastics during the conventional activated sludge process in one wastewater treatment plant of China. *Chemical Engineering Journal*, *362*, 176-182.
- Long, Z., Pan, Z., Wang, W., Ren, J., Yu, X., Lin, L., Lin, H., Chen, H., & Jin, X. (2019). Microplastic abundance, characteristics, and removal in wastewater treatment plants in a coastal city of China. *Water Research*, *155*, 255-265.
- Luo, Y., Xie, H., Xu, H., Zhou, C., Wang, P., Liu, Z., Yang, Y., Huang, J., Wang, C., & Zhao, X. (2023). Wastewater treatment plant serves as a potentially controllable source of microplastic: association of microplastic removal and operational parameters and water quality data. *Journal of Hazardous Materials*, *441*, 129974.
- Lv, L., He, L., Jiang, S., Chen, J., Zhou, C., Qu, J., Lu, Y., Hong, P., Sun, S., & Li, C. (2020). In situ surface-enhanced Raman spectroscopy for detecting microplastics and nanoplastics in aquatic environments. *Science of The Total Environment*, *728*, 138449.

- Lv, X., Dong, Q., Zuo, Z., Liu, Y., Huang, X., & Wu, W.-M. (2019). Microplastics in a municipal wastewater treatment plant: Fate, dynamic distribution, removal efficiencies, and control strategies. *Journal of Cleaner Production*, 225, 579-586.
- Ma, B., Xue, W., Hu, C., Liu, H., Qu, J., & Li, L. (2019). Characteristics of microplastic removal via coagulation and ultrafiltration during drinking water treatment. *Chemical Engineering Journal*, 359, 159-167.
- Ma, N., Fan, X., Quan, X., & Zhang, Y. (2009). Ag-TiO<sub>2</sub>/HAP/Al<sub>2</sub>O<sub>3</sub> bioceramic composite membrane: Fabrication, characterization and bactericidal activity. *Journal of Membrane Science*, 336(1-2), 109-117.
- Madkhali, N., Prasad, C., Malkappa, K., Choi, H. Y., Govinda, V., Bahadur, I., & Abumousa, R. (2023). Recent update on photocatalytic degradation of pollutants in waste water using TiO<sub>2</sub>-based heterostructured materials. *Results in Engineering*, 100920.
- Malato, S., Fernández-Ibáñez, P., Maldonado, M. I., Blanco, J., & Gernjak, W. (2009). Decontamination and disinfection of water by solar photocatalysis: recent overview and trends. *Catalysis Today*, 147(1), 1-59.
- Marinho, B. A., Cristóvão, R. O., Djellabi, R., Caseiro, A., Miranda, S. M., Loureiro, J. M., Boaventura, R. A., Dias, M. M., Lopes, J. C. B., & Vilar, V. J. (2018). Strategies to reduce mass and photons transfer limitations in heterogeneous photocatalytic processes: hexavalent chromium reduction studies. *Journal of Environmental Management*, 217, 555-564.
- Mason, S. A., Garneau, D., Sutton, R., Chu, Y., Ehmann, K., Barnes, J., Fink, P., Papazissimos, D., & Rogers, D. L. (2016). Microplastic pollution is widely detected in US municipal wastewater treatment plant effluent. *Environmental Pollution*, 218, 1045-1054.
- Michielssen, M. R., Michielssen, E. R., Ni, J., & Duhaime, M. B. (2016). Fate of microplastics and other small anthropogenic litter (SAL) in wastewater treatment plants depends on unit processes employed. *Environmental Science: Water Research & Technology*, 2(6), 1064-1073.
- Mishra, J. R., Samal, S. K., Mohanty, S., & Nayak, S. K. (2021). Polyvinylidene fluoride (PVDF)/Ag@ TiO<sub>2</sub> nanocomposite membrane with enhanced fouling resistance and antibacterial performance. *Materials Chemistry and Physics*, 268, 124723.
- Mishra, S., Rout, P. K., & Das, A. P. (2021). Emerging microfiber pollution and its remediation. *Environmental Pollution and Remediation*, 247-266.
- Molinari, R., Lavorato, C., & Argurio, P. (2021). The Evolution of photocatalytic membrane reactors over the last 20 years: a state of the art perspective. *Catalysts*, 11(7), 775.
- Molinari, R., Severino, A., Lavorato, C., & Argurio, P. (2023). Which Configuration of Photocatalytic Membrane Reactors Has a Major Potential to Be Used at an Industrial Level in Tertiary Sewage Wastewater Treatment? *Catalysts*, 13(8), 1204.

- Monira, S., Roychand, R., Hai, F. I., Bhuiyan, M., Dhar, B. R., & Pramanik, B. K. (2023). Nano and microplastics occurrence in wastewater treatment plants: A comprehensive understanding of microplastics fragmentation and their removal. *Chemosphere*, 334, 139011.
- Mosquera, A. A., Albella, J. M., Navarro, V., Bhattacharyya, D., & Endrino, J. L. (2016). Effect of silver on the phase transition and wettability of titanium oxide films. *Scientific Reports*, 6(1), 1-14.
- Mozia, S. (2010). Photocatalytic membrane reactors (PMRs) in water and wastewater treatment. A review. *Separation and Purification Technology*, 73(2), 71-91.
- Mu, H., & Chen, Y. (2011). Long-term effect of ZnO nanoparticles on waste activated sludge anaerobic digestion. *Water research*, 45(17), 5612-5620.
- Mujeriego, R., & Asano, T. (1999). The role of advanced treatment in wastewater reclamation and reuse. *Water Science and Technology*, 40(4-5), 1-9.
- Murphy, F., Ewins, C., Carbonnier, F., & Quinn, B. (2016). Wastewater treatment works (WwTW) as a source of microplastics in the aquatic environment. *Environmental science & technology*, 50(11), 5800-5808.
- Nayeri, S., & Parsa, J. B. (2024). High performance polyethersulfone/TiO<sub>2</sub>-AgBr-Ag photocatalytic membrane for Cefixime removal from water under visible light. *Desalination and Water Treatment*, 317, 100242.
- Novotna, K., Cermakova, L., Pivokonska, L., Cajthaml, T., & Pivokonsky, M. (2019). Microplastics in drinking water treatment—current knowledge and research needs. *Science of The Total Environment*, 667, 730-740.
- Osorio-Vargas, P., Pinotti, A., Campos, C. H., Macías-Quiroga, I. F., Manrique-Holguín, M., Pizzio, L. R., & Rengifo-Herrera, J. A. (2023). Flexible polymeric films containing nanoparticles of visible-light absorbing TiO<sub>2</sub> and their applications as photo-induced self-cleaning and antimicrobial surfaces. In *Novel Materials for Environmental Remediation Applications* (pp. 413-433). Elsevier.
- Ou, H., & Zeng, E. Y. (2018). Occurrence and fate of microplastics in wastewater treatment plants. In *Microplastic contamination in aquatic environments* (pp. 317-338). Elsevier.
- Paiman, S. H., Noor, S. F. M., Ngadi, N., Nordin, A. H., & Abdullah, N. (2023). Insight into photocatalysis technology as a promising approach to tackle microplastics pollution through degradation and upcycling. *Chemical Engineering Journal*, 143534.
- Pasichnyk, M., Gaálová, J., Minarik, P., Václavíková, M., & Melnyk, I. (2022). Development of polyester filters with polymer nanocomposite active layer for effective dye filtration. *Scientific Reports*, 12(1), 973.
- Patil, S., Kamdi, P., Chakraborty, S., Das, S., Bafana, A., Krishnamurthi, K., & Sivanesan, S. (2023). Characterization and removal of microplastics in a sewage treatment

- plant from urban Nagpur, India. *Environmental Monitoring and Assessment*, 195(1), 1-19.
- Peng, G., Qi, X., Qu, W., Shao, X., Song, L., Du, P., & Xiong, J. (2023). Photocatalytic degradation of PET microfibers and hydrogen evolution by Ni<sub>5</sub>P<sub>4</sub>/TiO<sub>2</sub>/C NFs. *Catalysis Science & Technology*, 13(20), 5868-5879.
- Pepper, L., & Truscott, L. (2021). Preferred fiber & materials market report 2021. In.
- Pérez-Jiménez, A. I., Lyu, D., Lu, Z., Liu, G., & Ren, B. (2020). Surface-enhanced Raman spectroscopy: benefits, trade-offs and future developments. *Chemical science*, 11(18), 4563-4577.
- Persson, L., Carney Almroth, B. M., Collins, C. D., Cornell, S., de Wit, C. A., Diamond, M. L., Fantke, P., Hassellöv, M., MacLeod, M., & Ryberg, M. W. (2022). Outside the safe operating space of the planetary boundary for novel entities. *Environmental science & technology*, 56(3), 1510-1521.
- Pico, Y., Alfarhan, A., & Barcelo, D. (2019). Nano-and microplastic analysis: Focus on their occurrence in freshwater ecosystems and remediation technologies. *TrAC Trends in Analytical Chemistry*, 113, 409-425.
- Pivokonsky, M., Cermakova, L., Novotna, K., Peer, P., Cajthaml, T., & Janda, V. (2018). Occurrence of microplastics in raw and treated drinking water. *Science of the Total Environment*, 643, 1644-1651.
- Poerio, T., Lavorato, C., Severino, A., Russo, B., Molinari, R., Argurio, P., & Figoli, A. (2024). Combined membrane separation and photocatalysis process for the recovery and decomposition of micro/nanoplastics from polyester fabrics. *Journal of Environmental Chemical Engineering*, 12(5), 113310.
- Pramanik, B. K., Pramanik, S. K., & Monira, S. (2021). Understanding the fragmentation of microplastics into nano-plastics and removal of nano/microplastics from wastewater using membrane, air flotation and nano-ferrofluid processes. *Chemosphere*, 282, 131053.
- Prata, J. C., da Costa, J. P., Lopes, I., Duarte, A. C., & Rocha-Santos, T. (2020). Environmental exposure to microplastics: An overview on possible human health effects. *Science of the Total Environment*, 702, 134455.
- Prata, J. C., Venâncio, C., da Costa, J. P., Lopes, I., Duarte, A. C., & Rocha-Santos, T. (2021). Considerations when using microplates and Neubauer counting chamber in ecotoxicity tests on microplastics. *Marine pollution bulletin*, 170, 112615.
- Praveena, S. M., Syahira Asmawi, M., & Chyi, J. L. Y. (2021). Microplastic emissions from household washing machines: preliminary findings from Greater Kuala Lumpur (Malaysia). *Environmental Science and Pollution Research*, 28(15), 18518-18522.
- Priya, K., Iqbal, S., Archana, A., Gopika, B., Mina, M., Haddout, S., & Madhu, A. M. (2023). Implications of solid waste dumps on the microplastic abundance in

- groundwater in Kollam, India. *Journal of Environmental Management*, 348, 119224.
- Qin, H., Guo, W., Gao, P., & Xiao, H. (2020). Spheroidization of low-cost alumina powders for the preparation of high-flux flat-sheet ceramic membranes. *Ceramics International*, 46(9), 13189-13197.
- Qiu, Y., Zhang, T., & Zhang, P. (2023). Fate and environmental behaviors of microplastics through the lens of free radical. *Journal of hazardous materials*, 453, 131401.
- Rajala, K., Grönfors, O., Hesampour, M., & Mikola, A. (2020). Removal of microplastics from secondary wastewater treatment plant effluent by coagulation/flocculation with iron, aluminum and polyamine-based chemicals. *Water research*, 183, 116045.
- Raju, M., Gandhimathi, R., & Nidheesh, P. (2023). The cause, fate and effect of microplastics in freshwater ecosystem: Ways to overcome the challenge. *Journal of Water Process Engineering*, 55, 104199.
- Rani, C. N., Karthikeyan, S., & Doss, S. P. A. (2021). Photocatalytic ultrafiltration membrane reactors in water and wastewater treatment-A review. *Chemical Engineering and Processing-Process Intensification*, 165, 108445.
- Reddy, A. S., & Nair, A. T. (2022). The fate of microplastics in wastewater treatment plants: An overview of source and remediation technologies. *Environmental Technology & Innovation*, 102815.
- Renner, G., Schmidt, T. C., & Schram, J. (2017). Characterization and quantification of microplastics by infrared spectroscopy. In *Comprehensive Analytical Chemistry* (Vol. 75, pp. 67-118). Elsevier.
- Rodriguez-Narvaez, O. M., Goonetilleke, A., Perez, L., & Bandala, E. R. (2021). Engineered technologies for the separation and degradation of microplastics in water: A review. *Chemical Engineering Journal*, 414, 128692.
- Rojas-Guerrero, C., Villanueva-Rodríguez, M., Guzmán-Mar, J., Hernández-Ramírez, A., Cedillo-González, E., Rodríguez, F. L., & Hinojosa-Reyes, L. (2023). Solar photocatalytic degradation of polyethylene terephthalate nanoplastics: Evaluation of the applicability of the TiO<sub>2</sub>/MIL-100 (Fe) composite material. *Journal of Environmental Chemical Engineering*, 11(5), 110415.
- Ruan, Y., Zhang, K., Wu, C., Wu, R., & Lam, P. K. (2019). A preliminary screening of HBCD enantiomers transported by microplastics in wastewater treatment plants. *Science of The Total Environment*, 674, 171-178.
- Saifuddin, M., Ghaffari, Y., Park, S. Y., & Kim, C. G. (2022). Rapid surface degradation of co-axially arranged polypropylene globules by nanoporous carbonized TiO<sub>2</sub> assisted with UV-C. *Environmental Research*, 212, 113422.

- Sajid, M., Ihsanullah, I., Khan, M. T., & Baig, N. (2022). Nanomaterials-based adsorbents for remediation of microplastics and nanoplastics in aqueous media: A review. *Separation and Purification Technology*, 122453.
- Saletnik, A., Saletnik, B., & Puchalski, C. (2021). Overview of popular techniques of Raman spectroscopy and their potential in the study of plant tissues. *Molecules*, 26(6), 1537.
- Salmi, P., Ryymin, K., Karjalainen, A. K., Mikola, A., Uurasjärvi, E., & Talvitie, J. (2021). Particle balance and return loops for microplastics in a tertiary-level wastewater treatment plant. *Water Science and Technology*, 84(1), 89-100.
- Salthouse, T. N., & Matlaga, B. F. (1975). Significance of cellular enzyme activity at nonabsorbable suture implant sites: silk, polyester, and polypropylene. *Journal of Surgical Research*, 19(2), 127-132.
- Sang, T., Wallis, C. J., Hill, G., & Britovsek, G. J. (2020). Polyethylene terephthalate degradation under natural and accelerated weathering conditions. *European polymer journal*, 136, 109873.
- Sangkham, S., Faikhaw, O., Munkong, N., Sakunkoo, P., Arunlertaree, C., Chavali, M., Mousazadeh, M., & Tiwari, A. (2022). A review on microplastics and nanoplastics in the environment: Their occurrence, exposure routes, toxic studies, and potential effects on human health. *Marine Pollution Bulletin*, 181, 113832.
- Sarkar, D. J., Sarkar, S. D., Das, B. K., Praharaj, J. K., Mahajan, D. K., Purokait, B., Mohanty, T. R., Mohanty, D., Gogoi, P., & Kumar, S. (2021). Microplastics removal efficiency of drinking water treatment plant with pulse clarifier. *Journal of Hazardous Materials*, 413, 125347.
- Schymanski, D., Oßmann, B. E., Benismail, N., Boukerma, K., Dallmann, G., Von der Esch, E., Fischer, D., Fischer, F., Gilliland, D., & Glas, K. (2021). Analysis of microplastics in drinking water and other clean water samples with micro-Raman and micro-infrared spectroscopy: minimum requirements and best practice guidelines. *Analytical and bioanalytical chemistry*, 413(24), 5969-5994.
- Shen, M., Song, B., Zhu, Y., Zeng, G., Zhang, Y., Yang, Y., Wen, X., Chen, M., & Yi, H. (2020). Removal of microplastics via drinking water treatment: Current knowledge and future directions. *Chemosphere*, 251, 126612.
- Shi, X., Chen, Z., Liu, X., Wei, W., & Ni, B.-J. (2022). The photochemical behaviors of microplastics through the lens of reactive oxygen species: Photolysis mechanisms and enhancing photo-transformation of pollutants. *Science of the Total Environment*, 846, 157498.
- Siipola, V., Pflugmacher, S., Romar, H., Wendling, L., & Koukkari, P. (2020). Low-cost biochar adsorbents for water purification including microplastics removal. *Applied Sciences*, 10(3), 788.
- Singh, R. P., Mishra, S., & Das, A. P. (2020). Synthetic microfibers: Pollution toxicity and remediation. *Chemosphere*, 257, 127199.

- Singh, S., Mahalingam, H., & Singh, P. K. (2013). Polymer-supported titanium dioxide photocatalysts for environmental remediation: A review. *Applied Catalysis A: General*, 462, 178-195.
- Sivaranjani, P., Janani, B., Thomas, A. M., Raju, L. L., & Khan, S. S. (2022). Recent development in MoS<sub>2</sub>-based nano-photocatalyst for the degradation of pharmaceutically active compounds. *Journal of Cleaner Production*, 352, 131506.
- Skaf, D. W., Punzi, V. L., Rolle, J. T., & Kleinberg, K. A. (2020). Removal of micron-sized microplastic particles from simulated drinking water via alum coagulation. *Chemical Engineering Journal*, 386, 123807.
- Song, Y. K., Hong, S. H., Jang, M., Han, G. M., Rani, M., Lee, J., & Shim, W. J. (2015). A comparison of microscopic and spectroscopic identification methods for analysis of microplastics in environmental samples. *Marine pollution bulletin*, 93(1-2), 202-209.
- Sonune, A., & Ghate, R. (2004). Developments in wastewater treatment methods. *Desalination*, 167, 55-63.
- Suaria, G., Achtypi, A., Perold, V., Lee, J. R., Pierucci, A., Bornman, T. G., Aliani, S., & Ryan, P. G. (2020). Microfibers in oceanic surface waters: A global characterization. *Science advances*, 6(23), eaay8493.
- Sun, J., Dai, X., Wang, Q., Van Loosdrecht, M. C., & Ni, B.-J. (2019). Microplastics in wastewater treatment plants: Detection, occurrence and removal. *Water research*, 152, 21-37.
- Talvitie, J., Mikola, A., Koistinen, A., & Setälä, O. (2017). Solutions to microplastic pollution—Removal of microplastics from wastewater effluent with advanced wastewater treatment technologies. *Water Research*, 123, 401-407.
- Talvitie, J., Mikola, A., Setälä, O., Heinonen, M., & Koistinen, A. (2017). How well is microlitter purified from wastewater?—A detailed study on the stepwise removal of microlitter in a tertiary level wastewater treatment plant. *Water Research*, 109, 164-172.
- Tang, N., Liu, X., & Xing, W. (2020). Microplastics in wastewater treatment plants of Wuhan, Central China: Abundance, removal, and potential source in household wastewater. *Science of the Total Environment*, 745, 141026.
- Tang, W., Li, X., Liu, H., Wu, S., Zhou, Q., Du, C., Teng, Q., Zhong, Y., & Yang, C. (2020). Sequential vertical flow trickling filter and horizontal flow multi-soil-layering reactor for treatment of decentralized domestic wastewater with sodium dodecyl benzene sulfonate. *Bioresource technology*, 300, 122634.
- Tao, H., Zhou, L., Qi, Y., Chen, Y., & Lin, T. (2023). Variation of microplastics and biofilm community characteristics along the long-distance raw water pipeline. *Process Safety and Environmental Protection*, 169, 304-312.
- Taylor, M., Gwinnett, C., Robinson, L. F., & Woodall, L. C. (2016). Plastic microfibre ingestion by deep-sea organisms. *Scientific reports*, 6(1), 33997.

- Tchobanoglous, G., Burton, F. L., & Stensel, H. D. (1991). Wastewater engineering. *Management*, 7(1), 4.
- Thompson, R. C., Olsen, Y., Mitchell, R. P., Davis, A., Rowland, S. J., John, A. W., McGonigle, D., & Russell, A. E. (2004). Lost at sea: where is all the plastic? *Science*, 304(5672), 838-838.
- Tseng, H.-C., & Chen, Y.-W. (2019). Facile synthesis of Ag/TiO<sub>2</sub> by photoreduction method and its degradation activity of methylene blue under UV and visible light irradiation. *Modern Research in Catalysis*, 9(1), 1-19.
- Uheida, A., Mejía, H. G., Abdel-Rehim, M., Hamd, W., & Dutta, J. (2021). Visible light photocatalytic degradation of polypropylene microplastics in a continuous water flow system. *Journal of Hazardous Materials*, 406, 124299.
- Üstün, G. E., Bozdaş, K., & Can, T. (2022). Abundance and characteristics of microplastics in an urban wastewater treatment plant in Turkey. *Environmental Pollution*, 310, 119890.
- Ütebay, B., Çelik, P., & Çay, A. (2020). Textile wastes: Status and perspectives. *Waste in textile and leather sectors*, 39-52.
- Van Do, M., Le, T. X. T., Vu, N. D., & Dang, T. T. (2022). Distribution and occurrence of microplastics in wastewater treatment plants. *Environmental Technology & Innovation*, 26, 102286.
- Vatanpour, V., Karami, A., & Sheydaei, M. (2019). Improved visible photocatalytic activity of TiO<sub>2</sub> nanoparticles to use in submerged membrane photoreactor for organic pollutant degradation. *International Journal of Environmental Science and Technology*, 16, 2405-2414.
- Vethaak, A. D., & Legler, J. (2021). Microplastics and human health. *Science*, 371(6530), 672-674.
- Viana, M., Mohallem, N., Miquita, D., Balzuweit, K., & Silva-Pinto, E. (2013). Preparation of amorphous and crystalline Ag/TiO<sub>2</sub> nanocomposite thin films. *Applied Surface Science*, 265, 130-136.
- Wang, C., Song, J., Nunes, L. M., Zhao, H., Wang, P., Liang, Z., Arp, H. P. H., Li, G., & Xing, B. (2024). Global microplastic fiber pollution from domestic laundry. *Journal of hazardous materials*, 135290.
- Wang, L., & Wang, X. (2006). Study of membrane morphology by microscopic image analysis and membrane structure parameter model. *Journal of Membrane Science*, 283(1-2), 109-115.
- Wang, S., Parajuli, S., Sivalingam, V., & Bakke, R. (2019). Biofilm in moving bed biofilm process for wastewater treatment. *Bacterial Biofilms*, 1(1), 1-15.
- Wang, Y., Chen, G.-E., Wu, H.-L., Xu, Z.-L., Wan, J.-J., Liu, L.-J., Xu, S.-J., Kong, Y.-F., Wu, Q., & Min, J. (2020). Fabrication of GO-Ag/PVDF/F127 modified



membrane IPA coagulation bath for catalytic reduction of 4-nitrophenol. *Separation and Purification Technology*, 235, 116143.

- Wang, Y., Liu, Y., Chen, Z., Liu, Y., Guo, J., Zhang, W., Rao, P., & Li, G. (2022). Recent progress in the pore size control of silicon carbide ceramic membranes. *Ceramics International*, 48(7), 8960-8971.
- Wang, Z., Lin, T., & Chen, W. (2020). Occurrence and removal of microplastics in an advanced drinking water treatment plant (ADWTP). *Science of the Total Environment*, 700, 134520.
- Wei, S., Luo, H., Zou, J., Chen, J., Pan, X., Rousseau, D. P., & Li, J. (2020). Characteristics and removal of microplastics in rural domestic wastewater treatment facilities of China. *Science of The Total Environment*, 739, 139935.
- Wodka, D., Bielanska, E., Socha, R. P., Elzbieciak-Wodka, M., Gurgul, J., Nowak, P., Warszynski, P., & Kumakiri, I. (2010). Photocatalytic activity of titanium dioxide modified by silver nanoparticles. *ACS applied materials & interfaces*, 2(7), 1945-1953.
- Wols, B., & Hofman-Caris, C. (2012). Review of photochemical reaction constants of organic micropollutants required for UV advanced oxidation processes in water. *Water Research*, 46(9), 2815-2827.
- Wu, M., Tang, W., Wu, S., Liu, H., & Yang, C. (2021). Fate and effects of microplastics in wastewater treatment processes. *Science of the Total Environment*, 757, 143902.
- Xu, J., Wang, X., Zhang, Z., Yan, Z., & Zhang, Y. (2021). Effects of chronic exposure to different sizes and polymers of microplastics on the characteristics of activated sludge. *Science of The Total Environment*, 783, 146954.
- Xu, X., Jian, Y., Xue, Y., Hou, Q., & Wang, L. (2019). Microplastics in the wastewater treatment plants (WWTPs): occurrence and removal. *Chemosphere*, 235, 1089-1096.
- Xu, Z., Bai, X., & Ye, Z. (2021). Removal and generation of microplastics in wastewater treatment plants: a review. *Journal of Cleaner Production*, 291, 125982.
- Yang, J., Monnot, M., Sun, Y., Asia, L., Wong-Wah-Chung, P., Doumenq, P., & Moulin, P. (2023). Microplastics in different water samples (seawater, freshwater, and wastewater): Removal efficiency of membrane treatment processes. *Water research*, 119673.
- Yang, X.-D., Gong, B., Chen, W., Qian, C., Du, M., & Yu, H.-Q. (2022). In-situ quantitative monitoring the organic contaminants uptake onto suspended microplastics in aquatic environments. *Water research*, 215, 118235.
- Yang, Z., Li, S., Ma, S., Liu, P., Peng, D., Ouyang, Z., & Guo, X. (2021). Characteristics and removal efficiency of microplastics in sewage treatment plant of Xi'an City, northwest China. *Science of The Total Environment*, 771, 145377.

- Yang, Z., & Tang, C. Y. (2018). Novel membranes and membrane materials. In *Membrane-Based Salinity Gradient Processes for Water Treatment and Power Generation* (pp. 201-221). Elsevier.
- Yaranal, N. A., Subbiah, S., & Mohanty, K. (2021). Identification, extraction of microplastics from edible salts and its removal from contaminated seawater. *Environmental Technology & Innovation*, 21, 101253.
- Yuan, F., Yue, L., Zhao, H., & Wu, H. (2020). Study on the adsorption of polystyrene microplastics by three-dimensional reduced graphene oxide. *Water Science and Technology*, 81(10), 2163-2175.
- Yuan, J., Ma, J., Sun, Y., Zhou, T., Zhao, Y., & Yu, F. (2020). Microbial degradation and other environmental aspects of microplastics/plastics. *Science of the Total Environment*, 715, 136968.
- Yuan, Z., Nag, R., & Cummins, E. (2022). Human health concerns regarding microplastics in the aquatic environment-From marine to food systems. *Science of the Total Environment*, 823, 153730.
- Zakria, H. S., Borhamdin, S., Ismail, N. J., Peechmani, P., Moslan, M. S., Othman, M. H. D., Rahman, M. A., Jaafar, J., Puteh, M. H., & Rajamohan, N. (2024). Novel Self-cleaning PVDF/MoO<sub>3</sub>/ZnO/GO Dual Layer Hollow Fiber Photocatalytic Membrane with Excellent Photocatalytic Performance of EDCs Removal and Energy Storage Capability. *Journal of Membrane Science*, 122842.
- Zhang, B., Wu, Q., Gao, S., Ruan, Y., Qi, G., Guo, K., & Zeng, J. (2023a). Distribution and removal mechanism of microplastics in urban wastewater plants systems via different processes. *Environmental Pollution*, 320, 121076.
- Zhang, B., Wu, Q., Gao, S., Ruan, Y., Qi, G., Guo, K., & Zeng, J. (2023b). Distribution and removal mechanism of microplastics in urban wastewater plants systems via different processes. *Environmental Pollution*, 121076.
- Zhang, C., Zhang, T., Wang, Y., Liang, Q., Zhou, M., Li, X., Li, Z., & Xu, S. (2022). In-situ synthesis of 3D CdMoO<sub>4</sub>@ CdS core-shell structure for efficient photocatalytic degradation. *Ceramics International*, 48(11), 15064-15072.
- Zhang, G., Yu, Y., Tu, Y., Liu, Y., Huang, J., Yin, X., & Feng, Y. (2023). Preparation of reusable UHMWPE/TiO<sub>2</sub> photocatalytic microporous membrane reactors for efficient degradation of organic pollutants in water. *Separation and Purification Technology*, 305, 122515.
- Zhang, H., Quan, X., Chen, S., Zhao, H., & Zhao, Y. (2006). Fabrication of photocatalytic membrane and evaluation its efficiency in removal of organic pollutants from water. *Separation and Purification Technology*, 50(2), 147-155.
- Zhang, J. (2020). Recent trends and research strategies for wastewater treatment in China. In *Water Conservation and Wastewater Treatment in BRICS Nations* (pp. 169-186). Elsevier.

- Zhang, J., Wang, L., Trasande, L., & Kannan, K. (2021). Occurrence of polyethylene terephthalate and polycarbonate microplastics in infant and adult feces. *Environmental Science & Technology Letters*, 8(11), 989-994.
- Zhang, J., Wu, H., Shi, L., Wu, Z., Zhang, S., Wang, S., & Sun, H. (2023). Photocatalysis coupling with membrane technology for sustainable and continuous purification of wastewater. *Separation and purification technology*, 125225.
- Zhang, W., Ding, L., Luo, J., Jaffrin, M. Y., & Tang, B. (2016). Membrane fouling in photocatalytic membrane reactors (PMRs) for water and wastewater treatment: A critical review. *Chemical Engineering Journal*, 302, 446-458.
- Zhang, Y., Jiang, H., Bian, K., Wang, H., & Wang, C. (2021). A critical review of control and removal strategies for microplastics from aquatic environments. *Journal of Environmental Chemical Engineering*, 9(4), 105463.
- Zhang, Y.-Q., Lykaki, M., Alrajoula, M. T., Markiewicz, M., Kraas, C., Kolbe, S., Klinkhammer, K., Rabe, M., Klauer, R., & Bendt, E. (2021). Microplastics from textile origin—emission and reduction measures. *Green Chemistry*, 23(15), 5247-5271.
- Zhang, Y.-T., Wei, W., Huang, Q.-S., Wang, C., Wang, Y., & Ni, B.-J. (2020). Insights into the microbial response of anaerobic granular sludge during long-term exposure to polyethylene terephthalate microplastics. *Water research*, 179, 115898.
- Zhang, Y.-T., Wei, W., Wang, C., & Ni, B.-J. (2022). Microbial and physicochemical responses of anaerobic hydrogen-producing granular sludge to polyethylene micro (nano) plastics. *Water research*, 221, 118745.
- Zhang, Z., Pan, S., Huang, F., Li, X., Shang, J., Lai, J., & Liao, Y. (2017). Nitrogen and phosphorus removal by activated sludge process: a review. *Mini-Reviews in Organic Chemistry*, 14(2), 99-106.
- Zhao, D. L., Zhou, W., Shen, L., Li, B., Sun, H., Qianqian, Z., Tang, C. Y., Lin, H., & Chung, T.-S. (2024). New directions on membranes for removal and degradation of emerging pollutants in aqueous systems. *Water Research*, 121111.
- Zhao, L., Su, C., Liu, W., Qin, R., Tang, L., Deng, X., Wu, S., & Chen, M. (2020). Exposure to polyamide 66 microplastic leads to effects performance and microbial community structure of aerobic granular sludge. *Ecotoxicology and Environmental Safety*, 190, 110070.
- Zheng, X., Shen, Z.-P., Shi, L., Cheng, R., & Yuan, D.-H. (2017). Photocatalytic membrane reactors (PMRs) in water treatment: configurations and influencing factors. *Catalysts*, 7(8), 224.
- Zhou, D., Luo, H., Zhang, F., Wu, J., Yang, J., & Wang, H. (2022). Efficient photocatalytic degradation of the persistent PET fiber-based microplastics over Pt nanoparticles decorated N-doped TiO<sub>2</sub> nanoflowers. *Advanced Fiber Materials*, 4(5), 1094-1107.

- Zhou, D., Wang, L., Zhang, F., Wu, J., Wang, H., & Yang, J. (2022). Feasible Degradation of Polyethylene Terephthalate Fiber - Based Microplastics in Alkaline Media with Bi<sub>2</sub>O<sub>3</sub>@ N - TiO<sub>2</sub> Z - Scheme Photocatalytic System. *Advanced Sustainable Systems*, 6(5), 2100516.
- Zhou, M., Zhang, X., Quan, Y., Tian, Y., Chen, J., & Li, L. (2024). Visible light-induced photocatalytic and antibacterial adhesion properties of superhydrophilic TiO<sub>2</sub> nanoparticles. *Scientific Reports*, 14(1), 7940.
- Zhou, X.-X., Liu, R., Hao, L.-T., & Liu, J.-F. (2021). Identification of polystyrene nanoplastics using surface enhanced Raman spectroscopy. *Talanta*, 221, 121552.
- Ziajahromi, S., Neale, P. A., Rintoul, L., & Leusch, F. D. (2017). Wastewater treatment plants as a pathway for microplastics: development of a new approach to sample wastewater-based microplastics. *Water research*, 112, 93-99.

Universiti Malaysia